




Universitetet
i Stavanger

FACULTY OF SCIENCE AND TECHNOLOGY

MASTER'S THESIS

Study programme/specialisation: Offshore Technology - Marine- and Subsea Technology	Spring / Autumn semester, 2017.. Open/ Confidential
Author: Jørgen Andresen	 (signature of author)
Programme coordinator: Prof. Ove Tobias Gudmestad Supervisor(s): Prof. Ove Tobias Gudmestad	
Title of master's thesis: Mooring Analysis of a Closed Fish Cage	
Credits: 30	
Keywords: Aquaculture AquaSim Mooring Wave and Current Forces Concept Fish Farm	Number of pages: 96..... + supplemental material/other: 116..... Stavanger, 13.06.2017..... date/year

This page is intentionally left blank.



Universitetet
i Stavanger

Mooring Analysis of a Closed Fish Cage

Jørgen Andresen

June 2017

MASTER THESIS

Department of Mechanical and Structural Engineering and Material Science

University of Stavanger

Supervisor: Professor Ove Tobias Gudmestad

This page is intentionally left blank.

Abstract

As of today, Norway is the second largest seafood exporter in the world after China, and Norwegian seafood is currently exported to more than 130 countries ([Laksefakta, n.d.](#)). In conjunction with the present growth of the aquaculture industry in Norway, there is a rising skepticism regarding the sustainability of the industry. Major concerns are fleeing, fish welfare, salmon louse and impact on marine life in close proximity to the fish farms.

The aim of this thesis is to investigate the possibility of exchanging a fish net, at an operational fish farm, with a newly proposed closed fish cage concept without altering the existing mooring system. The benefit will be reduced downtime and expenditure during setup, since there is no need to install a new mooring system.

A conventional fish net is analyzed to obtain comparable results to that of the fish cage, with identical mooring used by both systems. A numerical, and a simplified analytical method is used. AquaSim, which is a finite element analysis software, is used to perform the numerical comparison of both systems exposed to regular waves, while an analytical approach is used to derive static values, such as; wave and current forces, and static mooring line data. The focus is on mooring line loads, since these loads would be the governing factor regarding the interchangeability.

Drag loads of the fish net with varying amounts of marine fouling are calculated. The results show that there is an approximately linear increase in drag loads for current velocities between 0 m/s and 1,5 m/s. These drag loads are compared to the estimated loads of the fish cage, calculated by hand and through AquaSim.

By introducing a combination of waves and current in the numerical analysis, the results shows that the wave loads are within the same range for both solutions. The results also show that the mooring line loads are dominated by current forces, even for the largest wave conditions. Addi-

tionally, the results related to the fish net are higher than that of the fish cage for all simulated conditions, suggesting that it would be possible to exchange the fish net with the closed fish cage.

Although the simulations converge, there is some uncertainty related to the validity of the values obtained in the simulation of the fish cage, when exposed to the largest wave conditions. The fish cage picks up a slight rolling motion, and waves overtops the upper part of the structure on one side only, resulting in an unloading of the mooring lines, located in the direction opposite of the waves propagation. A comparison to experimental results obtained through model testing would be beneficial, but are not included since no experimental data is available.

Acknowledgment

This master thesis is written during the spring of 2017, as part of my studies for a Master of Science degree in Offshore Technology at the University of Stavanger.

I would like to thank my supervisor, Professor Ove Tobias Gudmestad for his support, interesting points of view, and the valuable contributions during our meetings. His knowledge and passion for this field of engineering has been an inspiration. Furthermore, I would like to thank Aquastructure for providing me with the AquaSim software package, that made this thesis possible. Ole Chr. Wroldsen, from Aquastructure, for his advice and clarification regarding problems related to the AquaSim software package, which made the program much easier to comprehend.

I would also like to thank my fellow students, for the valuable motivation, discussions, and feedback throughout the working period of this thesis. And finally, I would like to thank my family for their continuous support during my education.

Jørgen Andresen

Stavanger, 15th June 2017

Contents

Abstract	iv
Acknowledgment	vii
Nomenclature	xvi
1 Introduction	1
1.1 Background	2
1.2 Scope	3
1.3 Limitations	3
1.4 Methodology	4
1.5 Structure of the Report	5
2 The Fully Enclosed Egg Concept	7
2.1 The Cage	8
2.2 Water Circulation	8
2.3 Feeding Tube	9
2.4 Collection of Waste	10
2.5 Mooring	11
3 Theory	13
3.1 Important Assumptions	13
3.2 Potential Function	14
3.3 Dispersion Relation	16
3.4 Wave Theory Regimes	17
3.5 Morison Equation	18

3.6	Wave Loads on Large Structures	19
3.6.1	Diffraction Theory	20
3.6.2	Wave Loads on Floating Cylinders	24
3.6.3	Floating Dock Approximation	25
3.7	Drag Force	26
3.7.1	Drag Coefficient	28
3.8	Response Amplitude Operator	28
3.9	Mooring System	30
3.9.1	Equipment	30
3.9.2	Mooring Systems for Fish Farms	34
3.9.3	Catenary Mooring	35
3.10	Dynamic Mooring Motions	37
3.10.1	Loading Mechanisms	38
3.10.2	Dynamic Analysis	39
3.11	Solidity and Marine Growth	41
3.12	Net Membrane Elements in AquaSim	42
3.13	Dense Net Membrane Elements in AquaSim	43
4	Simulation Modelling	45
4.1	Genie and HydroD	45
4.1.1	Modelling in Genie	45
4.1.2	Setup in HydroD	46
4.2	AquaSim	47
4.2.1	Modelling of Fish Net	47
4.2.2	Modelling of Fish Cage	49
4.2.3	Modelling of the Mooring System	51
4.3	Drag Comparison	53

5 Results	55
5.1 Wave Force Calculations	55
5.1.1 Wave Parameteres	56
5.1.2 Diffraction Force	57
5.2 Drag Calculations	60
5.2.1 Drag Coefficient	60
5.2.2 Drag Force	61
5.3 RAO Estimation	63
5.3.1 Coarse Frequency Step	63
5.3.2 Refined Frequency Step With Coarse Mesh	64
5.3.3 Refined Frequency Step With Fine Mesh	65
5.4 Static Mooring Calculations	66
5.5 AquaSim	67
5.5.1 Static Mooring Analysis	69
5.5.2 Drag Comparison of Fish Net and Fish Cage Models	70
5.5.3 Mooring Analysis of Fish Net	73
5.5.4 Mooring Analysis of Fish Cage	78
5.5.5 Comparison of Mooring Analysis of Fish Net and Fish Cage	84
6 Conclusions	89
7 Further Work	91
Bibliography	92
A Environmental Classification	97
A.1 Wave parameters	97
A.2 Current parameters	97
B Wave Forces by Chadwick et al. (2010)	98

C Fish Net Deformation in Varying Current	99
C.1 Sinker tube weight 78 kg/m	99
C.2 Sinker tube weight 135 kg/m	100
D AquaSim Material Properties	101
D.1 Material properties for beam elements	101
D.2 Material properties for floater elements in the fish net	101
D.3 Mooring buoy properties	102
D.4 Net properties for fish net	102
D.5 Net properties for dense net	103
D.6 Mooring and bridle line 48mm properties	104
D.7 Anchor chain 36mm properties	104
E Properties for the time domain simulation	105
F Numerical Formulation of Sea Loads to Impermeable Nets	107
G Matlab Functions	115

List of Figures

1.1	World capture fisheries and aquaculture production, (FAO, 2014b)	2
2.1	Egg shaped fish cage concept, (Hauge Aqua, n.d.a)	7
2.2	Internal water circulation concept	9
2.3	Feeding tube	10
2.4	Top view of a typical mooring system	12
3.1	Sinosoidal wave	13
3.2	Wave force regimes, (Chakrabarti, 1987b , p. 323)	18
3.3	Bottom mounted cylinder	20
3.4	Wave diffraction and wave scattering	21
3.5	Inertia coefficient	23
3.6	Phase shift	24
3.7	Floating cylinder	25
3.8	Garret vs Van Oortmerssen approximation, (McCormick, 2010b , p. 322)	26
3.9	Water particles being forced around a cylinder	27
3.10	6 degrees of freedom	29
3.11	Mooring chain, Eiva-Safex (n.d.a)	31
3.12	Fiber rope, Eiva-Safex (n.d.c)	31
3.13	Shackle	31
3.14	Connection plate	32
3.15	Floating buoy	33
3.16	Anchor	33
3.17	Mooring system configuration for fish farms	35

3.18 Catenary profile	36
3.19 Catenary line motions caused by movement at swl	38
3.20 Finite Element Method	40
3.21 Solidity panel	41
3.22 2D view of one mask	41
3.23 Marine fouling of a fish net (Akva-Group, n.d.)	42
4.1 Coarse and fine meshed model	46
4.2 Programs included in the AquaSim package	47
4.3 Floater	48
4.4 Fish net	48
4.5 Lines in the fish net	49
4.6 Fish cage model without floating collar	50
4.7 Further refined fish cage model with floating collar	50
4.8 Composition of one mooring line	51
4.9 Mooring system model	52
4.10 Horizontal drag model for both systems	53
5.1 Essential dimentions	55
5.2 Velocity profile for wave condition nr 2	59
5.3 Cross section	61
5.4 Drag force variation with current velocity	62
5.5 Coarse frequency range	64
5.6 Coarse mesh with refined frequency range	65
5.7 Refined mesh with refined frequency range	66
5.8 Mooring line numbers	68
5.9 Mooring systems with straight mooring lines	69
5.10 Mooring systems at static equilibrium	70

5.11 Close-up of mooring systems at static equilibrium	70
5.12 Drag with sinker tube weight 75 kg/m	72
5.13 Drag with sinker tube weight 135 kg/m	73
5.14 Horizontal length between bouy and floater	74
5.15 Wave condition 1 with fish net	75
5.16 Wave condition 2 with fish net	75
5.17 Wave condition 3 with fish net	76
5.18 Axial force in mooring line 1 for condition 1, waves only	77
5.19 Axial force in mooring line 1 for condition 2, waves only	77
5.20 Axial force in mooring line 1 for condition 3, waves only	77
5.21 Wave condition 1	78
5.22 Wave condition 2	79
5.23 Wave condition 3	79
5.24 Horizontal translation of bridle line connection point	80
5.25 Vertical anchor chain node translation	81
5.26 Axial force in opposite mooring lines	82
5.27 Axial force in mooring line 1 for condition 1, waves only	83
5.28 Axial force in mooring line 1 for condition 2, waves only	83
5.29 Axial force in mooring line 1 for condition 3, waves only	83
5.30 Axial force in mooring line 1 for case 4, 5 , and 6	85
5.31 Axial force in mooring line 1 for case 7, 8 , and 9	87
5.32 Axial force in mooring line 1 for case 10, 11 , and 12	88
C.1 Sinker tube weight, 78 kg/m	99
C.2 Sinker tube weight, 135 kg/m	100

List of Tables

1.1	Wave parameters	4
1.2	Current parameters	4
5.1	Calculated Wave Parameters	57
5.2	Calculated wave forces, McCamy & Fuchs methods	57
5.3	Calculated wave forces, van Oortmerssen method	58
5.4	Cross-sectional areas and drag coefficients	61
5.5	Drag force at different current velocities	62
5.6	Static mooring line calculations	67
5.7	Simulated conditions with parameters	68
B.1	Horizontal wave forces [N] on one cylinder as presented by Chadwick et al. (2010)	98
E.1	Simulated conditions with time domain parameters	105

Nomenclature

Acronyms

3D	Three dimensional
CAD	Computer-aided design
CFD	Computational fluid dynamics
CFSBC	Combined free surface boundary condition
DEG	Degrees
DFSBC	Dynamic free surface boundary condition
DOF	Degrees of freedom
FEM	Finite element method
KC	Kuelegan-Carpenter
KFSBC	Kinematic free surface boundary condition
MF	McCamy & Fuchs
RAO	Response amplitude operator
SWL	Still water line
TDP	Touchdown point

Greek Symbols

α	Phase shift
ω	Angular frequency
ρ	Density
φ	Velocity potential
φ_i	Incoming velocity potential
φ_s	Scattered velocity potential
ξ	Wave amplitude

Latin Letters

a_m	Amplitude of motion
A	Cross sectional area
a	Radius
C_D	Drag coefficient
C_M	Mass coefficient
$C_{d,mem}$	Drag coefficient for a membrane panel
D	Diameter
d	Water depth
F_D	Drag force
g	Gravitational acceleration
H	Horizontal force in mooring
H	Wave height
h	Draft
k	Wave number
L_y	Net mask width
L_z	Net mask height
L	Projected floor length in mooring
L	Wave length
S_n	Solidity
s	Total mooring line length
T_p	Wave period
T	Total tension
t	Time
U	Velocity
V	Vertical tension
W	Submerged mooring line weight

This page is intentionally left blank.

1. Introduction

In the recent years, there have been a huge growth in the aquaculture industry in Norway ([Miljøstatus, 2015](#)). As a response to market demands, the industry has resolved to a solution of increasing the numbers of fish in the existing fish cages. However, the open fish nets are vulnerable to damage which can result in the fish escaping the fish net. As a response to the problem of escape, there have been conducted several studies on new concepts to reduce this risk, while increasing the production capacity ([Rosten et al., 2011](#)). The government of 2015 has proposed some development concessions, which can be granted to promising new concepts. The idea is to trigger the development of new technical solutions regarding the known problems of the open fish nets often seen in the industry today ([Fiskeridirektoratet, 2016](#)). A closed structure can be a great approach regarding some, if not all of the problems in the aquaculture industry. Problems such as fish welfare, risk of escape, impact of fish faeces from the different locations, and of course salmon lice.

One of the new concepts for a closed fish cage design is “The Egg”, which is a concept developed by Hauge Aqua ([Hauge Aqua, n.d.b](#)). The structure is a closed egg shaped fish cage, produced in composite material. Compared to traditional fish nets comprising a floating collar with a suspended net beneath the water surface, the egg shaped fish cage is a completely new design that addresses many of the problems associated with the nets. This paper will investigate the mooring line loads that are exerted on the system by the hydrodynamic loads of the design, and the possibility of utilizing the existing mooring solutions for the fish nets, which it seeks to replace. In addition, a general introduction to the concept will be given to highlight the potential benefits and challenges associated with this solution.

1.1 Background

Norway is currently the number one producer of Atlantic salmon with a market share of 53 percent while Chile, being the second largest producer, is at a mere 25 percent ([Laksefakta, n.d.](#)). This is a remarkable achievement for such a small country, and the business in Norway is expanding rapidly.

The experienced demand for higher production rates of fish is a result of the increasing need for a stable and sustainable food supply. At the same time, marine capture fisheries experiences that the fish is harder to find, and it looks like the sea might be depleted to some extent. The only alternative, if we want to increase the amount of seafood, is aquaculture. As a result, the annual increase for the last five decades have been around 3,2 percent. Figure 1.1 illustrates the global fish production from 1950 to 2012. This graph also indicates that the capture production has reached its limits, and are now stagnating at its current level ([FAO, 2014a](#)).

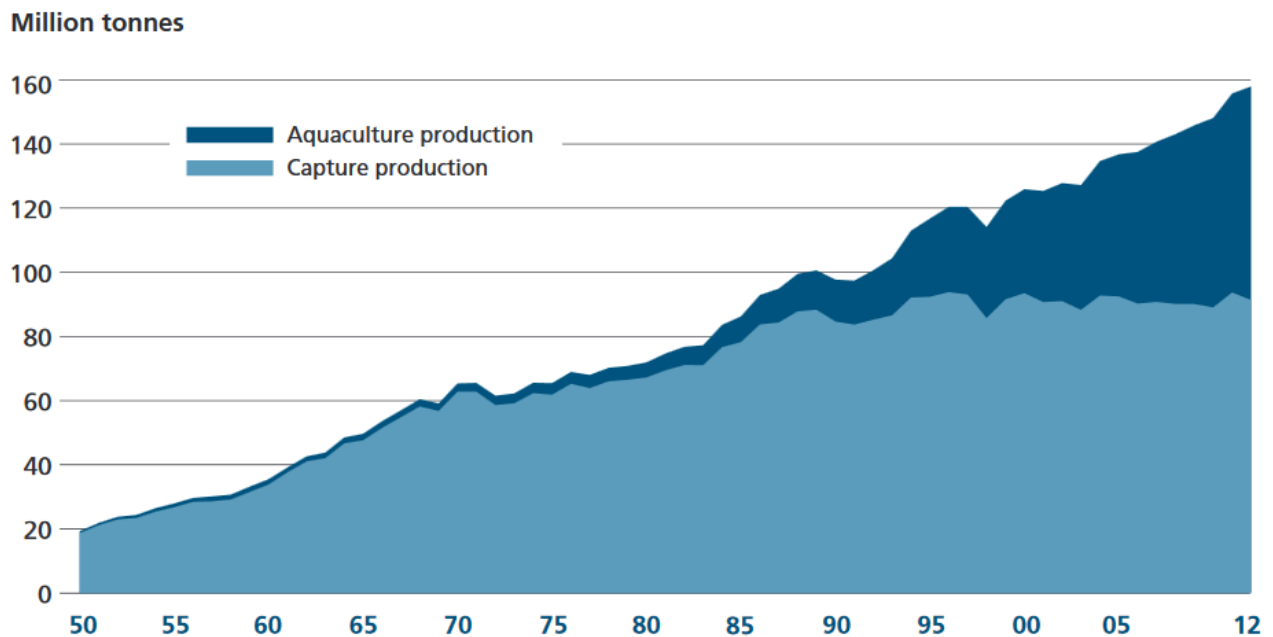


Figure 1.1: World capture fisheries and aquaculture production, ([FAO, 2014b](#))

1.2 Scope

In this Thesis, a concept for a closed fish cage are investigated through a combination of both analytical and numerical simulations. The objective of the thesis is to derive the mooring forces in two identical mooring systems, with a fish net and the fish cage. This analysis will make it possible to check whether the new fish cage can use the existing mooring system, originally designed for the fish net on a location of interest. The environmental conditions will be a combination of both current and waves. Mooring forces are calculated with input from the results of the wave and current analysis. Both a static analysis and a software analysis are performed. The static analysis serves as a good basis for the more demanding dynamic simulation, and presents the theoretical formulations for such calculations. The dynamic mooring simulations were performed with a software called AquaSim ([Aquastructures, n.d.](#)), which made it possible to determine the resulting loads in the mooring system.

1.3 Limitations

This thesis does not account for the motion of the internal water flow during the analysis, as well as the associated intake tubes that are suspended from the bottom of the egg. While the mass of the internal volume is still included in the calculations, even though the circulation is neglected. Waves are only calculated from one direction, and only one mooring system configuration was considered. Furthermore, a predefined set of wave and current conditions were set to maintain a realistic amount of work during the working period of the thesis. The parameters are chosen according to the classifications in the NS9415 standard ([Standard Norge, 2009](#)) and are defined in tables 1.1 and 1.2. Lastly, both the NYTEK ([Nærings- og fiskeridepartementet, 2011](#)) and NS9415 documents are followed as close as possible, to obtain results that can be related to a non-fictional scenario.

Table 1.1: Wave parameters

Wave height, H [m]	Wave period, T_p [s]
0,5	2
1	3,2
2	5,1

Table 1.2: Current parameters

Current velocity, C_x [m/s]	0,2	0,4	0,6	1	1,5

1.4 Methodology

The thesis uses both an analytical and numerical approach. The analytical approach results in a better understanding of the theoretical part regarding wave loads on large structures and the static mooring line calculations. However, it is more challenging to work with formulas for dynamic systems and the simulation software AquaSim was used to calculate the dynamic behavior, and dynamic mooring forces for both the fish net and the closed fish cage. An additional approach could have been to execute some model testing in a towing tank, but this was not an option. The sea states are chosen in accordance to classifications in the NS9415 standard to maintain relevance to a real certification procedure.

1.5 Structure of the Report

Chapter 2 presents the concept in detail and discusses some of the most important challenges and advantages of this particular system, and also includes a brief introduction to fish farm mooring systems.

Chapter 3 describes the necessary theory to be able to execute the hand calculations of interest. This includes wave theory for large structures, drag calculations, catenary mooring line theory and lastly it describes the finite element approach of the computer program AquaSim.

Chapter 4 includes the modelling method in Genie and Hydro D, associated with the estimation of the RAOs of the system. It also explains the modelling procedure of the fish net, fish cage, and the associated mooring system in Aquasim.

Chapter 5 presents the calculated and simulated results. This includes static mooring line analysis and results of the mooring system analysis performed in AquaSim. A comparison study of the different results, and a comprehensive discussion of their validity were carried out.

Chapter 6 concludes the results of the initial problem regarding the interchangeability of the fish containment systems within the same mooring system.

Chapter 7 outlines suggestions for further studies of the problem.

This page is intentionally left blank.

2. The Fully Enclosed Egg Concept

The egg concept in figure 2.1 is a large rigid containment tank built to replace the existing open fish nets that are commonly found in fish farms. Some of the biggest concerns in association with today's operation of fish farms is related to; escape, fish lice, predators, high risk operations and loss of stock due to death. In 2016, the Directorate of Fisheries registered 126 000 escaped salmon and in 2015 the numbers were even higher, at 170 000 salmon. Of all the 109 events for all types of fish that was reported in 2015, 27% were related to structural failure which lead to the escape of 160 000 fish. 42% were due to operational faults and the resulting number of escaped fish were 82 000 ([Fiskeridirektoratet, 2015](#)). A more robust structure that is easier to operate will clearly benefit the industry based on these statistics, as a majority of the incidents are connected to structural failure.



Figure 2.1: Egg shaped fish cage concept, ([Hauge Aqua, n.d.a](#))

2.1 The Cage

The walls of the egg are going to be constructed from composite materials (Hauge Aqua, n.d.b). The physical properties of a composites sandwich panel give the structure an extremely high stiffness and great impact strength. A buoyancy element, protruding through the still water line (SWL), will be added to the upper external part of the egg to ensure that the structure have enough buoyancy and stability. The buoyancy collar will act as a protection barrier from possible external impacts in the SWL, as well as being the holding tank for the collected biological waste material. The dome of the egg that is visible above the SWL provides shelter for the operators in cases where they have to be present while performing tasks on the structure. The effect is a reduction in risk for the operators in comparison to the exposed, small walkway around the collar on a conventional floating fish net.

2.2 Water Circulation

Another new and unique feature of this new concept is the proposed management of the water flow. The egg has two inlet tubes reaching several meters down beneath the still water line. At deeper depths, the water temperature is more stable, as well as being below the depth where salmon lice, *Lepeophtheirus salmonis*, is found to exist (Johnsen et al., 2014). At these depths, there is a more constant temperature which is thought to yield a faster growth, especially through the cold winter months. The water is sucked into the cage through these tubes and travels up and out of a set of outlets in the buoyancy collar (Hauge Aqua, n.d.b). The principle is shown in figure 2.2. These outlets might expose the system to salmon lice, as there have to be openings near the SWL. Protective measures are necessary to avoid contamination inside the cage, because of the higher density of salmon lice in water depths down to approximately 10m(Johnsen et al., 2014).

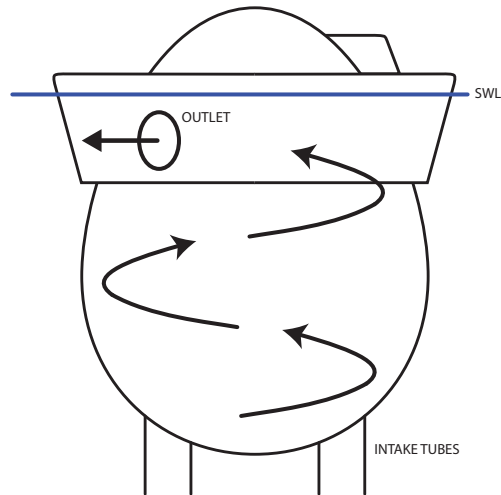


Figure 2.2: Internal water circulation concept

2.3 Feeding Tube

This concept also uses a new approach regarding the way of operating the feeding system. Instead of spreading the food pellets on the water surface with a turret like it is done with current standards, one wishes to inject the pellets through a vertical tube inside the egg, seen in figure 2.3. By doing this in combination with the swirling circulation of water inside, one can distribute the pellets more evenly. Two injectors ports are planned, and they are placed at different heights inside the cage to allow for a more even distribution of food throughout the height of the egg.

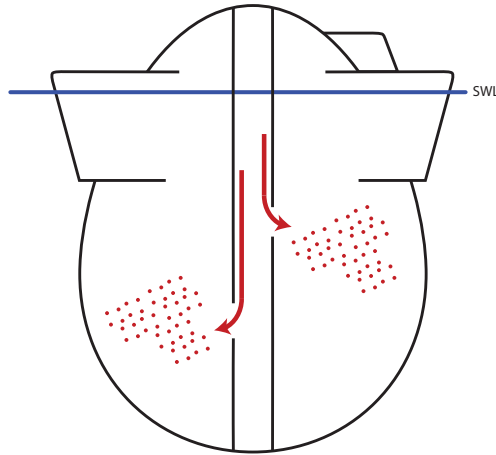


Figure 2.3: Feeding tube

However, an investigation regarding the buoyancy of the pellets would be beneficial to ensure maximum effect of the system, and to see how it compares to possible fish faeces. The solution in combination with the closed walls, also contributes to a reduction of food loss, as the pellets can't sink through the walls that enclose the cage, which results in smaller operational costs for the contractors. Another benefit of the vertical tube, is that it stiffens off the structure in the vertical direction.

2.4 Collection of Waste

All closed fish cages need a way of managing the natural generation of fish faeces to avoid unwanted build up in the bottom of the containment chamber. The proposed solution is to use the internal up-flow of the intake water to trap the particles of faeces in a circular holding tank inside the buoyancy collar, seen in figure 2.1. The collected waste material is planned to be extracted and used as a valuable resource, adding to the profitability of the facility. A possible area of use for the collected waste, is as bio-fuel to generate electricity to power the fish farm. Another possibility is to use the waste material as fertiliser in agriculture.

A questionable aspect of this method of waste collection is the fact that the fish have to swim in a swirl of its own faeces as it travels upward towards the holding tanks in the floating collar. Since this is an unproved concept, it remains to be seen, but methods to separate the injected food pellets from the faeces need to be established, and fish welfare must be taken into consideration. With the presence of the vertical tube already being established, one could try to incorporate a vacuum system to remove faeces from the bottom of the cage. This approach assumes that the faeces have negative buoyancy and will fall to the bottom of the cage, independent of the internal flow in the cage.

2.5 Mooring

The egg concept seeks to be a direct replacement for the existing open fish nets. The way a fish net is positioned is by a complex mooring system that uses a combination of anchors and anchor lines that are placed in a certain way around the fish net.

The environmental loads exerted on the closed cage must be compared to those of a fish net, to investigate if it is possible to use the existing mooring system for the new closed fish cage. If the loads are found to be within specifications, the benefit will offer a huge reduction in installation cost, and the exchange of a fish net with a closed cage can be performed in few days.

The system uses a suspended rectangle from 4 floating buoys, marked as yellow circles in figure 2.4. The buoys are designed to take the vertical force of the submerged anchor line. From the corners of the rectangle, bridle lines are attached to the fish cage to distribute the load as well as preventing yaw and horizontal displacement. The anchor lines themselves aren't directly connected to the fish cage, but they are attached to shackles and connection plates at each corner of the rectangle. The system components will be further explained in chapter 3.9.

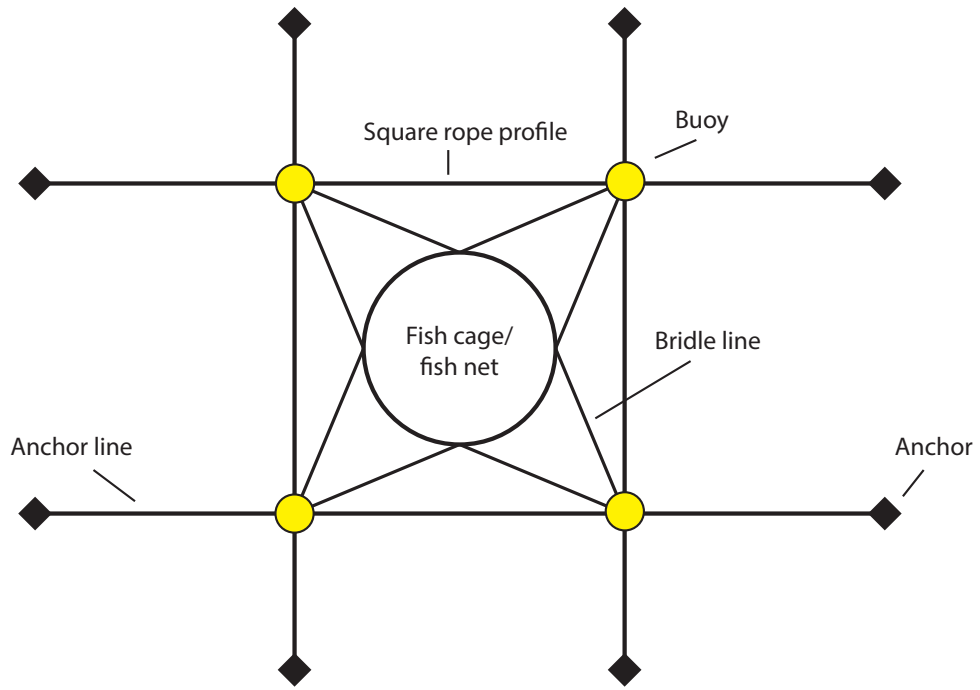


Figure 2.4: Top view of a typical mooring system

3. Theory

This Thesis uses linear wave theory throughout all the calculations, but in order to use such an approach there are certain requirements and assumptions that need to be taken into account. The simplifications and equations that are presented here are based on those presented by (Sarpkaya, 2010), and are presented due to their essentiality. In linear wave theory, the wave profile is of sinusoidal type. ξ denotes the surface elevation. At SWL the z coordinate is at 0, while the z coordinate is < 0 all the way down to the bottom at, $-d$.

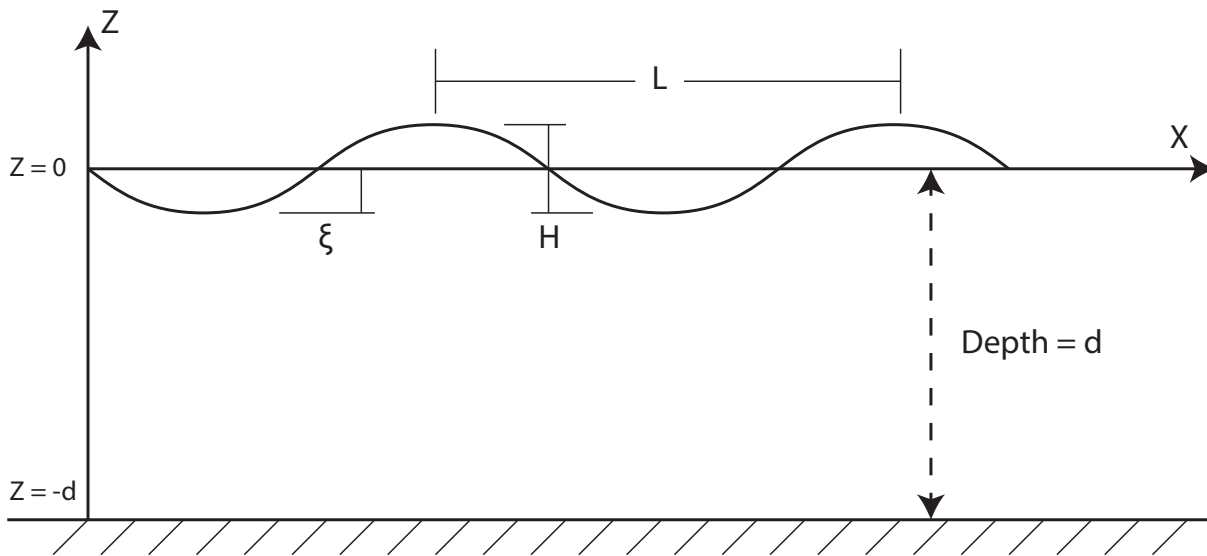


Figure 3.1: Sinosoidal wave

3.1 Important Assumptions

First, we assume that the flow is incompressible. This is a good approximation for water and is expressed in equation 3.2, where \vec{U} is the velocity vector in x -, y - and z -direction.

$$\frac{D\rho}{Dt} + \rho \left(\frac{\partial u}{\partial x} + \frac{\partial v}{\partial y} + \frac{\partial w}{\partial z} \right) \quad (3.1)$$

$$\frac{D\rho}{Dt} + \rho \nabla \cdot \vec{U} = 0 \quad (3.2)$$

$$\nabla \cdot \vec{U} = 0 \quad (3.3)$$

Furthermore, the flow is assumed to be non-rotational, which means that there are no shear forces acting between the water particles making it a frictionless flow. The equation expressing the non-rotational property of the flow can be seen in equation 3.4

$$\nabla \times \vec{U} = 0 \quad (3.4)$$

The last of the three most vital expressions is the Laplace differential equation of second order. φ , denotes the velocity potential, and will be investigated further in the next subsection.

$$\frac{\partial^2 \varphi}{\partial x^2} + \frac{\partial^2 \varphi}{\partial z^2} \quad (3.5)$$

3.2 Potential Function

With the definition of these three equations it is now possible to find the velocity potential function expressed by, $\varphi(x, y, z, t)$. Taking the derivative of φ with respect to direction, yields the property of the flow underneath the wave, such as velocity and acceleration. When the accelerations are found, we can find the forces. In order to get an expression for the velocity potential,

the solution for the second order Laplace equation have to be found. To do this, we establish three important boundary conditions.

Bottom boundary condition, no water can flow through the bottom, assuming a flat bottom.

$$\frac{\partial \varphi}{\partial z} = 0 \quad \text{at } z = 0 \quad (3.6)$$

Kinematic free surface boundary condition (KFSBC), a water particle at the free surface will always stay at the free surface.

$$\frac{\partial \xi}{\partial t} + \frac{\partial \varphi}{\partial x} \frac{\partial \xi}{\partial x} - \frac{\partial \varphi}{\partial z} = 0 \quad \text{at } z = \xi \quad (3.7)$$

Dynamic free surface boundary condition (DFSBC), the pressure at the free surface is constant and equal to the atmospheric pressure.

$$\frac{\partial \varphi}{\partial t} + \frac{1}{2} \left[\left(\frac{\partial \varphi}{\partial x} \right)^2 + \left(\frac{\partial \varphi}{\partial z} \right)^2 \right] + g\xi = f(t) \quad \text{at } z = \xi \quad (3.8)$$

The solution to these equations are very complex and we use the assumption of small wave amplitude theory. That is, H is smaller than L and d , and we disregard the nonlinear terms. By linearization we evaluate the equations at $z = 0$ and equation 3.7 and 3.8 reduces to

$$\frac{\partial \varphi}{\partial z} - \frac{\partial \xi}{\partial t} = 0 \quad \text{at } z = 0 \quad (3.9)$$

$$\frac{\partial \varphi}{\partial t} + g\xi = 0 \quad \text{at } z = 0 \quad (3.10)$$

A combination of the DFSBC and the KFSBC, known as the combined free surface boundary

condition (CFSBC) is expressed in equation 3.11:

$$\frac{\partial^2 \varphi}{\partial t^2} + g \frac{\partial \varphi}{\partial t} = 0 \quad \text{at } z = 0 \quad (3.11)$$

By solving the Laplace equation with these boundary conditions the velocity potential φ can be found. The procedure is quite complex and is not included here. The result of the mathematical process is the two-dimensional linearized potential function 3.12. k is the wave number, ξ is the wave amplitude, ω is the angular frequency, and x is the horizontal position of the wave propagation.

$$\varphi(x, y, z, t) = \frac{\xi g \cosh[k(z + d)]}{\omega \cosh(kd)} \sin(\omega t - kx) \quad (3.12)$$

3.3 Dispersion Relation

The dispersion relation is an important relation between wave length, L , and wave period T . The relation is expressed by substituting the first order velocity potential into the CFSBC (3.11) (Chakrabarti, 1987a). The result is known as the dispersion relation, as expressed in equation 3.13. By manipulating equation 3.13 we can get an expression for wave length, L eq(3.14), which is an essential parameter regarding wave loads.

$$\omega^2 = gk \tanh(kd) \quad (3.13)$$

$$L = \frac{g}{2\pi} T^2 \tanh(kd) \quad (3.14)$$

The k value represents the wave number, being a parameter that needs iterations in order to be calculated properly. The process can be very demanding if no computer programs are to be used. However, Matlab have a built-in solver to tackle such tasks, and it will be used later in the calculations with a custom function. There are also some simplifications to be made, depending on the condition of the water depth. In deep waters, we can simplify the both equation, which yields two new and simplified equations.

Since the NS 9415 standard only specify H and T_p , in conjunction to the classification, the wave length had to be calculated for the different wave conditions to be examined. The dispersion relation was used to calculate the wave number k .

3.4 Wave Theory Regimes

[Chakrabarti \(1987a\)](#) created the chart shown in figure 3.2, to decide what type of wave theory that is applicable in different conditions, depending on the Keulegan–Carpenter number, KC eq (3.15), and $\pi D/L$, alternatively expressed as ka . Both $\pi D/L$ and the KC number are parameters used to classify wave force regimes. KC is often expressed as $\pi H/D$ when considering deep water, and this Thesis assumes non-breaking waves which is part of the linearization. As observed in the graph, the diffraction region is valid if $\pi D/L > 0,5$. For values of $\pi D/L < 0,5$, we are in the regime where the Morison equation is applicable.

$$KC = \frac{u_0 T}{D} \quad (3.15)$$

$$KC = \frac{\pi H}{D} \quad (3.16)$$

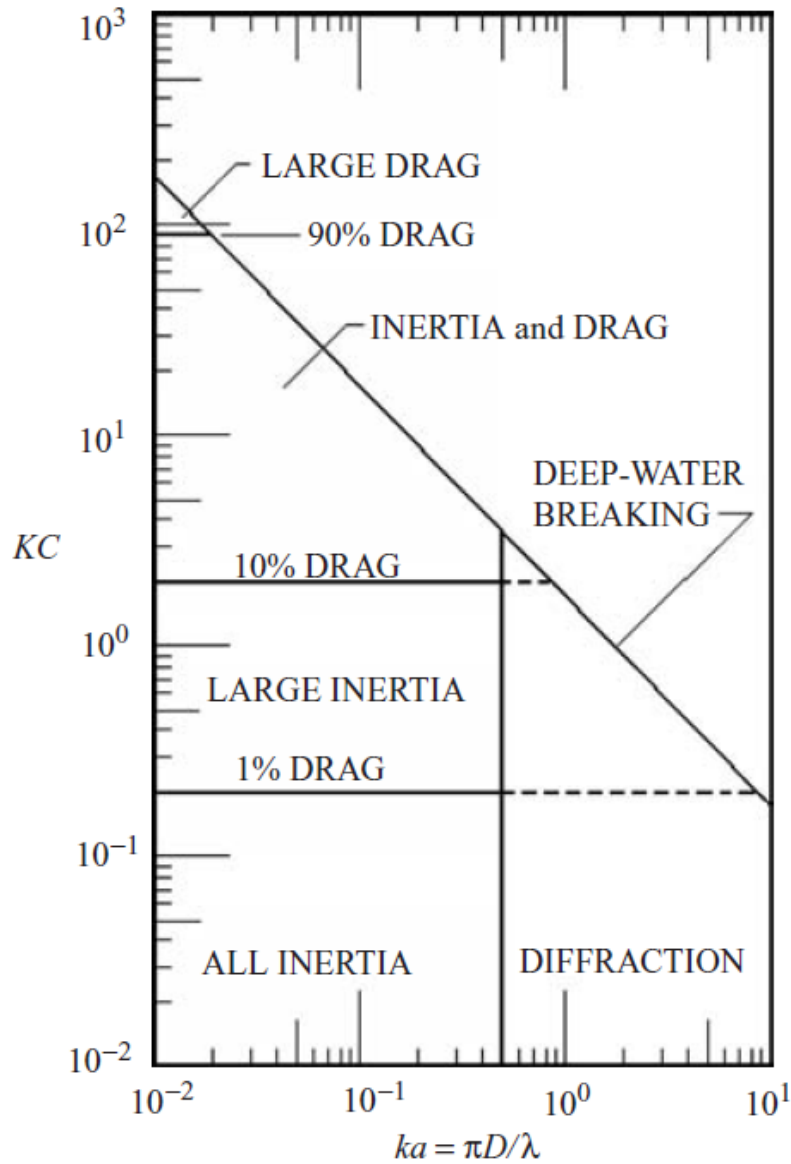


Figure 3.2: Wave force regimes, (Chakrabarti, 1987b, p. 323)

3.5 Morison Equation

The Morison equation (Morison et al., 1950) is one of the most widely used approaches for calculation wave loads in the case of a rigid circular cylinder exposed to oscillating waves. It comprises a combination of inertial and drag forces, as shown in equation 3.17, where F is the force

acting on a unit length of the body.

$$F = \frac{\pi D^2}{4} \rho C_M \dot{u} + \frac{1}{2} \rho C_D D u |u| \quad (3.17)$$

C_M and C_D are coefficients for mass and drag found from experiments, whereas u and \dot{u} are given respectively, as velocity and acceleration under the wave crest. D represents the diameter of the cylinder and ρ is the water density. However, there are limitations to the applicability of this formula which needs to be checked, considering the definition of slender elements.

In order to use the Morison's equation, the acceleration over the surface of the cylinder cannot change too much, reflected in the criteria, $D/L < 0,2$ (Faltinsen, 1990). Since the fish cage is 19 meters in diameter we have to assume that the structure cannot be considered as a slender element, since the ratio in the region of interest would exceed the criteria. Other methods have to be used to give a satisfactory result. Furthermore the amplitude of motion of the cylinder should not exceed the criteria, $a_m/D < 0,2$.

3.6 Wave Loads on Large Structures

Since the structure is considered to be of a large diameter, the Morison equation isn't applicable in the calculations of the wave loads on the closed fish cage. As a result, different methods regarding reflections and other effects behind the structure have to be explored. One of the most commonly used theories is that of McCamy and Fuchs (1954) (MF). The theory established the forces on a large, surface piercing cylinder, submerged in an ideal fluid, where the velocity potential, φ , is known to exist.

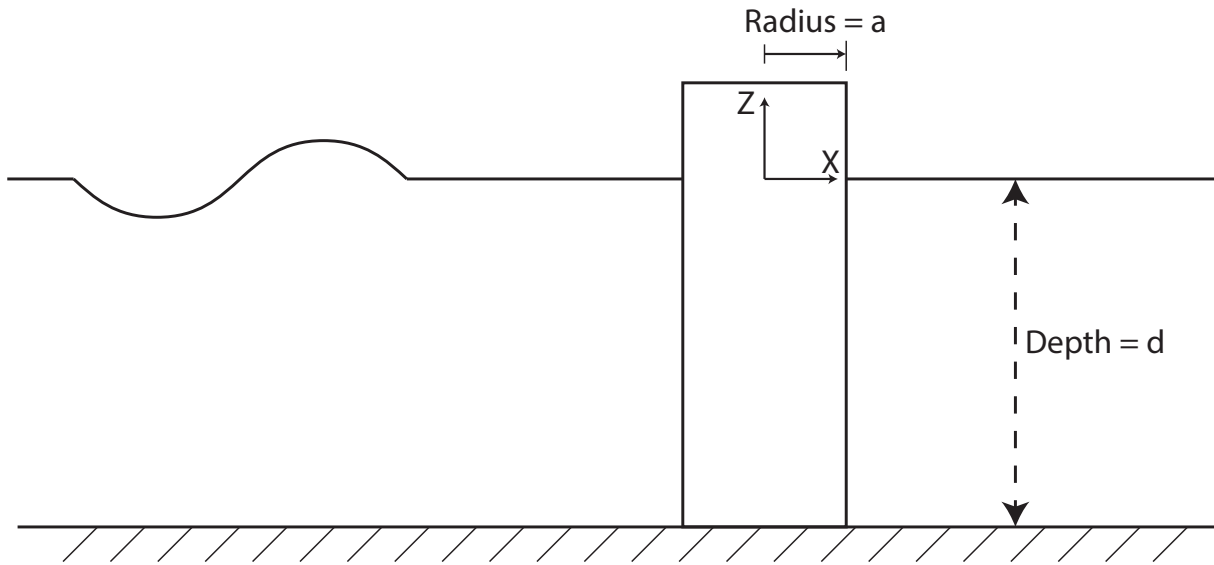


Figure 3.3: Bottom mounted cylinder

3.6.1 Diffraction Theory

The diffraction theory introduces a combined velocity potential, where φ is expressed as the sum of the potential of the incoming wave φ_i , and the scattered wave potential φ_s . The incident wave will get reflected outward as it impacts on the cylinder. Furthermore, the wave will get bent around the cylinder on the leeward side of the flow, which is known as diffraction. The combined effect of both the reflection and diffraction of the incident waves are known as wave scattering (Sumer and Fredsøe, 1997). The principle of this theory is illustrated in a very simplified manner in figure 3.4.

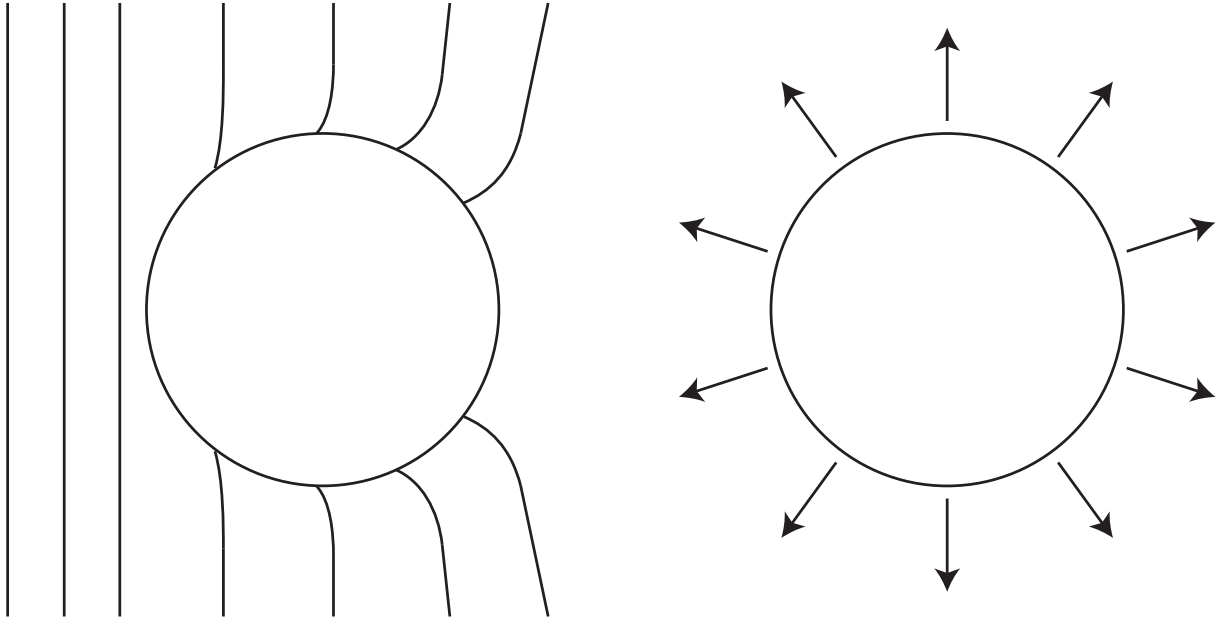


Figure 3.4: Wave diffraction and wave scattering

When we know the incoming potential, we can find the pressure. The pressure is expressed with the linearized Bernoulli equation 3.18, which describes the pressure variation in a fluid. The hydrostatic pressure is expressed as $\rho g z$ and changes with depth. The dynamic pressure is expressed as $\rho \frac{\partial \phi}{\partial t}$ and changes with the presence of waves.

$$P = -\rho g z - \rho \frac{\partial \phi}{\partial t} \quad (3.18)$$

With the equation for pressure being established, the result can be used to calculate the force.

$$F_z = \int_0^{2\pi} P \cos \theta d\theta \quad (3.19)$$

Integration of equation 3.19 represents the component of the force acting in the x-direction on the cylinder per unit length in the z-direction at depth z.

$$F_z = \frac{2\rho g H}{k} \frac{\cosh[k(z+d)]}{\cosh(kd)} A \left(\pi \frac{D}{L} \right) \cos(\omega t - \alpha) \quad (3.20)$$

Where:

$$\tan \alpha = \frac{J_1' \left(\pi \frac{D}{L} \right)}{Y_1' \left(\pi \frac{D}{L} \right)}$$

$$A \left(\pi \frac{D}{L} \right) = \frac{1}{\sqrt{J_1'^2 \left(\pi \frac{D}{L} \right) + Y_1'^2 \left(\pi \frac{D}{L} \right)}}$$

J_1 and Y_1 are Bessel function of first kind, with $\pi D/L$ as the argument. While J_1' and Y_1' are the first derivative of the same function. Alternatively, equation 3.20 can be expressed with C_M resulting in the following expression (Sarpkaya and Isaacson, 1981):

$$F_z = \frac{\pi}{8} \rho g H k D^2 \frac{\cosh[k(z+d)]}{\cosh(kd)} C_M \cos(\omega t - \alpha) \quad (3.21)$$

C_M is a complex mathematical term, as expressed in equation 3.22, and depends on the relation D/L (Sarpkaya and Isaacson, 1981). Matlab was used to produce the resulting graph in figure 3.5, which illustrates how C_M changes with different values of D/L . It is interesting to observe how the values are about the same for small values, ($< 0,2$) of D/L , and how they drop rapidly when the ratio increases in magnitude.

$$C_M = \frac{4A \left(\pi \frac{D}{L} \right)}{\pi \left(\pi \frac{D}{L} \right)^2} \quad (3.22)$$

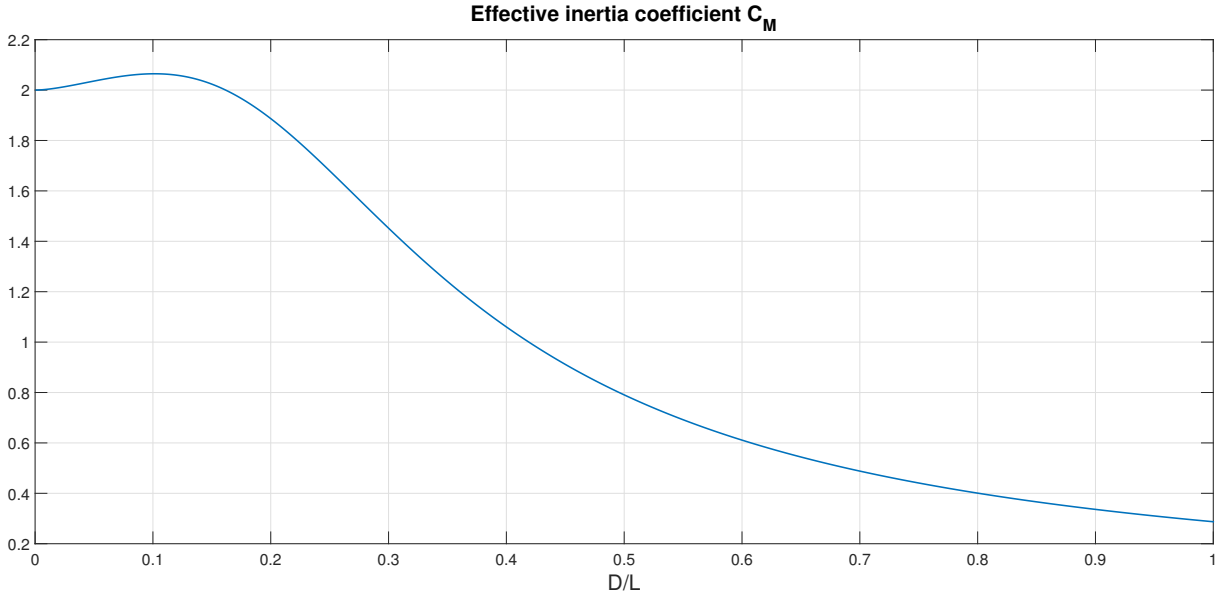


Figure 3.5: Inertia coefficient

The other constant, being α , is also dependent on the same Bessel functions and was calculated in Matlab. Alpha represent the phase shift that occurs when the wave passes over the surface of the cylinder, and provide a shift to the amplitude of the total horizontal force due to the diffraction effects behind the cylinder (Sumer and Fredsøe, 1997). The resulting values of the alpha constant was plotted, and are illustrated in figure 3.6 were D/L is defined from 0 to 1.

$$\alpha = \tan^{-1} \left(\frac{J_1'(\pi \frac{D}{L})}{Y_1'(\pi \frac{D}{L})} \right) \quad (3.23)$$

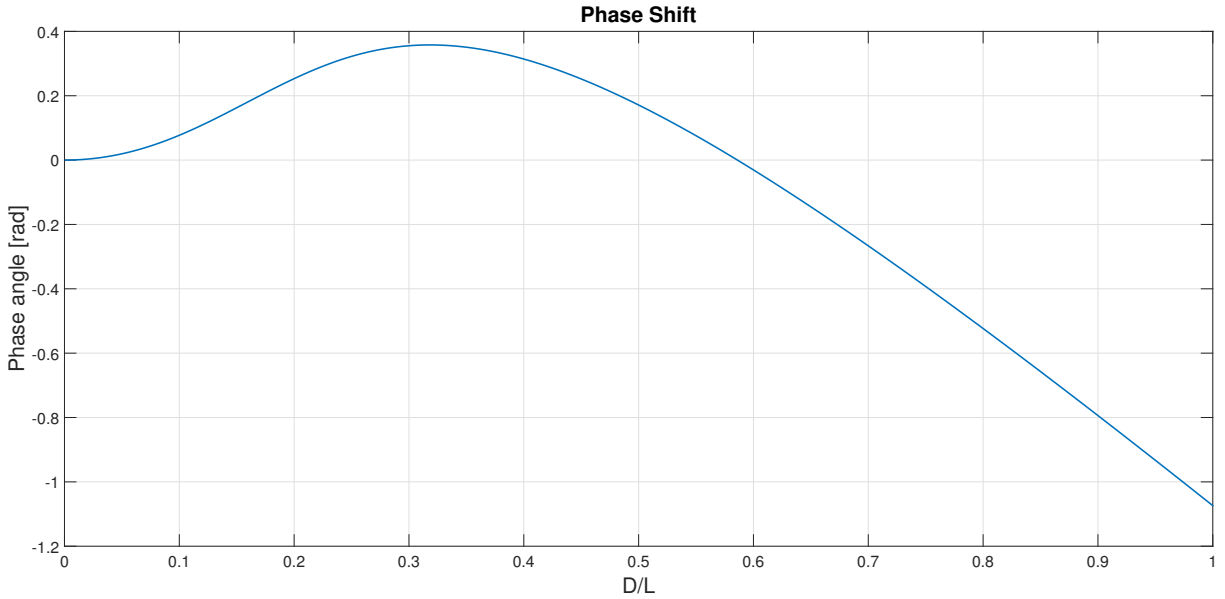


Figure 3.6: Phase shift

To express the total horizontal force, it was just a matter of integrating equation 3.21 over the height of the cylinder resulting in (Chakrabarti, 1987a):

$$F = \frac{\pi}{8} \rho g H D^2 \tanh(kd) C_M \cos(\omega t - \alpha) \quad (3.24)$$

3.6.2 Wave Loads on Floating Cylinders

Wave loads have until now been presented for vertical bottom-mounted surface-piercing cylinders. Since this is not the case for the floating fish cage, there is a need to modify the equations. The adapted equations were first presented by Miles and Gilbert (1968) and further revised by Garrett (1971). The approach is similar to that of a bottom mounted cylinder, and uses the integrated pressure over the surface of the structure. Additionally, a new set of boundary conditions for the flow that passes underneath the structure were established. The method is applicable in infinite water depths and is relevant for a great deal of different cases, and should improve on the diffraction theory since it allows the flow to pass underneath the structure. However, the

mathematical equations are complex and very demanding to solve. Consequently, other methods were investigated and checked for their analytical accuracy, and ease of application.

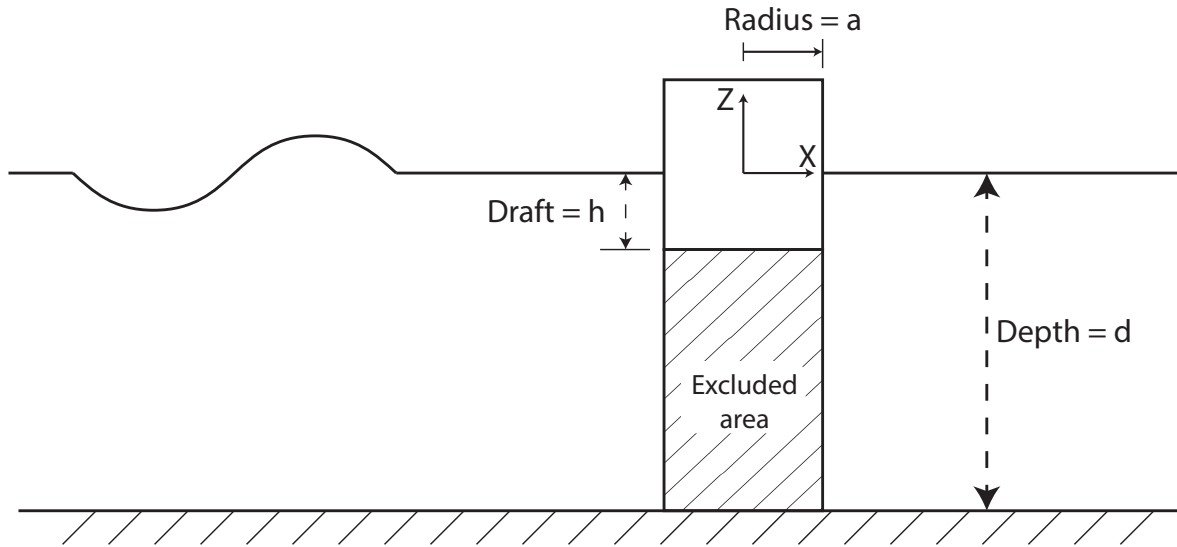


Figure 3.7: Floating cylinder

3.6.3 Floating Dock Approximation

van Oortmerssen (1971) developed a simpler approach based upon a ratio of the diffraction force for a bottom-mounted surface-piercing cylinder, but adapted for a circular dock with draft, h . The ratio is expressed in equation 3.25. While the oscillating horizontal force on a cylinder with draft h , can be approximated by equation 3.26, where F_x denotes the horizontal diffraction force from equation 3.24, for a bottom-mounted cylinder in water depth of d meters.

$$\frac{\sinh(kd) - \sinh(k(d-h))}{\cosh(kd)} \quad (3.25)$$

$$\frac{\sinh(kd) - \sinh(k(d-h))}{\cosh(kd)} \cdot F_x \quad (3.26)$$

This approximation have later been compared to the full Garret solution by [McCormick \(2010a\)](#), who proved that the van Oortmerssen approximation yields accurate results for values of ka above 1. $F(ka)$ is the non-dimensional horizontal force on a cylinder with draft d , radius a , in water depth h . However, van Oortmerssens results, marked with a solid line, overshoots the peak value and return a higher amplitude than the Garret analysis, marked with bullet points, as shown in figure 3.8.

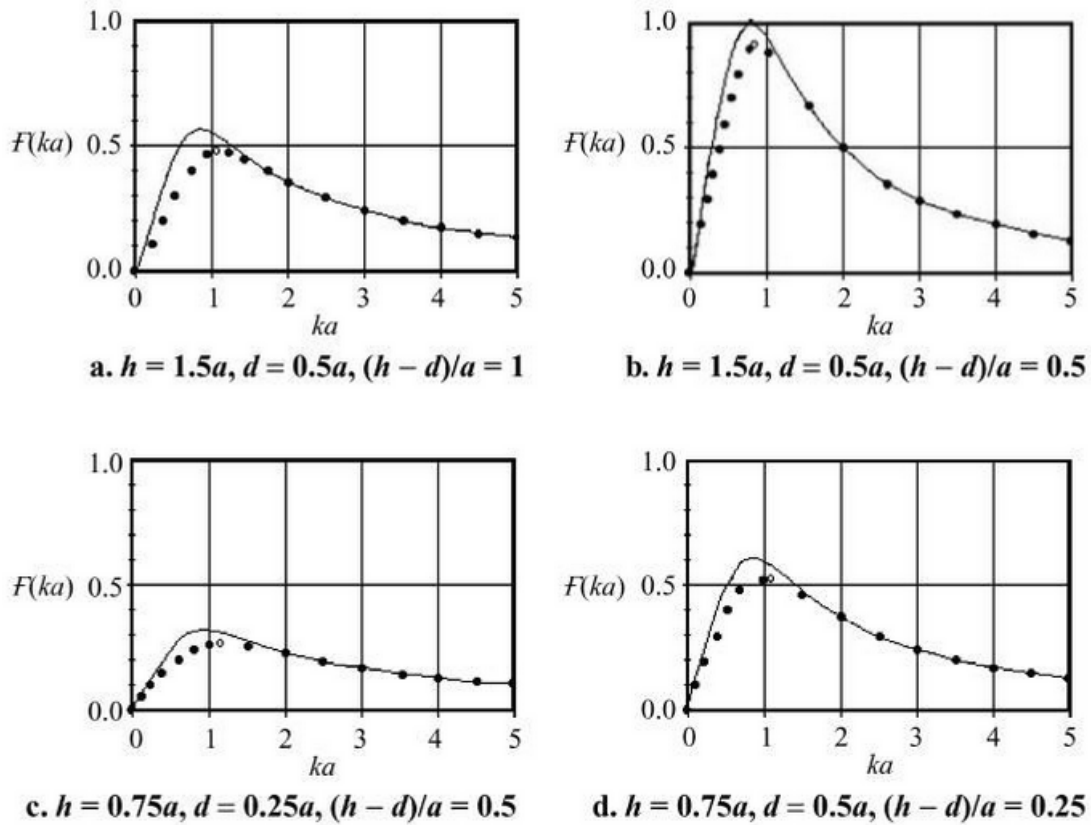


Figure 3.8: Garret vs Van Oortmerssen approximation, ([McCormick, 2010b](#), p. 322)

3.7 Drag Force

A structure submerged in a fluid will experience forces due to the static pressure of the fluid. If the fluid moves, there will also be a force contribution from the dynamic pressure that occurs

when water particles are forced around the structure, as seen in figure 3.9. This force is known as a drag force and is expressed in equation 3.27. In this equation ρ represents the density of the fluid of interest, A is the projected cross-sectional area in the flow direction, C_D is the drag coefficient of the structure, and U is the velocity of the fluid flow (Çengel and Cimbala, 2014).

$$F_D = \frac{1}{2} \rho A C_D U^2 \quad (3.27)$$

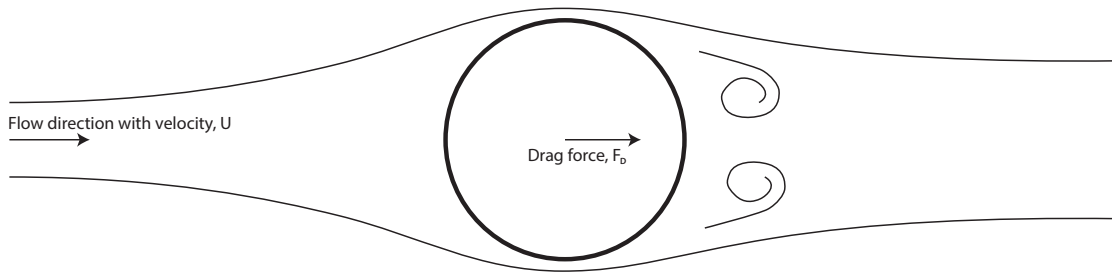


Figure 3.9: Water particles being forced around a cylinder

Such forces on marine structures occur due to the water currents, and can be a large dominant force. Therefore, it is necessary to understand how we can accurately predict these forces. Model tests are a well proven method of establishing the force variation at different velocities. Another possibility is to use computational fluid dynamics (CFD) to model the fluid-structure interactions (Chadwick et al., 2010). CFD could have been used in this thesis to establish such loads and a corresponding drag coefficient, but an estimated drag coefficient were sourced from Çengel and Cimbala (2014), due to the high complexity of such analysis types, and because experimental data obtained through model testing weren't an option.

3.7.1 Drag Coefficient

The drag coefficient, C_D , is a dimensionless number that represents the drag characteristics of the geometry (Çengel and Cimbala, 2014). It is a combination of a pressure coefficient, C_p resulting in a pressure force when integrated over the area of the fish cage. And a viscous coefficient, C_v due to friction at the surface, which is used to calculate the shear force. For large structures, we can neglect this viscous coefficient, C_v since it is only 1 – 3 % of the magnitude in comparison to the pressure coefficient (Faltinsen, 1990).

$$C_D = C_p + C_v \quad (3.28)$$

3.8 Response Amplitude Operator

Until now the fish cage has been considered as fixed in space. In reality, the cage will experience wave induced motions and have 6 degrees of freedom (DOF). For a floating object, these motions are divided into translational and rotational movement. The translational movements will follow the x-, y- and z-axis. The vertical motion is known as heave and is measured on the z-axis. The forward and backward motion are known as surge, and can be measured as displacement along the x-axis. The last movement is sway and is measured as translation along the y-axis. The rotational movement rotates about the same axis. The rotations are: roll, pitch and yaw. Roll is measured as rotation about the surge axis. Pitch is measured as rotation about the sway axis, and yaw is measured as rotation about the heave axis. The DOF with respect to the fish cage can be seen in figure 3.10.

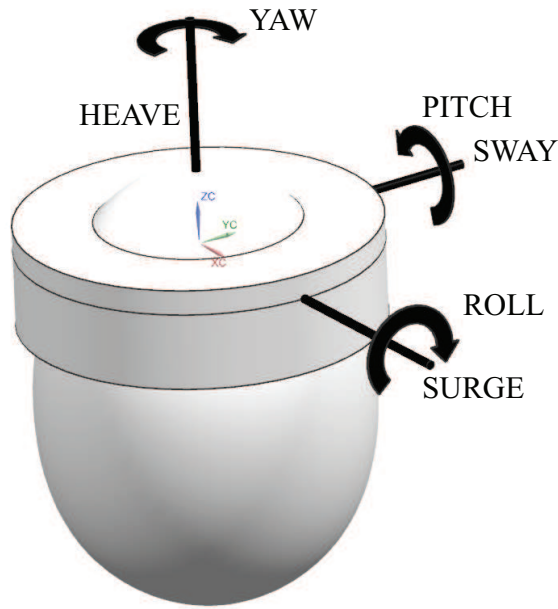


Figure 3.10: 6 degrees of freedom

In ship theory, the notation *response amplitude operator* (RAO) is often used and denotes the ratio between the response amplitude of the variable of interest to one meter of wave amplitude. The RAO of a vessel operates on the frequency spectrum and creates a spectrum of motion response (Bergdahl, 2009). The motion of special interest regarding the fish cage are the heave, which is the vertical motion. The RAOs of the fish cage were investigated to identify the wave frequencies where the response is of highest magnitude. A periodic, vertical translation of the fish cage will produce an oscillating tension force with a higher peak value compared to the static forces in the mooring lines, which is undesired. Consequently, one tries to design the structure or vessel with the peak response outside of the typical sea states experienced on location.

3.9 Mooring System

A catenary mooring system is used to position the fish cage. The system is similar to those used in station keeping for floating offshore structures (Faltinsen, 1990). This chapter presents the equipment involved in the mooring system and the necessary equations and assumptions to perform a static mooring analysis.

3.9.1 Equipment

Since the mooring systems for fish farms shares a lot of its technical features with the offshore equivalent, there is naturally similar components as well. However, there are differences and the next subchapters outline the equipment that are regularly used in fish farm mooring systems.

Mooring lines

The mooring lines themselves are often made of a light chain or a synthetic fibre rope. Figure 3.12 and 3.11 displays a typical fibre rope and a chain configuration. Bridle lines are smaller chains or ropes depending on the system, and connects the fish cage/net to the mooring system. The bridle lines are connected to the four corners of the square robe profile that surrounds the fish cage, and to connections points at the fish cage. The configuration will be explained in greater detail in the next chapter.

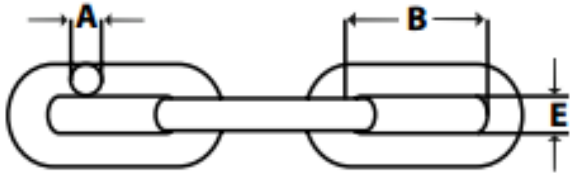


Figure 3.11: Mooring chain, [Eiva-Safex \(n.d.a\)](#)



Figure 3.12: Fiber rope, [Eiva-Safex \(n.d.c\)](#)

Connectors

A typical connector that is being used in mooring systems are shackles. A shackle is a U-shaped metal piece whose main purpose is to provide a strong and reliable connection of two elements in the mooring system. The connector is design to take the maximum breaking load of the mooring lines it connects ([Chakrabarti, 2005](#)). The shackle is secured with a clevis pin or a bolt that closes the profile.



Figure 3.13: Shackle, ([US Cargo Control, n.d.](#))

Connection Plate

The connection plate is a steel plate with holes that connects the ropes in the square rope profile that surrounds the fish cage to the floating buoys at the surface. The plate is submerged at a desired depth of a couple of meters below the SWL. It uses shackles to connect all the different components that are being attached. The hoop on the upper surface connects a rope between a floating buoy at the SWL and the plate itself, keeping it from sinking to the bottom.

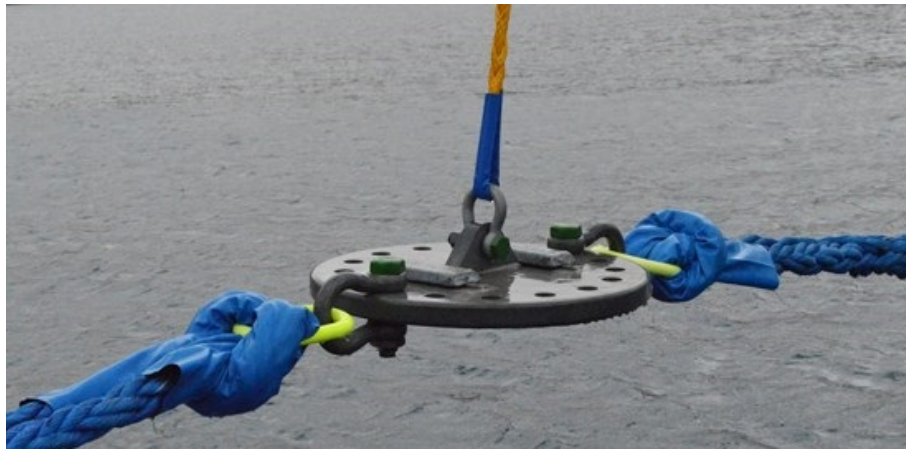


Figure 3.14: Connection plate, (Vónin, n.d.a)

Mooring Buoys

The mooring buoys are a buoyancy element used to manage the vertical forces in the mooring system. They are constructed from the plastic material, polyethylene, and filled with either polystyrene or polyurethane foam, depending on the needs. A continuous chain, or similar structural member, is pulled through the buoy and terminated at each end with a steel plate and a connection point. Sizes vary depending on the buoyancy need of the mooring system (Eiva-Safex, n.d.). A representative cross section can be examined in figure 3.15.

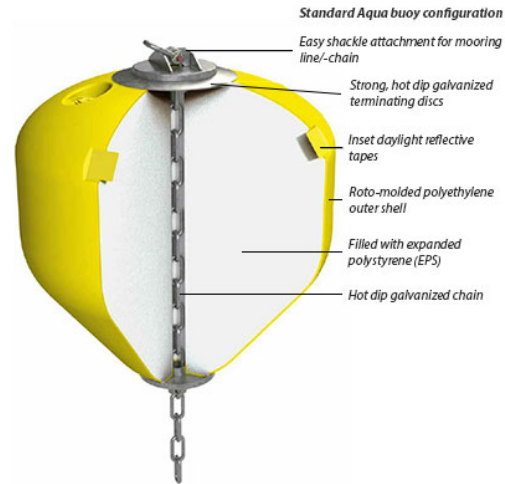


Figure 3.15: Floating buoy, (Eiva-Safex, n.d.b)

Anchors

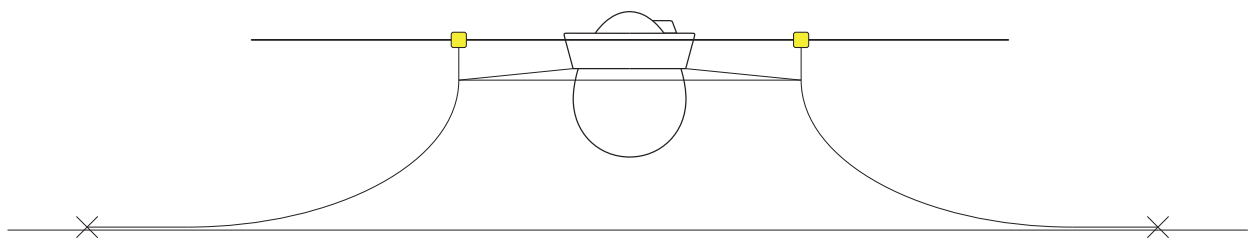
There are several anchor choices based on the geology of the location. The most popular type of anchor today, is the drag type anchor, and other anchors are thus not included. The anchor penetrates the seabed upon installation and provides great resistance against horizontal loads, generated by the resistance of the soil. On the other hand, these anchors are prone to being pulled out if vertical forces are present (Badinotti Group, n.d.).



Figure 3.16: Anchor, (Vónin, n.d.b)

3.9.2 Mooring Systems for Fish Farms

Because the fish cage needs to be permanently positioned, anchors and anchor lines are configured as a spread mooring system around the fish cage (Faltinsen, 1990). There is obviously a need for more than one anchor and anchor line to distribute the load depending on the direction. Figure 3.17 represents the state of art regarding mooring of fish cages. It is interesting to investigate whether or not it is possible to utilize the existing mooring system on location to reduce the installation expenditure of the new fish cage. The way the mooring system is set up, is by suspending a rectangle from 4 floating buoys, marked as yellow circles in figure 3.17b and 3.17a. From the corners of the rectangle, bridle lines are attached to the fish cage to prevent yaw and horizontal displacement. These lines form a “V”, and are connected to each corner of the square rope profile and to the fish cage. The anchor lines themselves aren’t directly connected to the fish cage, but they are attached to connection plates at each corner of the square rope profile. This way of mooring fish cages is convenient with respect to the calculations and load directions. There will always be at least 2 anchors to distribute the load, independent on the load direction. And arguments can be made to include another equivalent for the 4 anchors placed at 90 degrees to the loading direction, but this not implemented in the calculations.



(a) Sideview

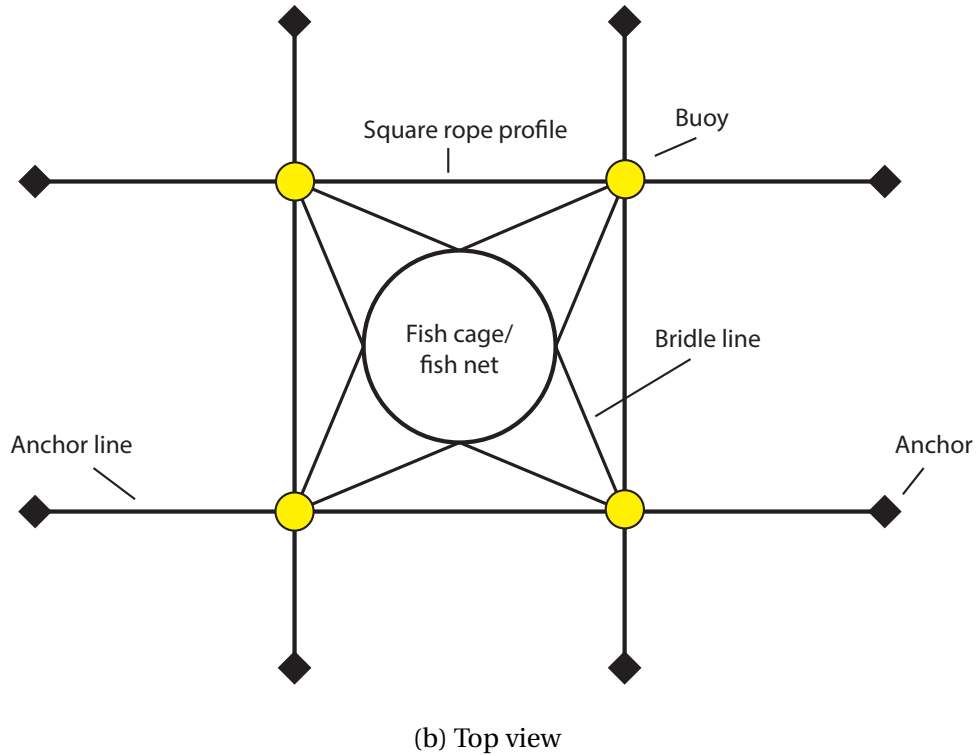


Figure 3.17: Mooring system configuration for fish farms

3.9.3 Catenary Mooring

The mooring lines are assumed to take on a catenary profile. That shape of a catenary is described as the resulting shape of a free hanging line under the action of gravity, where we define the coordinate system with origin at the touchdown point (Chadwick et al., 2010). Consequently, the coordinate system was defined in such a way that at $x = 0, z = 0$. The horizontal distance, x , to the fish cage is measured from the touchdown point, and reaches a maximum at $x = L$, as it is illustrated in figure 3.18. A catenary mooring system provides the needed station keeping through a combined action of the suspended line weight and changes in the lines configuration from the movement of the vessel it secures. The equation for the catenary mooring line profile is expressed as 3.29, and involves the parameters; W and H . W is the submerged weight of the anchor line, and H is the horizontal load that is exerted on the system by current and wave forces.

The water depth varies along the z-axis, until it reaches its maximum at $z = d$, (Chakrabarti, 2005).

$$y = \frac{H}{W} \left(\cosh^{-1} \left(\frac{W}{H} x \right) - 1 \right) \quad (3.29)$$

$$L = \frac{W}{H} \left(\cosh^{-1} \left(\frac{H}{W} d \right) + 1 \right) \quad (3.30)$$

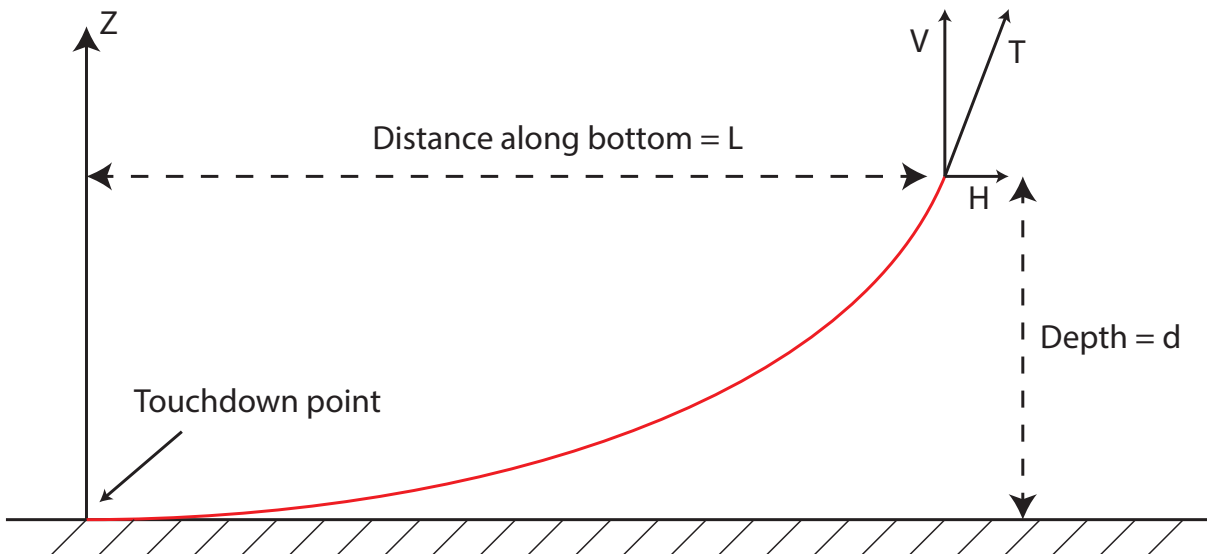


Figure 3.18: Catenary profile

Another parameter of great importance, is the actual length of the mooring line, s , defined by eq 3.31. The total length will vary with the curve of the mooring line, which changes with the submerged weight. Furthermore, the added length caused by the curvature of the mooring line in comparison to a straight line, will increase the vertical force expressed in eq 3.32. The total length, s , is then used to estimate the vertical force, as the product of the submerged weight per unit length times the length of the catenary.

$$s = \frac{H}{W} \left(\sinh^{-1} \left(\frac{W}{H} L \right) \right) \quad (3.31)$$

$$V = W \cdot s \quad (3.32)$$

The horizontal force, H , is defined as the load from the waves and/or current, acting on the cage. And finally, when values for both H , and V have been established, the total tension in the cable, T eq (3.33) can be calculated.

$$T = \sqrt{H^2 + V^2} \quad (3.33)$$

3.10 Dynamic Mooring Motions

In its static position, the mooring line is connected to the floating buoy and the square rope profile through the connection plate, while the end of the line rest at the seabed in the initial touchdown point. When waves and currents are introduced as loading factors, the fish cage is shifted horizontally and lifts an additional length of mooring line off the sea bed, while shifting the touchdown point in the opposite direction of the translation of the fish cage. The increased weight of the lifted line, increases the horizontal restoring force, while the tension in the line in close proximity to the connection point to the fish cage increases until the maximum horizontal displacement is reached (Chakrabarti, 2005). Since the restoring force is highly dependent on the submerged weight, mooring lines composed of different elements are often used to obtain the desired properties. Such an example is the use of heavy anchor chain in the vicinity of the anchor. The chain provides better resistance to vertical forces in the anchor which can lead to the undesirable event of the anchor being pulled out of the soil.

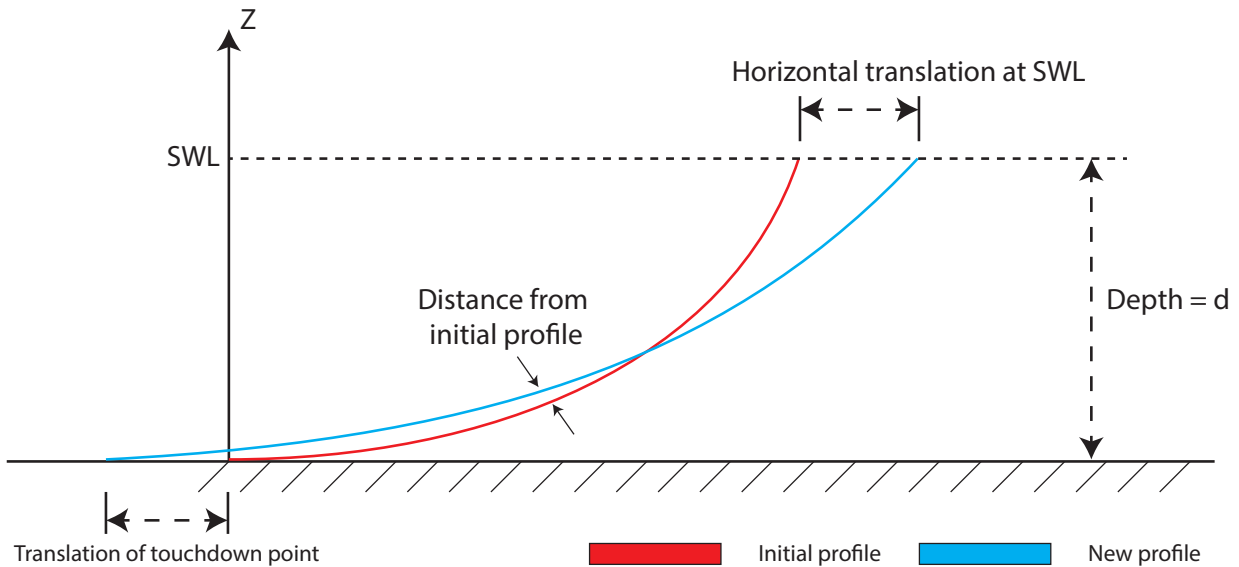


Figure 3.19: Catenary line motions caused by movement at swl

3.10.1 Loading Mechanisms

A set of different loading factors act on the fish cage and they are usually considered to be:

- Current
- Waves
- Wind

Both the wind and current can be assumed as constant loads while wave forces contribute with a time varying load on the system. The RAO of the fish cage will be a good indication for which wave frequencies it is easily excited. Theory regarding the RAOs were presented in chapter 3.8 and the resulting RAO for the heave motion can be inspected in chapter 5.3. Note that these RAOs are estimated without the added damping of the mooring system, which will decrease some of the motion.

3.10.2 Dynamic Analysis

A dynamic analysis is performed in the time domain and are known to be computationally intensive. By utilizing this type of simulation, one can estimate the connected system response and the resulting forces for different sets of environmental loading. An important aspect of the dynamic simulation in comparison to the static equivalent, is the inclusion of the hydrodynamic damping. Secondly, the inertial effects of the fluid interaction of the mooring line is included, but the effect are often considered to be minor ([Chakrabarti, 2005](#)). Furthermore, the time step of the simulation need to be of a magnitude that is small enough to capture the wave induced oscillations in the system. Simulations often tend to be long so they can capture the larger response periods of the system. This is especially true for simulations that uses an irregular sea, with a Spectrum such as JONSWAP that contains waves with different height and occasional high amplitude waves. For simulations that uses a regular sea, one can reduce the simulation time at the expense of accuracy, but computational cost is also drastically reduced. The computer software often uses a finite element method (FEM), which decompose the elements and lines into shorter or smaller elements with linear shape elements. AquaSim, provided by Aquas-structures, was used to perform the dynamic analysis and uses this approach. The basic principle of the FEM method is illustrated in figure 3.20.

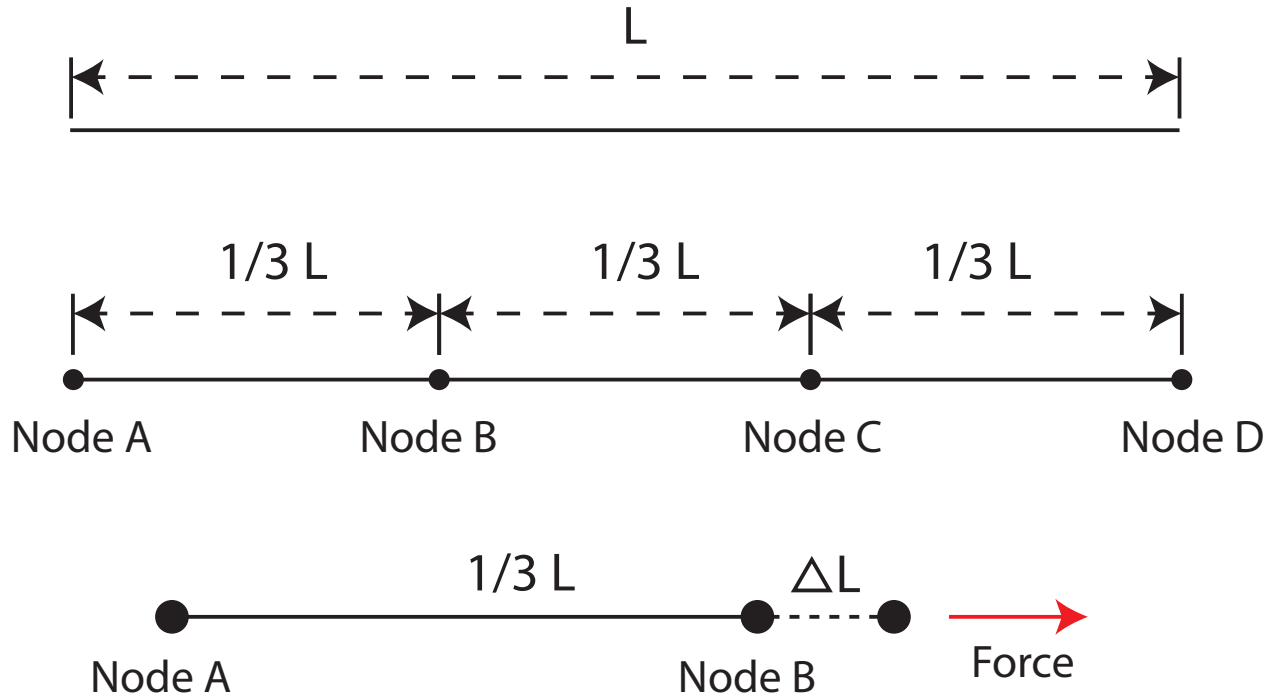


Figure 3.20: Finite Element Method

A truss such as the mooring line in figure 3.20 with length, L , is decomposed into a decided amount of elements connected by nodes. In this case 3 elements with length $1/3 L$, with 4 associated nodes. In a case considering node A to be fixed and by applying a force at node B. the element will deform a distance ΔL . By applying Hookes law eq (3.34), which states that the force, F , needed to extend or compress a spring by a distance, is proportional to that distance. In which, k , is the characteristic stiffness of the material of interest. Equilibrium is obtained when the internal forces of the truss are equal to the external applied forces. This is established for the whole structure in both a static or dynamic analysis ([Aquastructures, 2014](#)).

$$F = k\Delta L \quad (3.34)$$

3.11 Solidity and Marine Growth

Important load affecting parameters for the fish net was studied, since the loads in the mooring system of the closed fish cage is to be compared to that of a fish net. Two factors of considerable importance are the solidity and marine growth. The solidity, S_n , of the net is a parameter that defines the percentage of an area covered by the twines in the net (Gansel et al., 2015). The solidity will change with mask size in the net and line diameter. And increase for finer mask sizes or higher line diameter, since a greater area is covered.

$$S_n = \frac{\text{area}}{\text{total net outline area}} = \frac{d}{L_y} + \frac{d}{L_z} \quad (3.35)$$

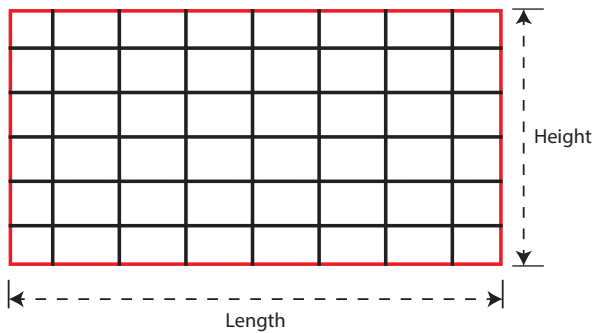


Figure 3.21: Solidity of a panel

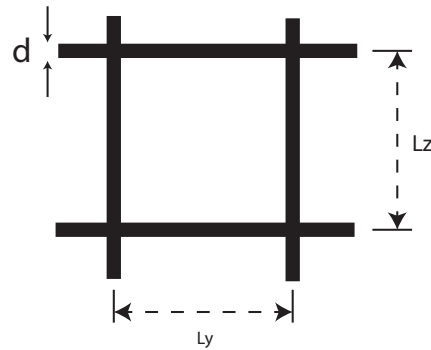


Figure 3.22: 2D view of one mask

Marine growth, also known as biofouling, “is the undesirable accumulation of microorganisms, plants and animals on artificial surfaces (nets, trays, cages), when they are immersed in the sea, with considerable economic consequences” (Mark G. J. Hartl and Davenport, 2006). Biofouling will also influence the solidity and drag loads of the fish net by increasing the effective line diameter in the net. The increase in drag caused by marine growth often causes additional deformation of the net, increasing the risk of wear and tear as a result of contact between the net

and the rest of the system. Figure 3.23 shows a fish net with marine fouling, and it is clear to see how it increases the solidity of the net.

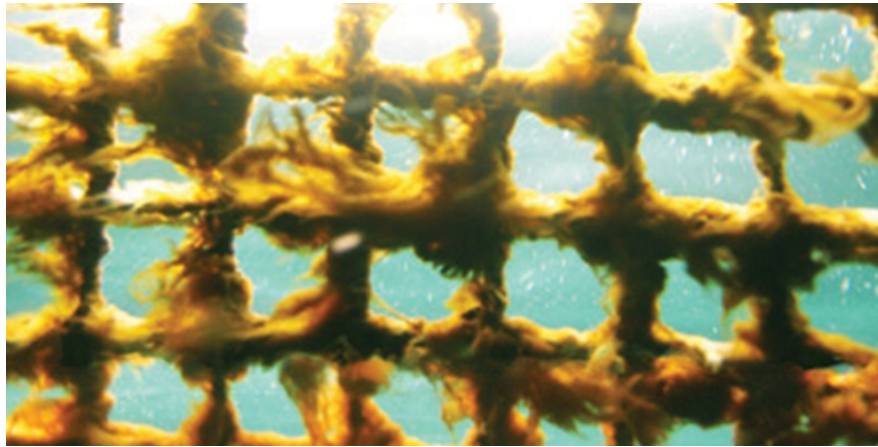


Figure 3.23: Marine fouling of a fish net (Akva-Group, n.d.)

The technical standard, NS9415, acknowledge the effect of marine growth and states that the dimensional fish net analysis shall use a line diameter increase of at least 50% when marine growth is considered (Standard Norge, 2009). Aquasim have an integrated option called “growth coefficient”, which accounts for increased diameter of the lines from fouling. Setting this coefficient to 1.5, increases the line diameter by 50% (Aquastructures, 2014). Other than increasing the weight, and hydrodynamic loads on the system and mooring, marine growth also affect the fish welfare. A significant amount of marine growth reduces the water exchange through the net due to the higher solidity, and consequently reduces the oxygen supply of the fish stock (Gansel et al., 2015).

3.12 Net Membrane Elements in AquaSim

AquaSim uses membrane elements to calculate the incident wave and current forces acting on a panel with solidity, S_n , as described in the previous section. A complete net consist of several panels similar to that of figure 3.21, comprising a mesh model. The modeling approach is

covered in chapter 4. There are three different load options to choose from, but the default option, M1, are used in this thesis since it shows good agreement to experimental measurements, and account for shading of consecutive lines as presented by [Berstad et al. \(2012\)](#). The drag coefficient for a single line in the net is used to calculate the appropriate drag coefficient for the membrane panel with equation 3.37, which is dependent on the solidity, S_n . The equation for the drag force of a net panel is defined in equation 3.36.

$$F = C_{d,mem} \frac{\rho}{2} d L_y U^2 \quad (3.36)$$

Where:

$$C_{d,mem} = C_{d,cyl} \frac{L_y L_z^2}{(L_y - d)(L_z - d)^2} \quad (3.37)$$

By introducing a net panel where $L_y = L_z = L$, equation 3.37 reduces to

$$C_{d,mem} = C_{d,cyl} \frac{1}{(1 - \frac{S_n}{2})^3} \quad (3.38)$$

3.13 Dense Net Membrane Elements in AquaSim

The “dense net” option is another option in AquaSim primarily meant to calculate the forces on lice skirts, but can also be used to calculate the forces on large closed volume bodies, such as the fish cage. However, the net doesn’t have bending stiffness and requires an underlying rigid structure to maintain its shape. The modelling of such a structure is described in chapter 4. Furthermore, it includes an option for added mass, as the internal volume multiplied with an added mass coefficient. Wave forces from the incident wave are calculated as a combination of the Froude-Kriloff force, and the diffraction force calculated according to McCamy and Fuchs ([Berstad and Heimstad, 2015](#)), which was presented in chapter 3.6.

This page is intentionally left blank.

4. Simulation Modelling

The purpose of this chapter is to cover the simulation modelling in the different programs that have been used, since all of the simulation setups are exclusive to this thesis. Some values are included in this chapter, but the complete list of variables and assigned values are included in Appendix D. The different programs are branded as:

- Genie
- HydroD
- AquaSim

4.1 Genie and HydroD

The simulation in Genie ([DNV GL, n.d.a](#)) and HydroD ([DNV GL, n.d.b](#)) are closely related and are therefore combined in this chapter. The purpose of implementing these programs was to estimate the RAOs of the fish cage. Genie was used as the modelling program while HydroD was used to calculate the RAOs.

4.1.1 Modelling in Genie

A cross section line was modelled and rotated 360° to produce the surface shape of the fish cage. Then the surfaces that are in contact with water and consequently should receive a hydrodynamic pressure, was specified. The generated model was meshed with a combination of a

regular structured mesh around the buoyancy collar. While a tetrahedral mesh was specified on the cage walls, to better capture the curvature of the egg. Genie had some problems to mesh the curve of the fish cage with a rectangular mesh, especially in the lower part of the cage with high curvature. Note that both programs only consider the area under the SWL, and subsequently, the structure above the SWL was not modelled.

Next, a secondary mesh was generated to see if further mesh refinement would improve or change the results to some extent. A better resolution in the calculated RAOs are generally expected by implementing a finer mesh. However, one tries to find a compromise between numerical accuracy and computational time. Both meshes are displayed in figure 4.1.



Figure 4.1: Coarse and fine meshed model

4.1.2 Setup in HydroD

In total, 3 simulations were carried out. All simulations used incoming waves with varying direction from 0° to 180° with an interval of 15° between the waves. The frequency set was specified to start at 0.2 rad/s and continue throughout 2 rad/s , with a steady progression of 0.1 rad/s . Then the frequency set was further refined, based on the results from the first simulations that yielded a poor resolution, but indicated the region of interest, even with a lack of measurements.

4.2 AquaSim

The software package called AquaSim, provided by Aquastructures was used to perform the dynamic simulations of both a open fish net with a floating collar and the closed fish cage. The program consist of 4 individual programs, each serving its own specialized purpose. The model is created in AquaEdit and environmental conditions are defined in the same program. AquaBase can be used to view the model, and evaluate the data regarding the different elements, but has been less important in the newest release of the program. AquaView displays the results from AquaEdit in an intuitive environment and lastly AquaTools lets the user plot and display results of interest. Lastly, Matlab was used to post-process the data and make combined plots of the data, extracted from AquaTools. All the material data can be inspected in appendix D.

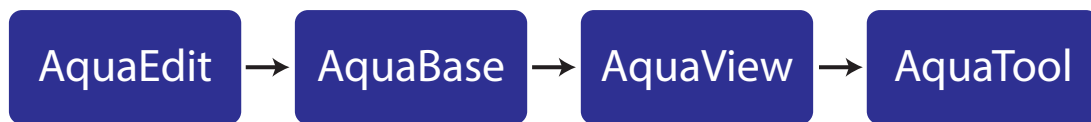


Figure 4.2: Programs included in the AquaSim package

4.2.1 Modelling of Fish Net

To generate the model, a circle with radius 16m, was drawn at $z = 0$, and divided into 36 elements distributed along the circumference. Another circle was extruded at a distance of 0,72m outwards from this circle, complete with connecting elements. These two circles comprise the floating collar and are defined as beam elements, assigned with properties and cross section of a circular plastic tube, included in appendix D.2.

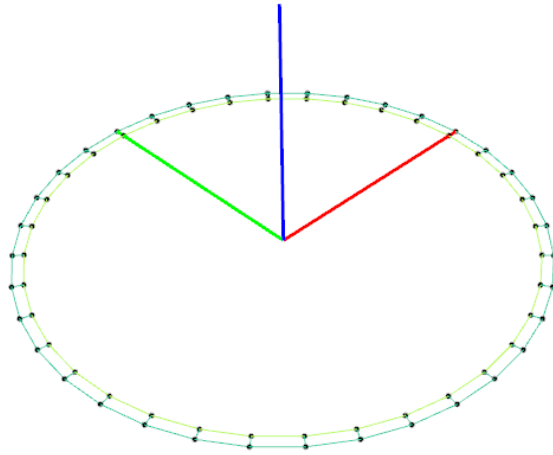
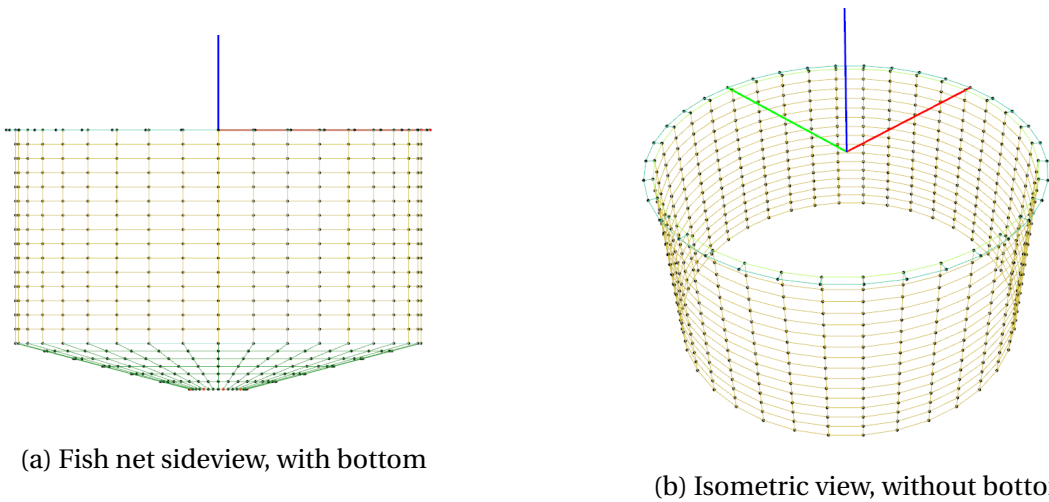


Figure 4.3: Floater

The fish net was extruded from the inner circle and along the negative z-axis for a distance of 20m distributed over 15 elements. To close off the net, a conical mesh was extruded from the bottom of the vertical sidewalls of the net, with a vertical distance of 5 meters and 6 elements in the radial direction. Then, all the elements of the extruded mesh was selected and the element type was set to membrane which defines a net type load to the selected mesh elements in AquaSim. The net has a baseline solidity of 15,9%, with another two simulations accounting for additional marine growth of 20% and 50%, with a resulting net solidity of 19,2% and 23,9% respectively.



(a) Fish net sideview, with bottom

(b) Isometric view, without bottom

Figure 4.4: Fish net

Another circle was extruded at the bottom of the sidewalls of the net. This circle represents a sinker tube, which purpose is to maintain the shape of the net while put under horizontal loading. This circle was attached to the inner circle of the floater with 9 vertical lines, distributed around the net. These lines are also connected to the net, and relief it from most of the vertical loads induced by the sinker tube, and provides strength to the system.

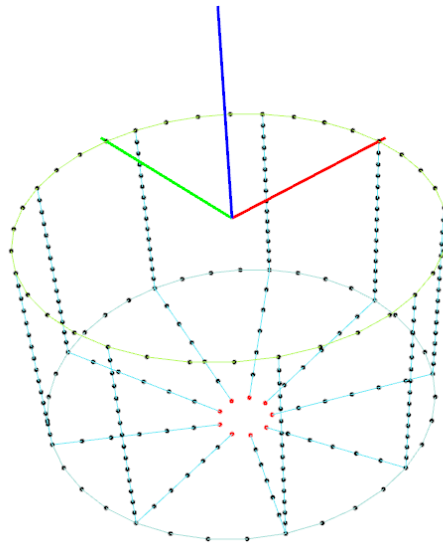


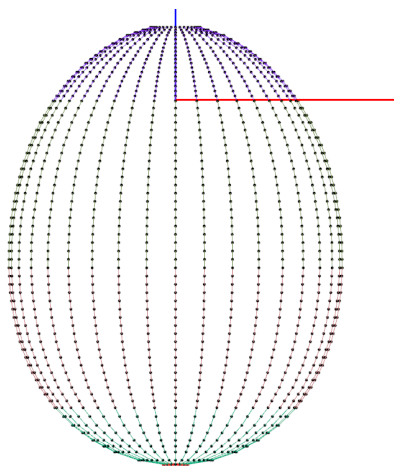
Figure 4.5: Lines in the fish net

4.2.2 Modelling of Fish Cage

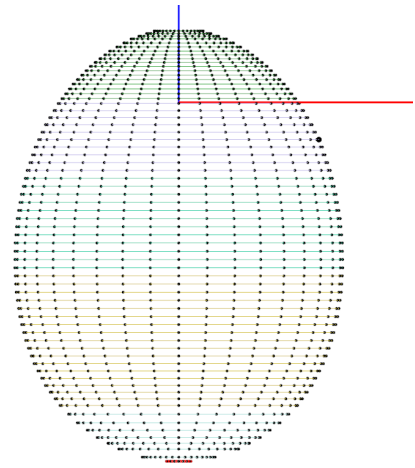
To model the fish cage, a set of 25 points were exported from a CAD modelling software, along the cross section of the egg shape. The coordinates of these points were used to draw the vertical cross section of the fish cage, before 1 refinement point were inserted between each of the original nodes to provide a smaller element size. The 3-dimensional shape was modelled by rotating the line 360 degrees and distributing 36 elements along the circumference. A similar approach was used to model the horizontal connections between the lines, as these needed to be different elements.

The floating collar comprises four different structural elements. Internal rectangular beams pro-

vide the necessary stiffness, while the circular elements at the outer perimeter of the floating collar connects these beams to create a rigid structure. A membrane element of type “dense net” is then defined at the outer perimeter of the whole structure, as seen in figure 4.7a. The internal water volume of the structure is accounted for by introducing this type of element to the model, as proved by [Berstad and Heimstad \(2015\)](#). Furthermore, the inclusion of the internal water volume for such a large volume structure is important to be able to capture the dynamic effect of the large mass of the structure, as it moves with the waves and currents.

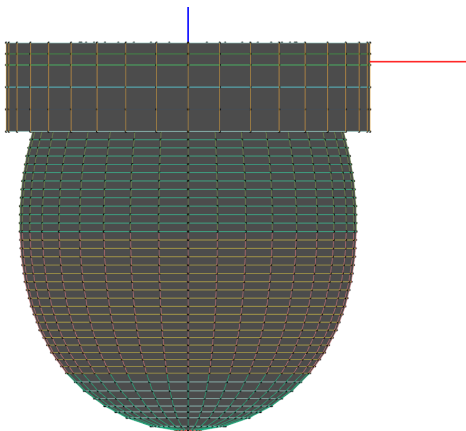


(a) Fish cage vertical elements

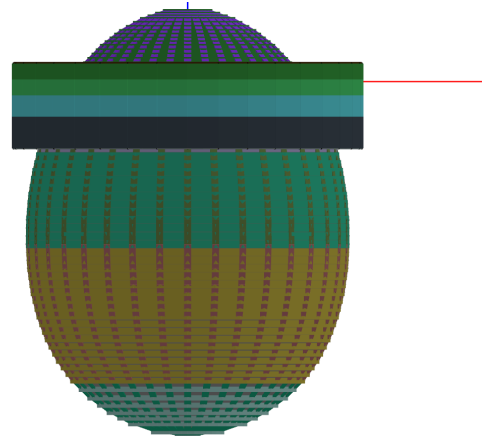


(b) Fish cage horizontal elements

Figure 4.6: Fish cage model without floating collar



(a) Dense net elements



(b) complete fish cage model

Figure 4.7: Further refined fish cage model with floating collar

4.2.3 Modelling of the Mooring System

The mooring system, illustrated in figure 4.9, is identical for both the fish net and the fish cage, since the purpose is to investigate their interchangeability. A 60 by 60 meter square rope profile, as described in section 3.9.2, was modelled at a depth of 5m. Buoys were defined at each corner, with properties found in appendix D.3. These elements have properties of a spring with a vertical force component to simulate the bouyancy. The bridle lines connect the square rope profile to the fish cage and fish net. Furthermore, the ends of the mooring lines were placed at an estimated distance of 400 meters away from the square rope profile, at a constant angle all the way down to the seabed at $z = 100m$. A further 70 meters of line was added from the touchdown point (TDP) to the anchor, to accommodate for some vertical movement, as the fish net and cage moves with the waves. The line resting at the seabed is given properties of a chain, while the longer lines are defined as fiber ropes. The anchors are held in place by introducing a constraint in the x -, y -, and z -direction for the node at the end of all the mooring lines.

The mooring lines are split into 7 elements of 51,4 meters for the major distance of the mooring line. 3 shorter refinement sections of 17,1 meters are specified near the square rope profile, to better capture the dynamic motions in this area. The anchor chain near the tdp are split into 8 sections, since some translation of the tdp is expected, when the mooring system moves with the waves, fish net, or the fish cage.

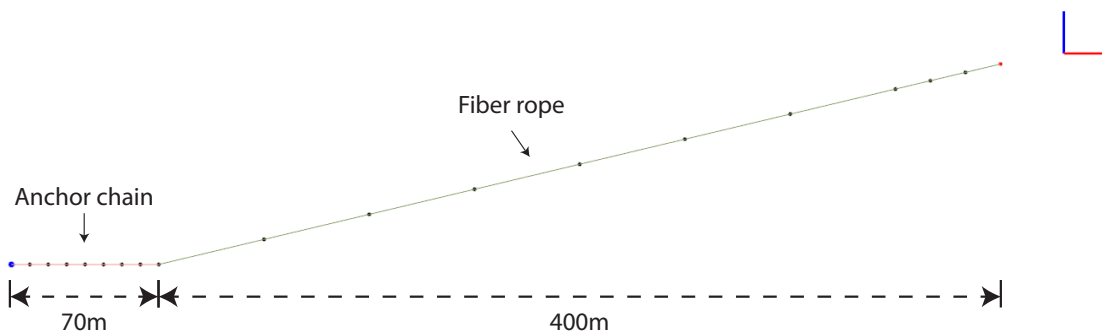
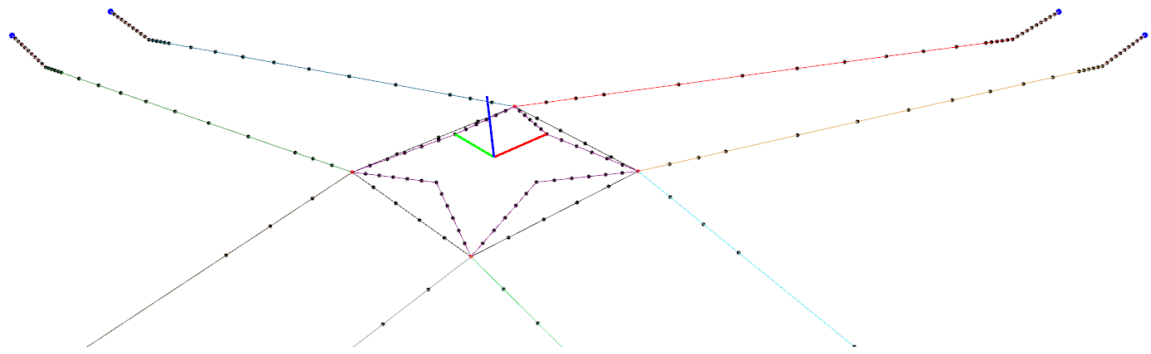
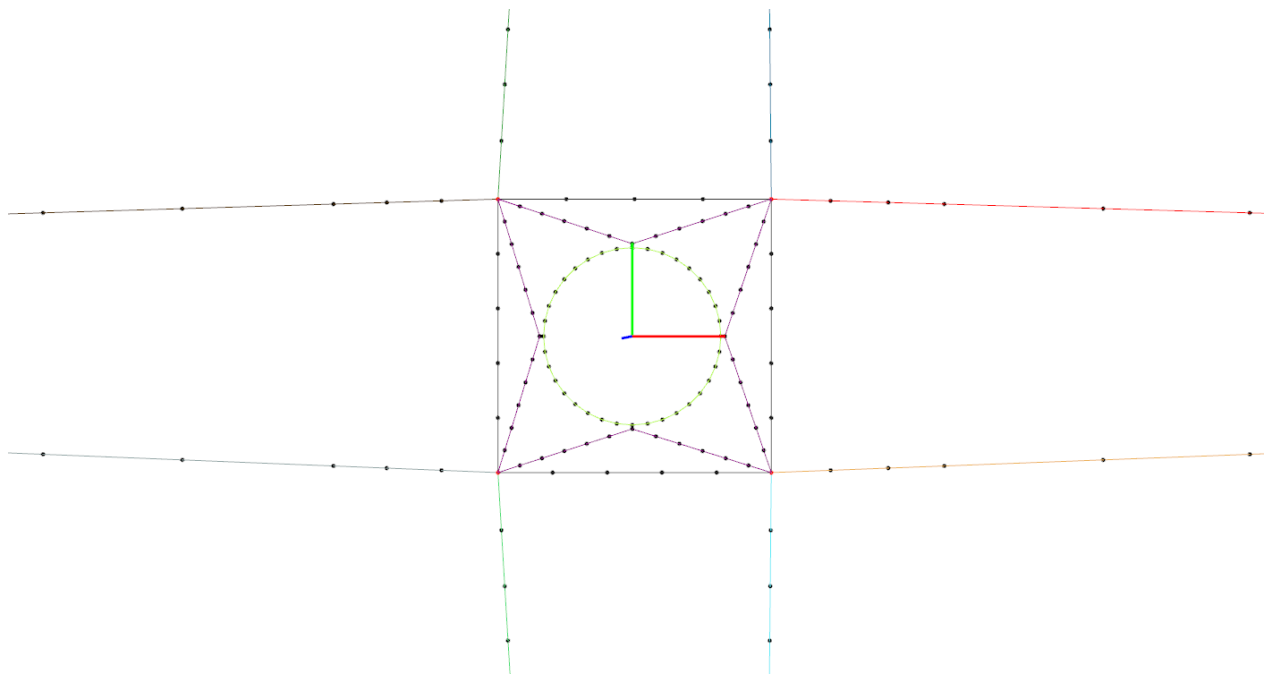


Figure 4.8: Composition of one mooring line



(a) Isometric view of mooring system



(b) Top view of mooring system

Figure 4.9: Mooring system model

4.3 Drag Comparison

Initially, only current was considered, and a setup were established to compare the drag loads from the fish net to the drag loads of the closed fish cage. A horizontal mooring line was placed at a distance of 50 meters from the center of the structure, and ended at 100m in the x-direction. The end-point at 100m were constrained in all directions. Additionally, 3 bridal lines connected the floater and fish cage to the mooring line to better distribute the load. Current of varying velocity was simulated, and the axial tension in the horizontal mooring line was inspected. This approach is similar to the one used by [Berstad and Heimstad \(2015\)](#) and [Lien and Volent \(2012\)](#). Figure 4.10 shows a top view of the setup for both the fish net and the closed fish cage.

Furthermore, these simulations only consider the containment systems, and the influence of the biomass, represented by the presence of fish, is not accounted for in the drag analysis of the fish net. A high density of fish inside the fish net will probably influence the flow pattern, and affect the incoming water velocity as it passes the structure. The fish cage does not have the same issue, due to the closed walls which provides a constant barrier against the surroundings. This makes the results more independent regarding the effect of the contained biomass.

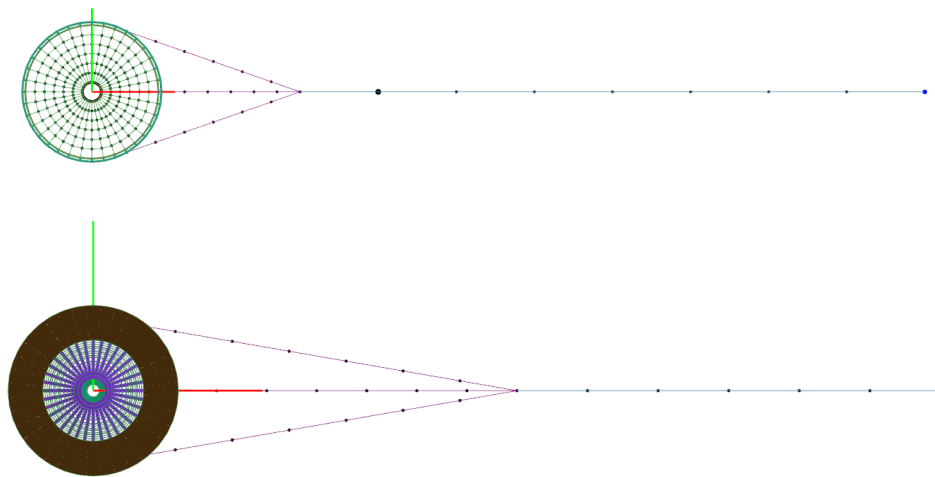


Figure 4.10: Horizontal drag model for both systems

This page is intentionally left blank.

5. Results

5.1 Wave Force Calculations

The geometry of the fish cage projects a horizontal cross section of a cylinder, and a vertical cross section as seen in figure 5.1. The horizontal load for an infinitesimal section will still be that of a cylinder, so the principle of calculation would be similar, except that we need to sum the forces from the different sections. However, the geometry of the whole structure makes it possible to justify a simplification were the shape is defined as a cylinder with constant diameter. The diameter is kept at 19m, and the cross-sectional area is assumed to be equal to the actual shape of the fish cage, which yields an equivalent draft of 17,8 m. This assumption should compensate for some of the geometrical differences. The result can be seen in figure 5.1.

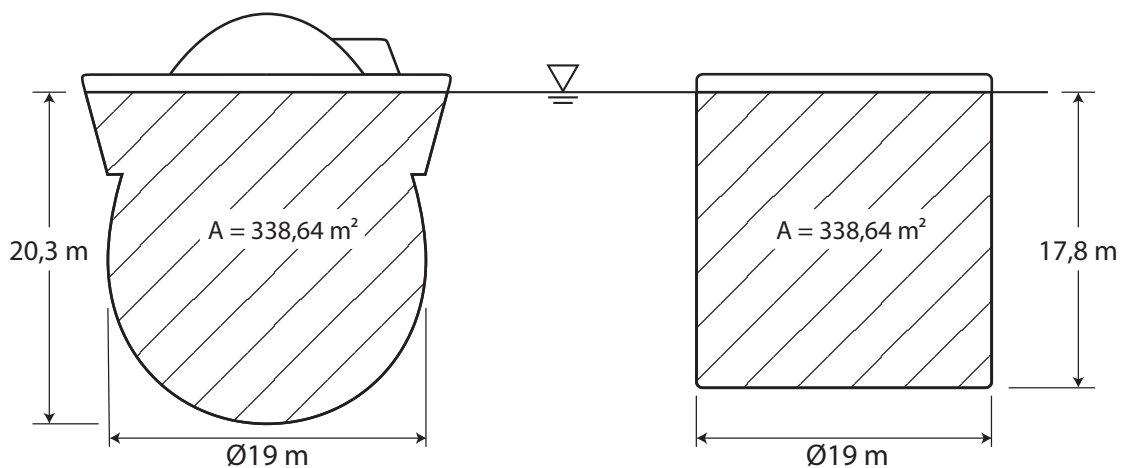


Figure 5.1: Essential dimensions

Geometric values of the fish cage	
Cross sectional area [m ²]	338,6
Draft [m]	20,3
Equivalent cylinder draft [m]	17,8

5.1.1 Wave Parameteres

The wave parameters of interest were defined in chapter 1 and are a direct result of the different wave classifications, sourced from the NS9415 standard. Supplementary parameters such as wave number, diffraction coefficient, and wave length were calculated because the NS9415 standard only list the wave height and the associated wave period. Note that all conditions are within the criteria for the diffraction regime of $\frac{\pi D}{L} < 0,5$, where condition nr 3 is getting closest to the “all inertia” region in figure 3.2.

A maximum wave height of 2m was chosen, since the freeboard of the floating collar was set at approximately 1,4m, and higher waves would overtop the floating collar with unknown effects. Furthermore, the fish cage is expected to be used at fish farms that already use fish nets. These tend to be located in sheltered locations with limited wave height, and consequently, higher waves were not included.

The theory regarding wave forces that was initially presented in chapter 3.6, investigates the total force on a cylinder that is piercing through the water surface and rigidly mounted to the sea bottom. Since the fish cage is in fact floating in the upper part of the water zone, there is a need to slightly modify the approach. The mooring lines are thought to secure the cage in such a way that free movement is restricted. Aquasim includes wave drift and should produce a more correct estimation, that contains all parameters of the floating body.

Table 5.1: Calculated Wave Parameters

Nr	H [m]	T _p [s]	k	d [m]	L [m]	C _M (Fig.3.5)	$\pi \frac{D}{L}$
1	0,5	2	1,006	100	6,25	0,0541	9.56
2	1	3,2	0,393	100	15,99	0,2218	3,73
3	2	5,1	0,1547	100	40,61	0,8655	1,47

5.1.2 Diffraction Force

The resulting force for each condition was calculated using McCamy and Fuchs's approach and are included in table 5.2. By comparing condition 2 and 3 as an example, one can observe how the wave load increase by a factor close to 8, with a doubling of the wave height and a slight increase in wave period. These loads are known to be overpredicted as they implement the water depth as the cylinder height, and don't account for the draft which allows some of the water to pass under the structure.

Table 5.2: Calculated wave forces, McCamy & Fuchs methods

Nr	Wave force [N]
1	38 559
2	316 171
3	2 467 499

Van Oortmerssens method of multiplying the MF force with a ratio was used to account for the floating body and the passing of water particles underneath the structure. The resulting

force for each condition are included in table 5.3. The calculated ratio is dependent on both the draft, water depth and the wave number. It is interesting to see how the wave number, k , is the deciding factor, as the other parameters are constant for all cases.

Table 5.3: Calculated wave forces, van Oortmerssen method

Nr	Ratio	Wave force [N]
1	1,000	38 559
2	0,999	315 883
3	0,937	2 310 819

The results in table 5.3 correlate to those produced by [Chadwick et al. \(2010\)](#), which used a floating cylinder with diameter of 20m, and a draft of 8m. They used the same approach as above, assuming that the cylinder does not move. A selection of the results are included in appendix B. Interestingly, [Chadwick et al.](#) decided to neglect the dynamic effect of the wave forces in the further work in relation to the mooring line analysis, “due to the large associated uncertainty of the wave parameters”.

Even though the results of these two independent studies are closely related, there is an uncertainty associated to how the spherical shape of the closed fish cage would impact the total forces, that are calculated for a floating cylinder. Model testing should be conducted to establish the dynamic effects of the fish cage, and to which degree these calculations are conservative or not. Nevertheless, one should acknowledge the magnitude of the potential diffraction forces and account for such forces, both structurally, and with respect to the dimensioning of the mooring system. These calculations must include the dynamic effect of the floating object, which they are applied to. Such effects are the horizontal-, rolling-, and vertical movements, which are believed to impact the result. The fish cage is in fact free to move with the waves to some extent,

since the mooring system has a moderate restoring force. This is one of the biggest differences in comparison to a rigidly mounted cylinder for which the amplitude of motion shall not be too large to use the McCamy and Fuchs theory.

The same level of force is not observed in the dynamic analysis, presented in chapter 5.5.4, but the reported force in this analysis only consider the axial tension in one mooring line. And consequently, one cannot compare these results directly, as the total force would be a combination of the oscillating force in all the mooring lines.

Another interesting discovery in the wave calculations is that the wave loads are close to that of a bottom mounted cylinder, even though there is a difference of 82.2 meters in draft. This is especially true in deep waters where there is a drastic decay of water wave particle velocity with increasing depth. Which means that the maximum amount of wave load will be experienced in the upper part of the total depth of water. Wave condition 2 have been used to highlight this property, as seen in figure 5.2, where a red marker has been included to highlight the draft of the equivalent cylinder and the SWL.

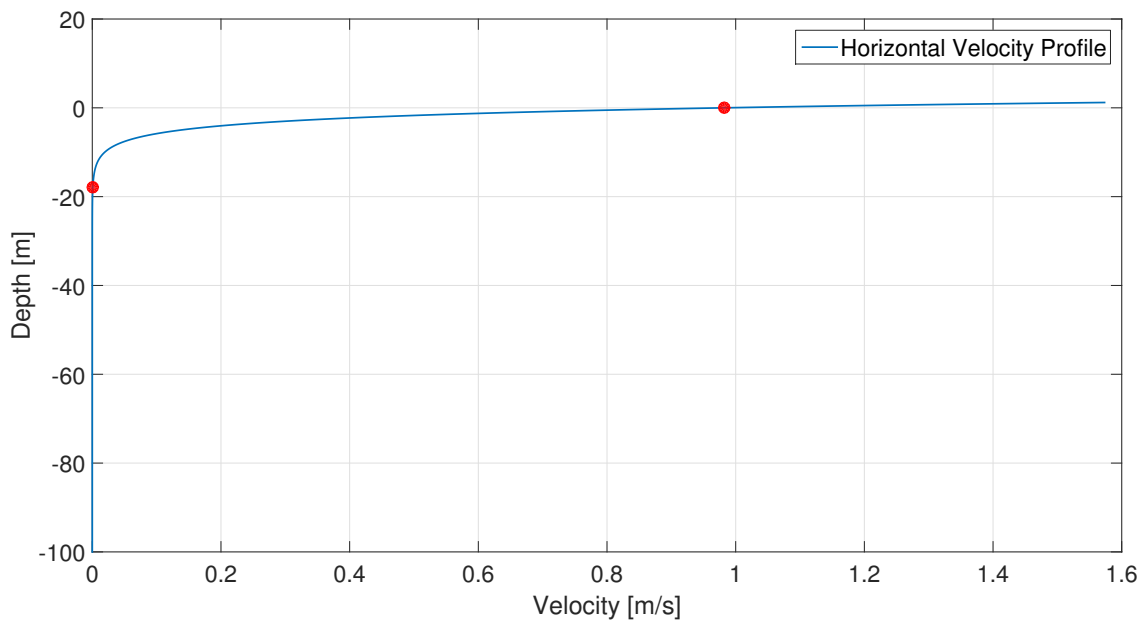


Figure 5.2: Velocity profile for wave condition nr 2

5.2 Drag Calculations

5.2.1 Drag Coefficient

As previously stated, the drag coefficient is a dimensionless number that represents the drag characteristics of the geometry. The drag coefficient that was used in this thesis is a combination of the drag coefficient of an elongated sphere, and a cylinder with aspect ratio of approximately 0,6. The elongated sphere with an aspect ratio of 0,75 have a drag coefficient of approximately 0,2 according to [Çengel and Cimbala \(2014\)](#). While a cylinder with an aspect ratio of 1 have a drag coefficient of 0,6. By inspecting the cross-sectional area, it is evident that the cross section is a combination of a cylinder and a capped elongated sphere. Figure 5.3 shows the two different cross sections, CS1 and CS2. Where CS1 represents the capped elongated sphere and CS2 represents the cylinder shape. Table 5.4 includes the cross-sectional areas and their percentage of the total area. The drag coefficient of both objects were weighted based on their percentage of covered area in relation to the submerged cross-sectional area, to establish the resulting drag coefficient. A resulting drag coefficient of approximately 0,3 is obtained by combining these two scaled drag coefficients, included in table 5.4 and were used in the Aquasim input data.

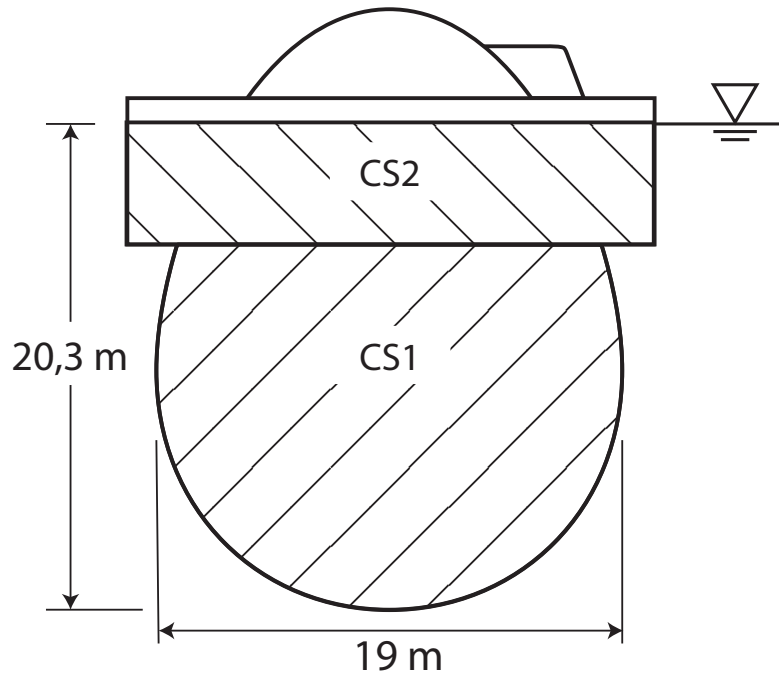


Figure 5.3: Cross section

Table 5.4: Cross-sectional areas and drag coefficients

	Cross section [m ²]	Cross section [%]	Original C _D	Scaled C _D
CS ₁	252,65	74,6	0,2	0,1492
CS ₂	86	25,4	0,6	0,1524
CS _{total}	338,65	100	-	0,3016

5.2.2 Drag Force

The total drag force was calculated by introducing the estimated drag coefficient of 0,3 into eq 3.27. The reference area is the projected area in the flow direction. The area was found to be 338.65m^2 in CAD software. The resulting force varies with the current velocity squared, as seen

by the exponential increase of force in figure 5.4. The drag force was plotted against current velocities from 0 to 1,5 m/s, since higher current velocities are rarely observed at fish farming locations. Furthermore, these current velocities covers all classifications in the NS9415 standard. By comparing the drag force to the wave forces obtained in table 5.3, it is evident that the drag force is of a much smaller magnitude. The combined effect of both factors will be further examined in the dynamic analysis.

Table 5.5: Drag force at different current velocities

Nr	Current velocity [m/s]	Drag coefficient	Drag force [N]
4	0,2	0,3	2 152
5	0,4	0,3	8 608
6	0,6	0,3	19 369
7	1	0,3	58 801
8	1,5	0,3	121 053

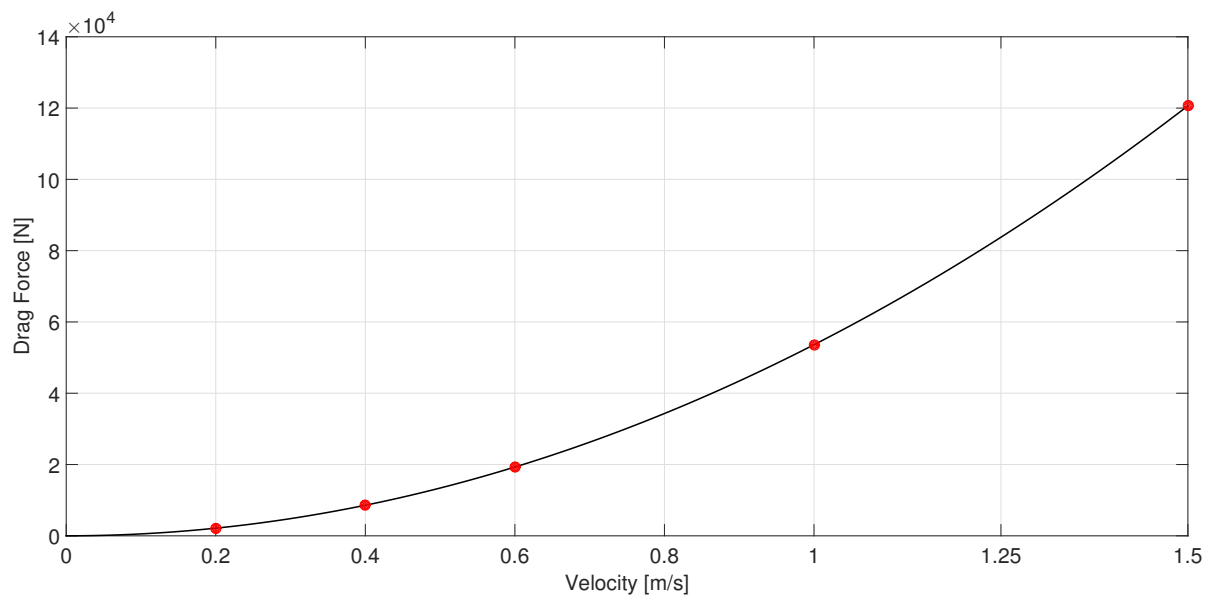


Figure 5.4: Drag force variation with current velocity

5.3 RAO Estimation

The RAOs were calculated in HydroD and the fish cage was modelled in Genie. Both software programs are products offered by DNV GL. Genie was used to construct the necessary panel model to perform the simulation, while HydroD was used to calculate the actual RAOs. The model generated in Genie was meshed with a combination of a regular structured mesh around the buoyancy collar. While a tetrahedral mesh was used on the cage walls to better capture the curvature of the egg. Note that both of the programs only consider the area under the SWL.

The results are plotted for the heave response as the waves propagate in the primary direction for all cases. The primary direction is defined to be parallel to the x-axis, that is at 0° . Additional directions such as, 45° and at 90° could have been implemented, but were excluded since a thorough investigation of the RAOs wasn't the objective of this thesis, and the fact that the fish cage is axisymmetric, which made the results identical for all directions. It is also important to notice that these simulations doesn't include the viscous damping of the water that surrounds the structure, which would most likely cause the amplitude to be smaller. Nonetheless, the frequency range would still be accurate.

5.3.1 Coarse Frequency Step

The first simulation run executed the calculations fast, and the resulting RAO for heave at 0° was found. In postprocessing Matlab was used to convert the frequency from rad/s to Hz. From the resulting plot, it is clear that there are some missing values at the peak, recognized by the sudden and nearly horizontal translation near the peak. Which in return suggest that there might be a point in between with a higher corresponding value that are excluded due to the coarse frequency step size.

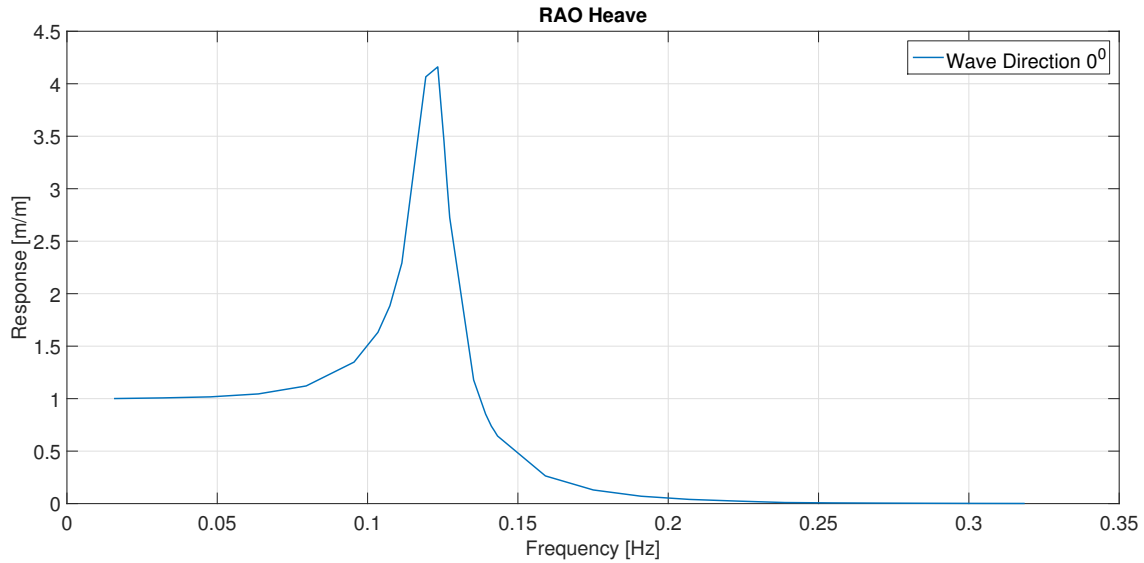


Figure 5.5: Coarse frequency range

5.3.2 Refined Frequency Step With Coarse Mesh

The following simulation implement a model with a finer frequency step in the frequency range of the peaks of the obtained spectrum. The frequency range in need of refinement was established in the previous simulation, and values was added manually in this range to increase the resolution. As a result, the peak was calculated to be higher. The graph also maintains a smoother profile, which is a good indication of adequate calculation steps. However, we see a small dent on the graph, which suggests that further refinement should be made.

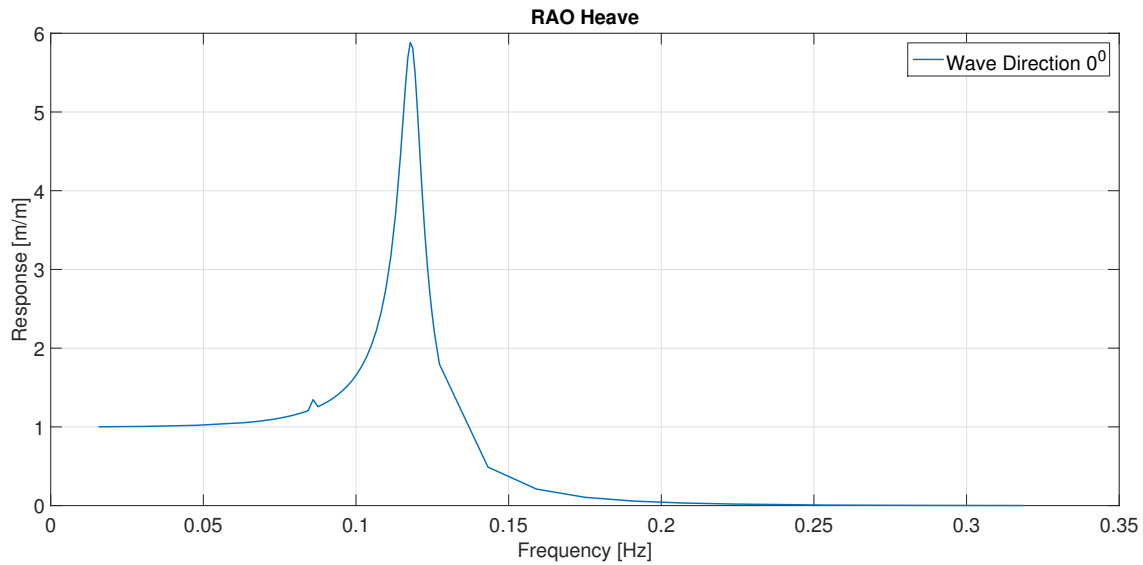


Figure 5.6: Coarse mesh with refined frequency range

5.3.3 Refined Frequency Step With Fine Mesh

The last simulation uses the same frequency set as the previous simulation, but the model was exchanged with a finer meshed model. The results were marginally higher for the heave motion. However, it is interesting to notice how the graph no longer contains the little peak at the start of the graph. By introducing a finer mesh, the simulation yielded a more robust and trustworthy solution. While the simulation gives more accurate results, there is a downside of higher computational time in comparison to the second simulation, with a computational time of 255s, compared to 72s for the coarse mesh with a fine resolution frequency set.

The peak of the graph with respect to wave frequency is at about 0,12 Hz, which equates to a wave period of 8,33s. The fish cage will have the highest response in this region, with a response close to 6 meters per meter wave height, without the viscous forces being accounted for. The highest wave period that was used in this thesis is at 5s, which is the same as a wave frequency of 0,2 Hz. In this area of the spectrum, there is a very small response and resonance in heave should not be a problem. On the other side of the graph one can see how the fish cage would follow the

waves in a harmonic motion in swell waves, when the wave period reaches approximately 20 seconds or higher.

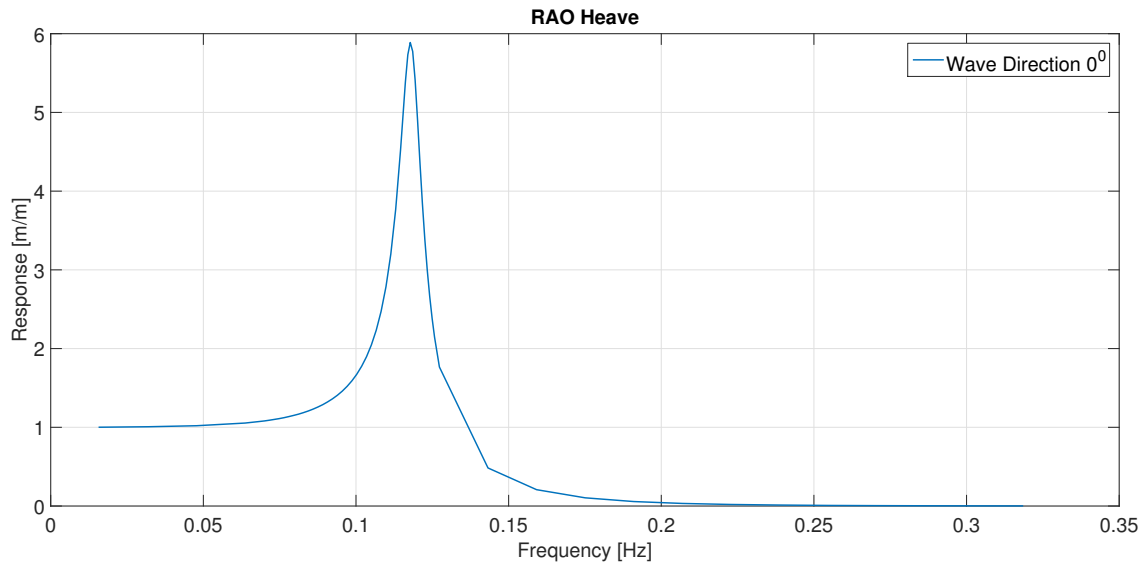


Figure 5.7: Refined mesh with refined frequency range

5.4 Static Mooring Calculations

Equation 3.29, which was presented in chapter 3.9.3, were used to calculate the static profile of the lines. The mooring lines were defined as a stud link chain, with a submerged weight of 39 N/m. To increase the safety of the system and make it more redundant to environmental loads, an extra length of 70m heavier anchor chain is added from the touchdown point to the anchor. This is a remedial action to mitigate the risk of vertical forces in the anchor. The sea bed was assumed to be completely flat for both the static and the dynamic analysis. The horizontal load, H , is divided by two, to better capture the nature of the spread mooring configuration that distribute the loads to at least two anchors at all times.

The static calculations only use the current loads as these are constant with time. Wave loads have been included in the simulations in AquaSim, which is covered in the next chapter. The input values and the results for the system at varying current speed is included in table 5.6.

One can clearly see that the vertical force is of great concern when the current loads are small, contributing to almost all the tension at the top of the line. The vertical force contributes to more than 50% of the total tension for $U_c < 0,6$.

Table 5.6: Static mooring line calculations

Current speed [m/s]	0,2	0,4	0,6	1,5
Drag coefficient	0,3	0,3	0,3	0,3
Drag force [N]	2 152	8 608	19 369	121 053
Stud link chain size 1-3/4 inch [N/m]	39	39	39	39
Estimated line length, s [m]	119,4	173,2	210,8	540,3
Seafloor projected length, L [m]	59,9	136,0	237,1	551,3
Chain on bottom [m]	70	70	70	70
Vertical leader [m]	5	5	5	5
Vertical tension [N]	4 658	6 754	9 246	21 499
Tension at top [N]	4 781	8 009	13 390	64 232
Water depth, d [m]	100	100	100	100

5.5 AquaSim

The two models of the fish net and fish cage described in chapter 4 were used throughout all simulations. A set of simulation conditions were established, included in table 5.7, to capture a broad spectrum of scenarios and wave classes as defined in the NS9415 standard. This table

employ the predefined environmental conditions, governing the wave height, wave period and current speed presented in Appendix A. The resulting tension plots for the complete mooring system in this chapter are taken from mooring line 1, as defined in figure 5.8.

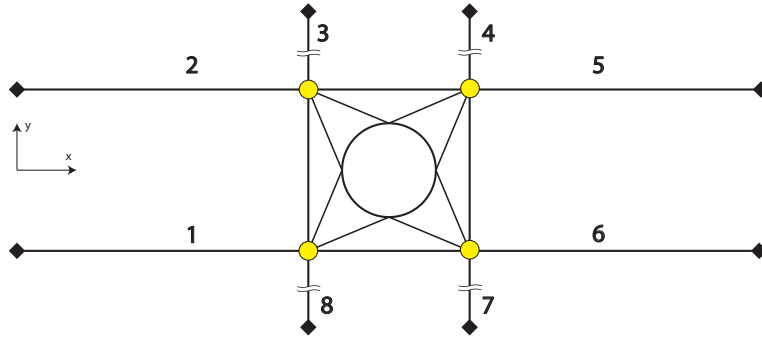


Figure 5.8: Mooring line numbers

Table 5.7: Simulated conditions with parameters

Condition	H[m]	T_p [s]	C_x [m/s]
1	0.5	2	0
2	1	3.2	0
3	2	5.1	0
4	0.5	2	0.2
5	1	3.2	0.2
6	2	5.1	0.2
7	0.5	2	0.4
8	1	3.2	0.4
9	2	5.1	0.4
10	0.5	2	0.6
11	1	3.2	0.6
12	2	5.1	0.6

5.5.1 Static Mooring Analysis

A short note on the initial steps and the static mooring calculations performed in Aquasim are included for convenience sake, and to illustrate the catenary profile and how it is obtained. The modeling method was covered in chapter 4.2.3, where the mooring lines are modelled as straight lines between the estimated touchdown point and the connection plate, as seen in figure 5.9.

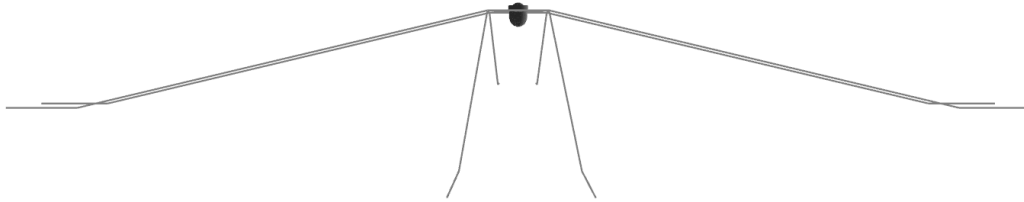


Figure 5.9: Mooring systems with straight mooring lines

The static condition is then calculated by the method described in chapter 3.10.2, until equilibrium is obtained. The program calculates the profile over several incremental steps, until the catenary profile in figure 5.10 was obtained. This procedure is executed at the beginning of each simulation. One can see a slight curvature in the square rope profile and bridle lines before any waves or current are introduced in figure 5.11. Furthermore, all lines in figure 5.11 are lifted to some extent in the corner of the square rope profile where the mooring buoy is attached, which provides a buoyancy force. The static tension can be found by inspecting the axial tension in mooring line 1, which is 12 568 N, which will be used as a reference for the axial tension in the succeeding chapters.

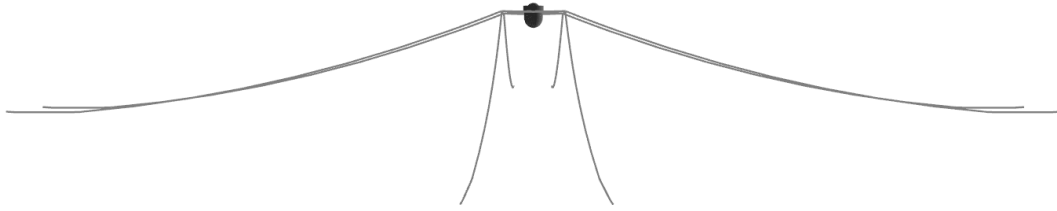


Figure 5.10: Mooring systems at static equilibrium

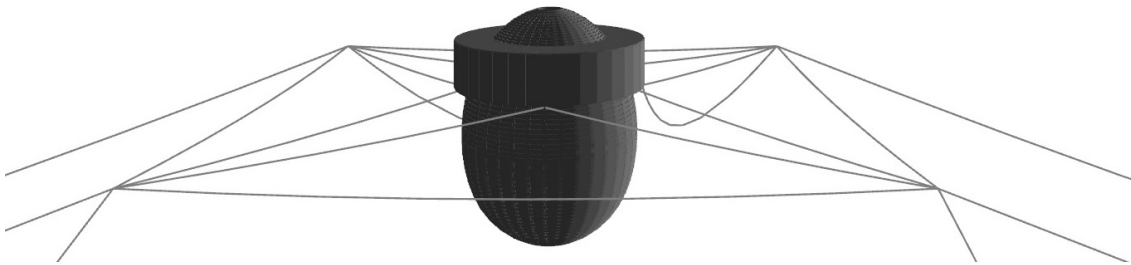


Figure 5.11: Close-up of mooring systems at static equilibrium

5.5.2 Drag Comparison of Fish Net and Fish Cage Models

Initially the simulations only considered constant current, since this setup is less complicated than a dynamic simulation with waves. The simulation model did not contain the full mooring system, but used the setup described in chapter 4.3. The fish cage was compared to the fish net with three different states of fouling and two different sinker tubes. The states of fouling were set to be a clean net with 0% growth, a net with 20% growth, and a net with 50% growth. The obtained results are a valuable contribution to the complete load picture, and understanding of how the system behaves after some exposure in the sea. The load variation in connection to the surface roughness of the egg have not been studied because of the conceptual state of the

fish cage. The change of surface roughness caused by marine growth will alter the total load and tension in the mooring lines, but the clean fish cage will serve as a benchmark in the further evaluation of the conducted work. Additionally, calculated drag results using the basic drag equation was included to compare the output from that obtained in AquaSim.

The drag force from the fish cage is represented in figure 5.12 with a cyan color and the fish net results are generated using a sinker tube weight of 75 kg/m. The drag loads on the fish cage are behaving almost linear and the increase in drag with increasing fouling is close to constant. However, in the event of 50% marine growth, there is a slight decrease in the progression of the drag load between 1m/s and 1,5m/s. This is most likely a result of the large deformation of the fish net that occurs at such high current velocities. The deformation of the fish net at all current velocities are included in Appendix C.

The drag load of the fish cage model closely resembles a quadratic line similar to that of the analytical results plotted with a pink line. This is expected when equation 3.27 is used to calculate the drag load, as presented in chapter 3.7. Even though the drag coefficient is identical in the analytical result and the AquaSim model, there is quite a difference in the resulting drag force. Lastly, the drag force stays below the load range of the fish net for all current speeds below 1,2 m/s. Which, by these drag-only simulations, makes it plausible to exchange the fish net with a fish cage, but simulations with full mooring systems should be evaluated as well, to capture the forces and dynamic behavior of the fully coupled system.

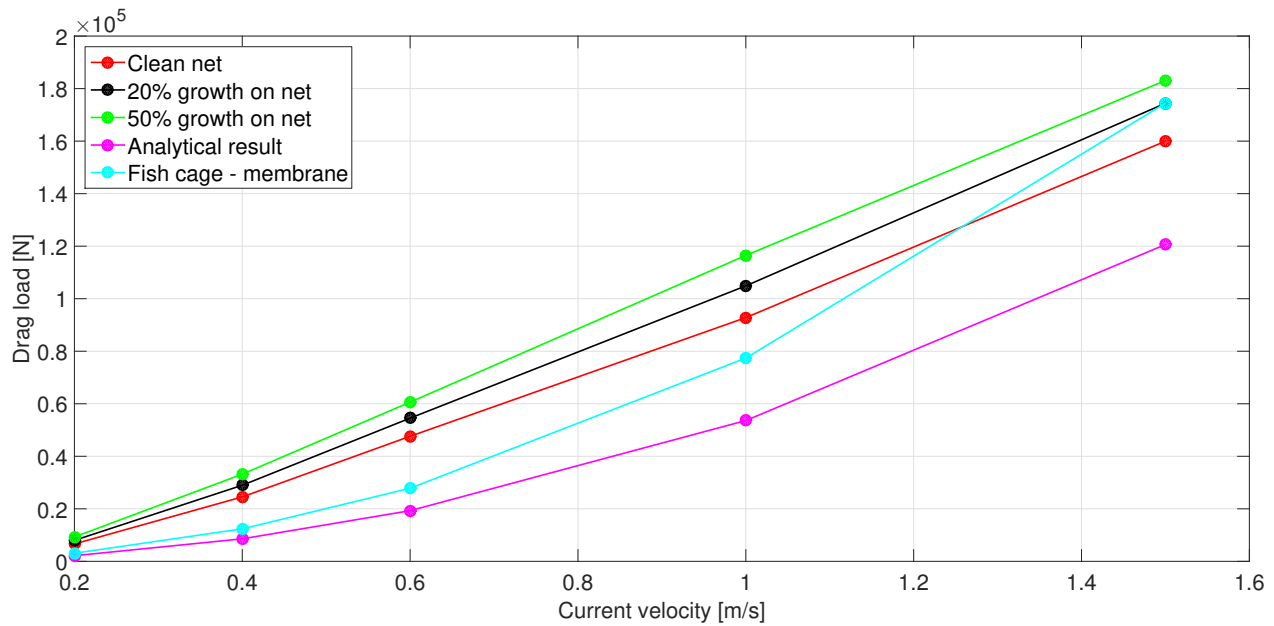


Figure 5.12: Drag with sinker tube weight 75 kg/m

Another set of simulations were executed with a heavier sinker tube, weighing 135 kg/m, to investigate the effect of this component. The immediate effect is that the fish cage maintains its initial shape for higher current speeds and the drag loads increase compared to the results in figure 5.13 using a sinker tube weight of 75 kg/m. The drag loads of the fish net also maintain an almost linear progression in this case, but shifts all of its drag values higher up on the y-axis, surpassing the drag loads of the fish cage for all current velocities.

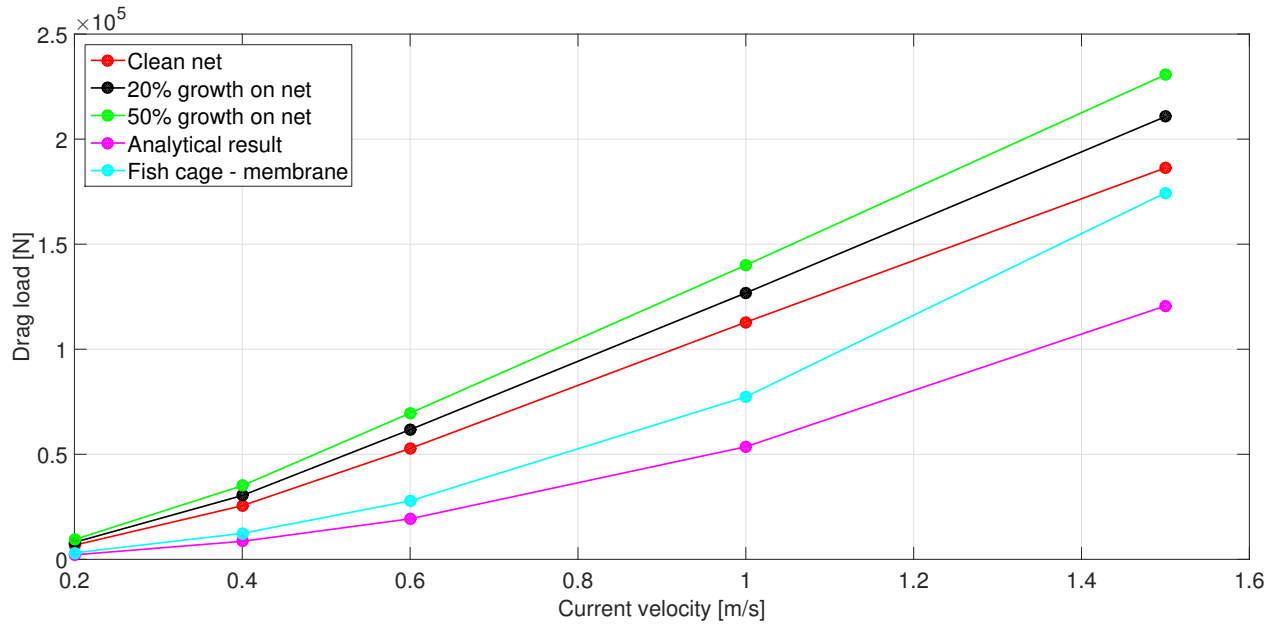


Figure 5.13: Drag with sinker tube weight 135 kg/m

These simulations clearly suggest that the sinker tube weight is a major factor regarding the deformation of the fish net with increasing current. A heavier sinker tube is able to maintain the shape of the fish net for higher current velocities, and the resulting drag force is increasing because of the larger projected area in the loading direction. Lastly the welfare of the fish stock needs to be maintained and is an important, but non-structural aspect of the fish net deformation.

5.5.3 Mooring Analysis of Fish Net, Waves Only

To comply with the NS9415 standard, all analyses used a growth coefficient of 50%. Tension plots from simulation condition 1, 2, and 3 are included in figure 5.18, 5.19 and 5.20. These simulations use the full mooring system, but only include waves. The initial steps calculate the static tension due to the submerged weight of the mooring line and are equal for all three simulations. This static result can be seen as the starting point on the y-axis in the plots. The oscillating motion of the waves causes the line to experience a periodic increase and decrease of tension, due

the wave forces and the induced motion of the floating collar and net.

The mooring system configuration in this case, separates the top of the mooring line and the floating collar by a horizontal distance of 14 meters, as seen in figure 5.14. The floating buoy at each corner of the square rope profile follows the waves as they pass its location, but the horizontal distance between the floating collar and the floating buoy can make them translate in- or out of synchronization, dependent on the wave length. Which in a worst-case scenario can make them translate in opposite directions, which will make the system experience snap loads. Snap loads are identified as short but rapidly increasing loads, often seen as sharp peaks in the results.

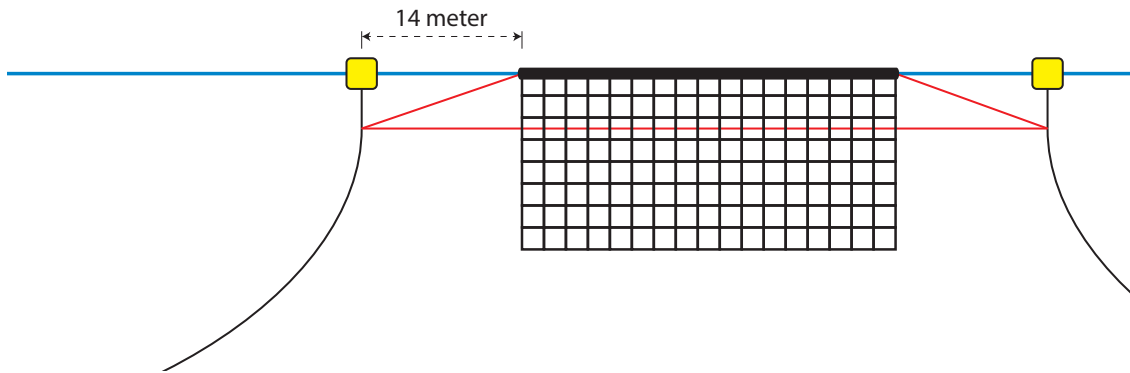


Figure 5.14: Horizontal length between bouy and floater

Condition 1, starts at a static tension value of 12 568 N, found from the initial tension due to the submerged weight of the mooring line. The tension plot starts out a bit rough as the first two waves propagate past the net, before the tension oscillation settles in a repeating pattern for the whole length of the simulation. The load variations are small, as a result of the small wave height specified in this wave condition. Figure 5.15 illustrate the wave height in comparison to the floating collar of the fish net.

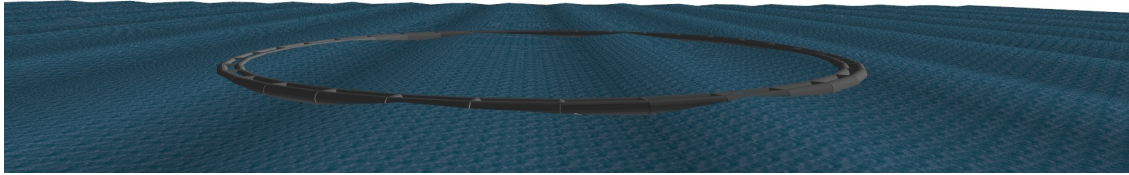


Figure 5.15: Wave condition 1 with fish net

Condition 2 behave similar to condition 1, but contains much higher peak values. This happens because the fish net does not follow the waves in a harmonic motion. The high peak values occur because the fish net doesn't follow the waves in a harmonic motion, but the floater remains mostly level with some short free spans between the waves. The floating buoy however, does follow the waves, and the vertical difference in movement adds to the high load fluctuation. Wave condition 2 in relation to the fish is included in figure 5.16.

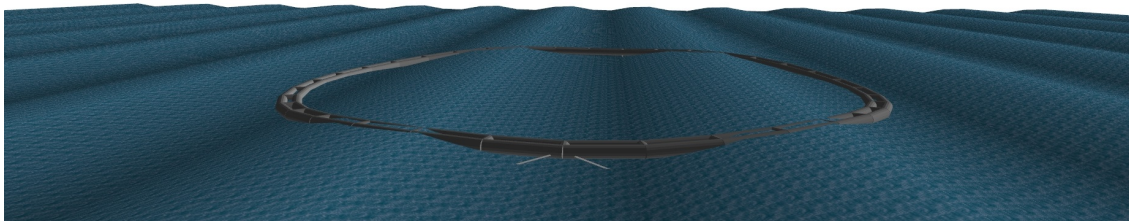


Figure 5.16: Wave condition 2 with fish net

This is not the case for condition 3, were the peak values are mostly snap loads, indicated by the sharp peak at each top. Such loads are undesirable as they tend to put immense fatigue on the system. Additionally, there was exerted a large amount of bending forces on the floater as

it deformed in the waves, however, the structural integrity of the fish net was assumed to be adequate. The load variation on the other hand is much smaller than in condition 2. Also note how there is a slow increase in mean tension during the first 80 seconds of simulated time, most likely caused by wave drift, which puts an increasingly larger mean tension load in the mooring line.

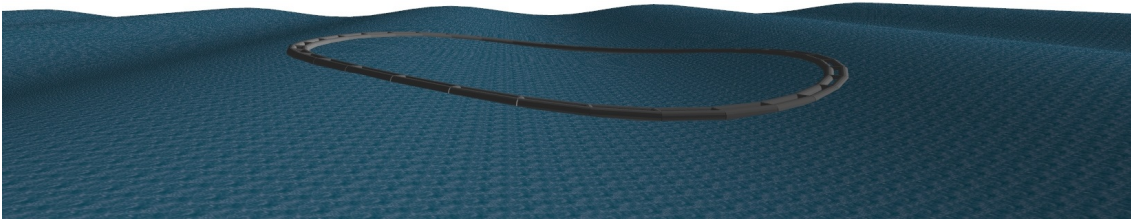


Figure 5.17: Wave condition 3 with fish net

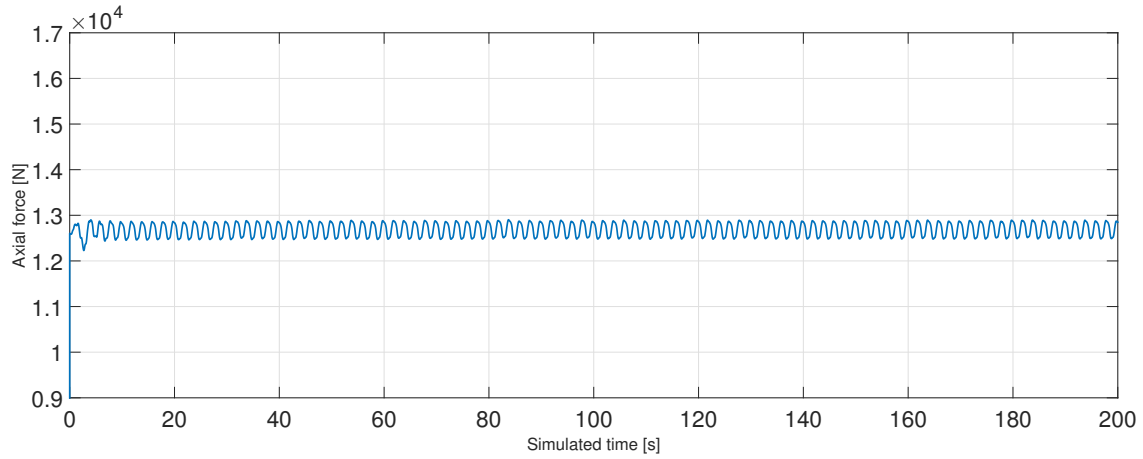


Figure 5.18: Axial force in mooring line 1 for condition 1, waves only

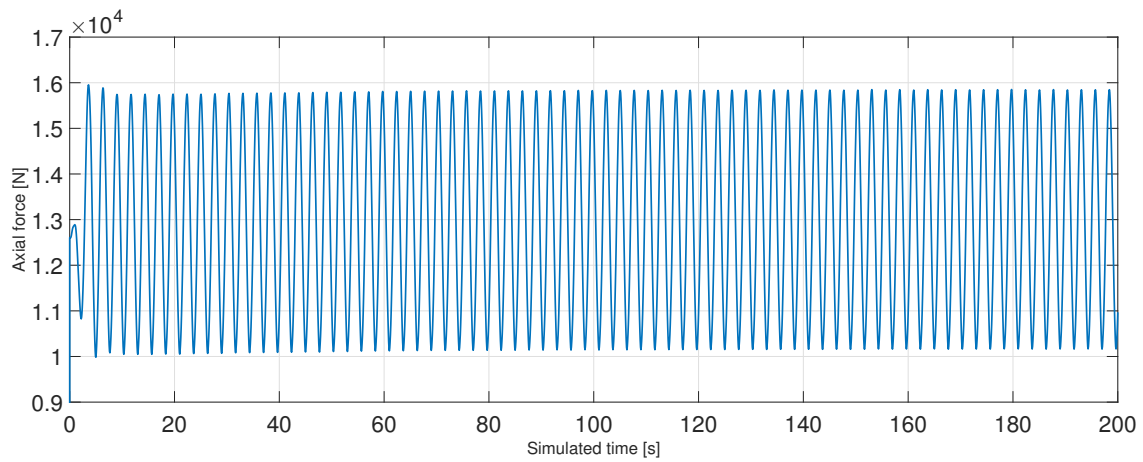


Figure 5.19: Axial force in mooring line 1 for condition 2, waves only

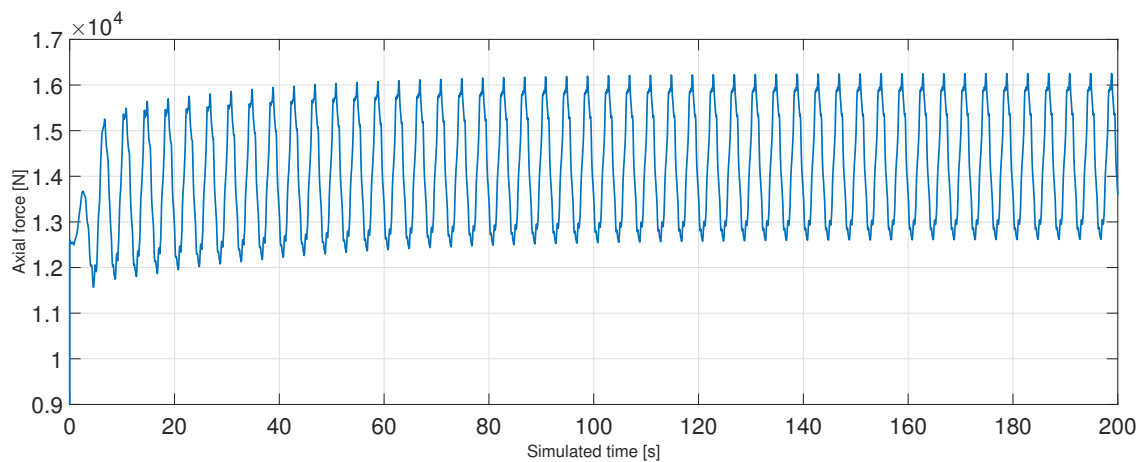


Figure 5.20: Axial force in mooring line 1 for condition 3, waves only

5.5.4 Mooring Analysis of Fish Cage, Waves Only

The fish cage behaves similar to the fish net for simulation case 1 and 2 with a load that oscillates around the static tension value at the top of the mooring line. Recalling that the heave response is particularly high for waves in the frequency range of 0,11 – 0,13Hz, equaling a wave period of 9,1s – 7,7s. And the fact that the wave frequency is out of the critical range of the RAO of the system for all simulation conditions, should keep the heaving motion under control. The resulting load variation is thus smaller for this system which is partly due to the large mass of the water filled fish cage, which causes the system oscillation to be out of synchronization with the harmonic frequency of the waves, as proven through the RAO results. Another important contributing factor to the reduced load variation is the smaller dimensions of the fish cage, with an outer diameter of 19m compared to the fish net with a floater diameter of 32m. Figure 5.21 shows the fish cage exposed to wave condition 1, that contains the smallest wave amplitude. The fish cage remains stable and no waves overtops the floating collar.

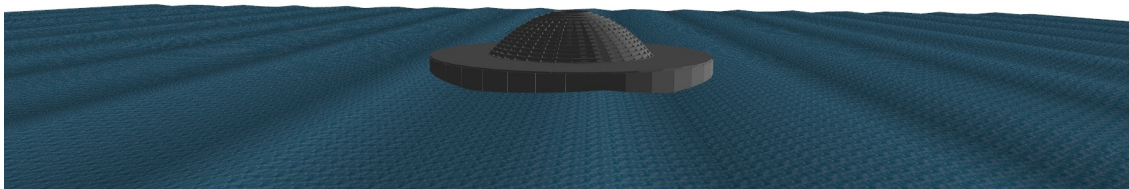


Figure 5.21: Wave condition 1

The results of wave condition 2 are very similar to wave condition 1, but with fewer waves in the same time frame as the wave length is longer. The load oscillation peaks are higher as expected from larger waves, and no waves overtops the floating collar. Furthermore, the fish cage remains stable without much rolling or heaving motions.

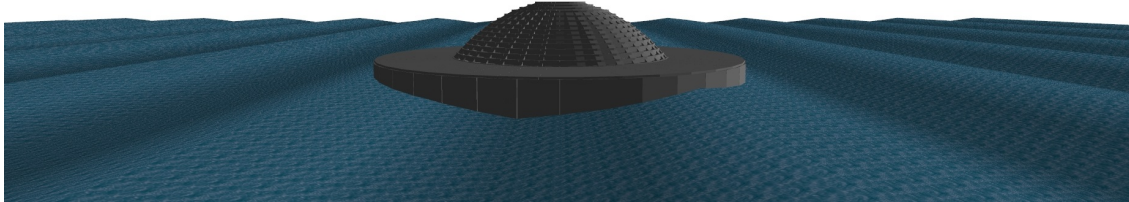


Figure 5.22: Wave condition 2

Simulation case 3 is the most interesting as it behaves quite different than the other simulated cases. The system experience a mean reduction of the tension in mooring line 1, before the load oscillations stabilize at a mean value much lower than for the previous cases. This unpredicted result was further inspected in Aquaview, to supplement the plots with a graphical animation.

During the simulation runs, the wave crest elevation reached above the top of the floating collar with wave conditions at 2m wave height, and 5,1s period, as seen in figure 5.23. However, the waves only overtop the floating collar in the upwind direction, which pushes the fish cage down into the water on one side, contributing to a rolling motion.

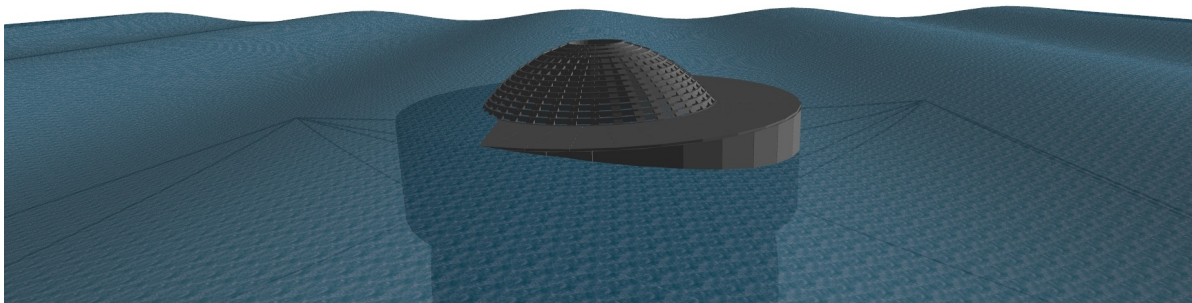


Figure 5.23: Wave condition 3, overtopping the floating collar

This is an interesting and important discovery, since it could be the main limiting factor with respect to certification of the system according to the classification of the NS9415 standard, assuming that waves overtopping the upper part of the floating collar is undesirable. When waves progress above the floating collar, they are in direct line with the control room, and working area of the operating personnel, endangering their working environment as well as increasing the operational risk. The results have been included since the structure itself is expected to withstand such loads, despite the evident disadvantage of such an event, and the associated uncertainty of how the wave propagation above the floating collar affect the credibility of the results.

Furthermore, there is a horizontal translation in the opposite way of the wave propagation which is in the positive x-direction. This translation causes mooring line 1 and 2 to slacken, which moves the tdp towards the fish cage, and that effectively removes some tension from the lines due to a shorter amount of suspended mooring line. The translation continues until the restoring force of the opposing mooring lines equals the translating force, and the system stabilizes after a translation of approximately 3,5 meter.

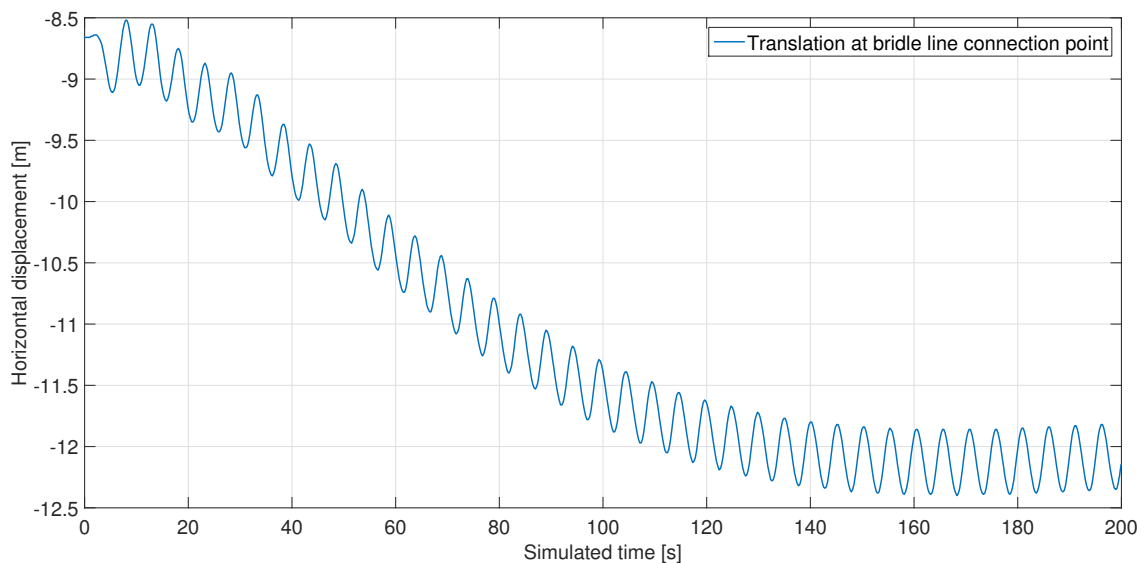


Figure 5.24: Horizontal translation of bridle line connection point

By inspecting the vertical translation of the first anchor chain node point for both anchor chain 1 and 6, it is clear to see how the movement of the tdp affects the difference in suspended length of mooring line at each side of the fish cage. The anchor chain in mooring line 1 settles at the bottom, and only minor oscillations are visible in figure 5.25. The first anchor chain node in mooring line 6 is lifted approximately 1,2 meters of the sea bed, which causes a tension increase due to the increased suspended length. Thus, the load increase is higher for mooring line 6 in comparison to the load reduction in mooring line 1, since the increased suspended length is comprised of heavier anchor chain, while the decreased length of mooring line 1 only consists of lightweight fiber rope.

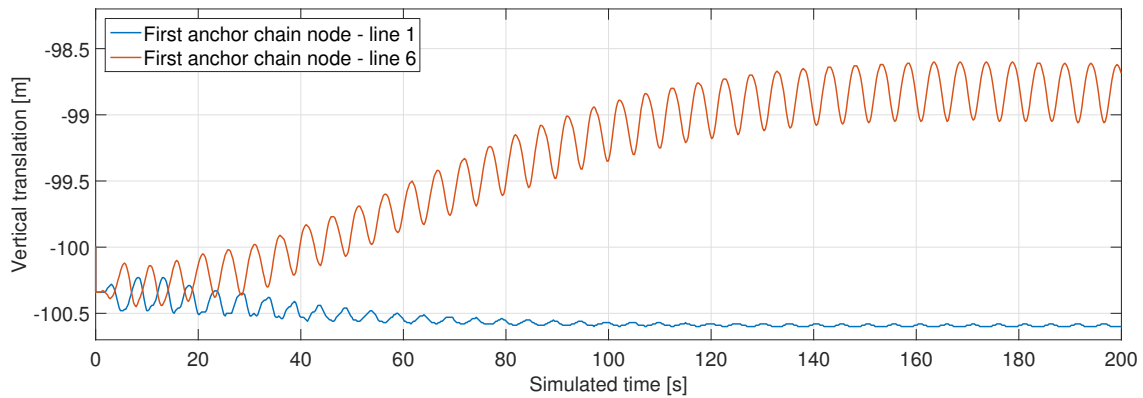


Figure 5.25: Vertical anchor chain node translation

Figure 5.26 shows the relation between the tension build-up in mooring line 1 and mooring line 6. Note how there is a unsymmetrical difference in the load reduction in mooring line 1 and the load increase in mooring line 6. Similar comparisons of these specific mooring line results are not included in the following chapters, as the inclusion of current forces moves the fish cage in the same way as the wave propagation. The associated drag load in these simulations causes mooring line 1 to retain the highest tension for all conditions including current.

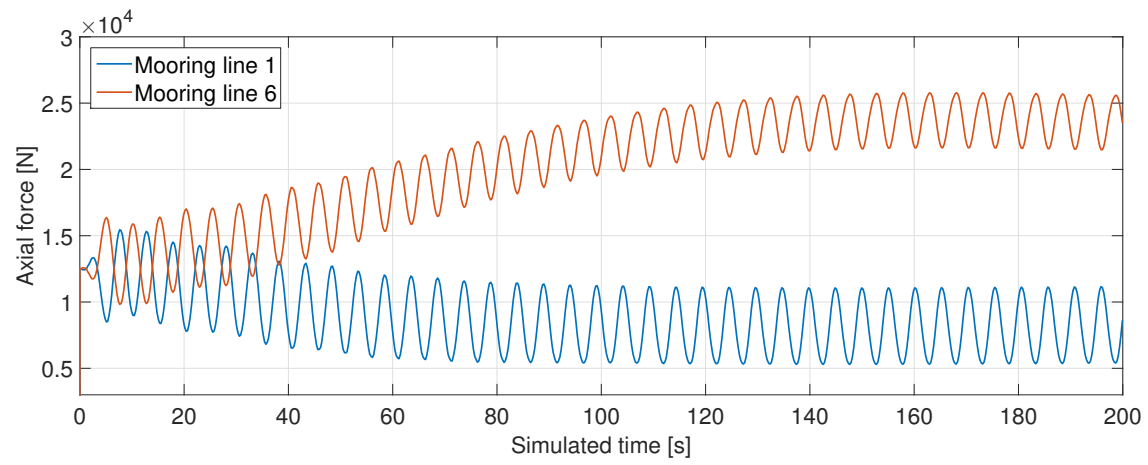


Figure 5.26: Axial force in opposite mooring lines

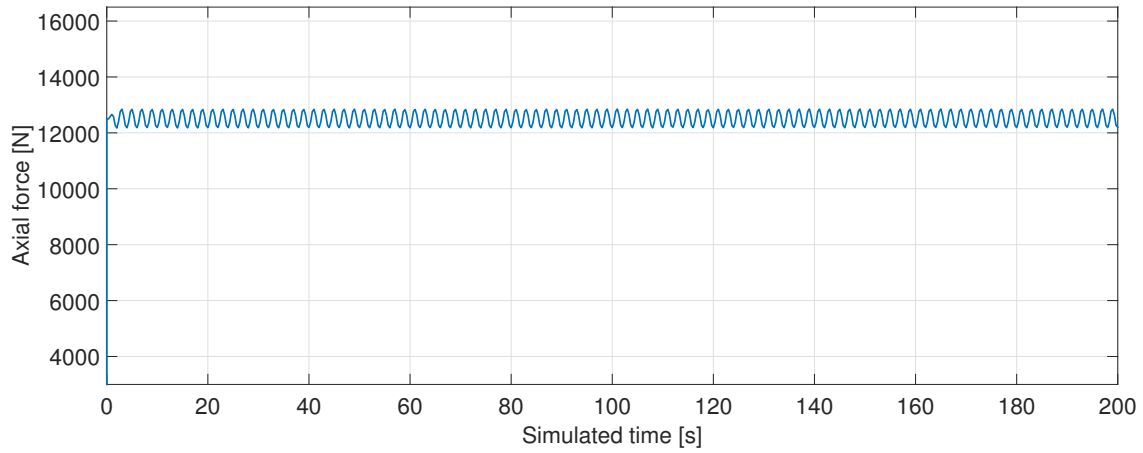


Figure 5.27: Axial force in mooring line 1 for condition 1, waves only

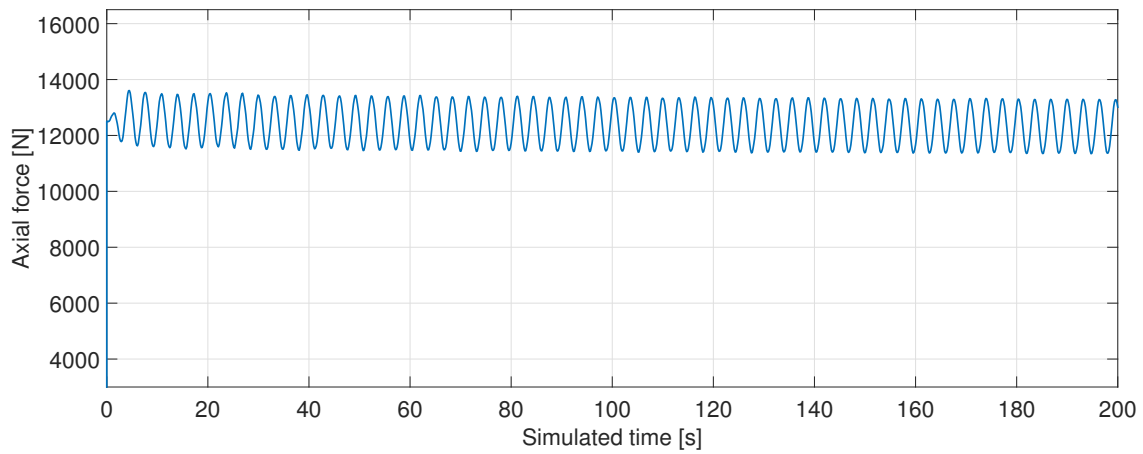


Figure 5.28: Axial force in mooring line 1 for condition 2, waves only

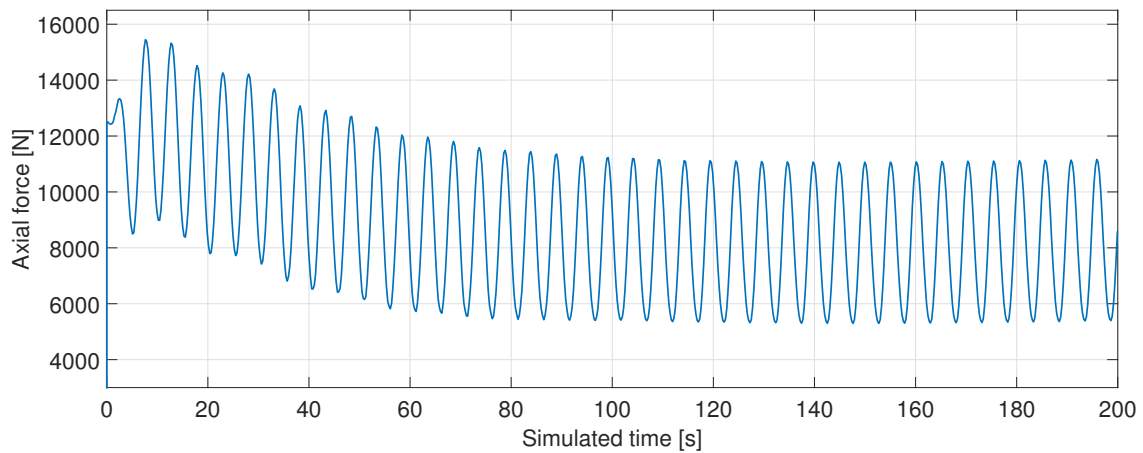


Figure 5.29: Axial force in mooring line 1 for condition 3, waves only

5.5.5 Comparison of Mooring Analysis of Fish Net and Fish Cage

A comparison study of the predefined conditions was conducted to better identify differences between both systems. Current were introduced to analyze a combined loading condition with both waves and current, as the previous chapter only considered waves. All simulation conditions containing the same current velocity are plotted in the same plots. That equates to 6 plotted lines per plot, representing 3 conditions for the fish cage and 3 conditions for the fish net. Due to time constraints and long simulation runs, conditions with current velocities at 1 and 1,5 m/s were abandoned. This is partly justified with the high deformation of the fish net at these velocities, which makes it debatable whether the fish welfare is maintained, and the rarity of such high current events.

Condition 4, 5, and 6

Case 4, 5, and 6 simulates the combined loading of all wave conditions with a current velocity of 0,2 m/s. Figure 5.30 clearly captures the different drag forces of the two systems, and the oscillating load due to the waves. The static condition with current only is calculated during the first 5 initial steps of the simulation. Then the wave height gradually builds up during the first two generated waves in the simulation, before the regular wave set remains constant for the rest of the simulation. The difference in initial tension was expected because of the different values of tension in figure 5.12 and 5.13. By inspecting this drag only plot, one expect to see an incremental increase in static tension, with increasing current velocity. The static tension in the mooring line for the fish cage settles at around 13 780 N, which is approximately 1 200 N higher than in conditions with zero current. The additional tension in comparison to condition 1, 2 and 3 are a result of the horizontal drag load imposed on the system. The fish net maintains a marginally higher drag load which contributes to a slightly higher static tension of 16 000 N at a current velocity of 0,2 m/s.

Another interesting feature of the same plot is the difference in tension build-up in both systems. The fish net reaches a steady state at approximately 80 seconds while the fish cage needs around 160 seconds to reach the same steady state of tension.

There is also a difference in the behavior of the tension build-up in the mooring line for the two systems. When the fish net was attached to the mooring system, there was a rapid increase in tension for the two wave conditions containing the biggest waves. In comparison, there was a different pattern regarding the load build-up for the closed fish cage, where the tension gradually builds up over a longer time period and settles at a lower mean value. As expected, the oscillating tension due to the difference in wave parameters stays incrementally higher for higher wave conditions.

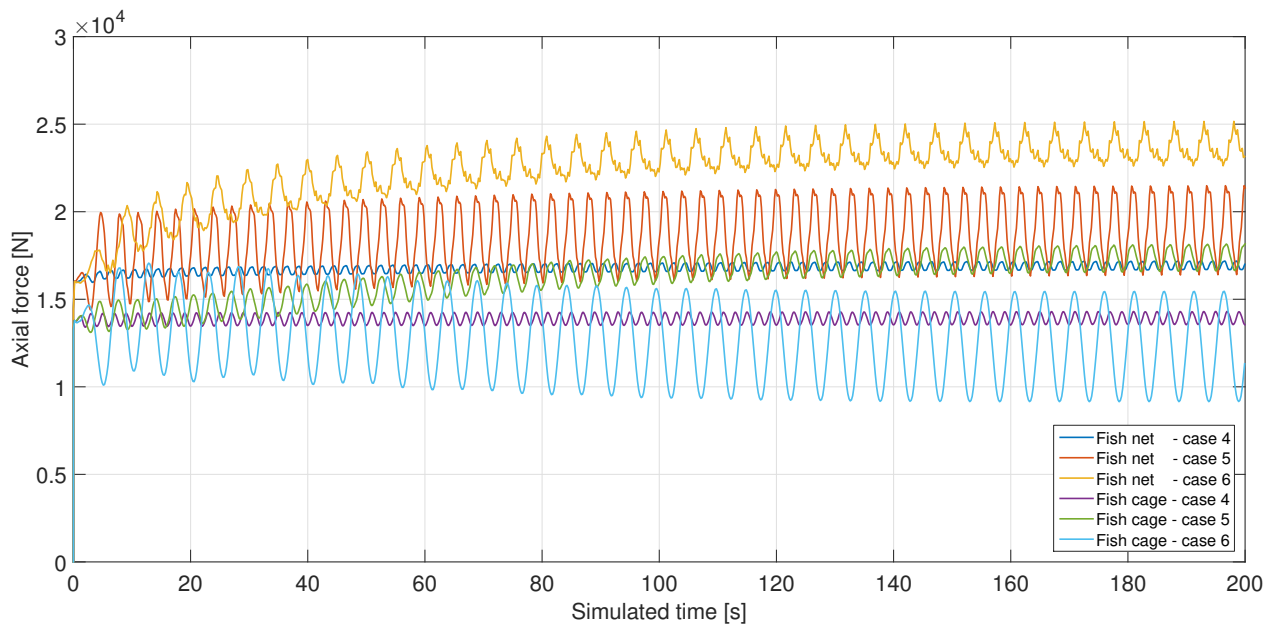


Figure 5.30: Axial force in mooring line 1 for case 4, 5 , and 6

Condition 7, 8, and 9

The fish net behaves as expected, with tension plots of increasing magnitude for higher wave period and wave height. The result of simulation condition 9 is noticeably different to the other two lines which follows a symmetric, oscillating pattern. There is a smaller load variation caused by the waves, and the load follows a rougher path. Once again, the source of these ragged load peaks, are a direct consequence of a snap load transferred through the bridal line as the floater follows the waves at a different rate than the top of the mooring line. The plot still maintains a positive incline after the simulation stops at 200 sek, which implies that the maximum value is of even higher magnitude than that obtained in the simulation. A longer simulation timeframe should be set up to capture the maximum value. However, the difference between these values and those representing the highest values of the fish cage are already such difference that the results were kept as is. The load variation of condition 7 and 8, are close to that of condition 4 and 5, but with a more defined spread and doesn't overlap each other no more.

By inspection of the results for the fish cage, one can see that the load condition with the highest mean tension are condition 8. Despite being the resulting simulation with the highest mooring line tension, it never reaches the tension value of the fish net exposed to the smallest wave condition. This difference will be reduced by altering the amount of marine growth of the fish net, which was set to 50%, as explained in chapter 5.5.3. Condition 9 contains the highest waves and corresponding wave periods, but levels out at a lower mean value than condition 8. Nonetheless, it contains the biggest load fluctuation as expected because of the larger waves. Once again, the result seems to be effected by the reduction in mooring line tension observed in case 3, but experience an incremental increase in comparison to the previous simulation set, that shifts it closer to case 8.

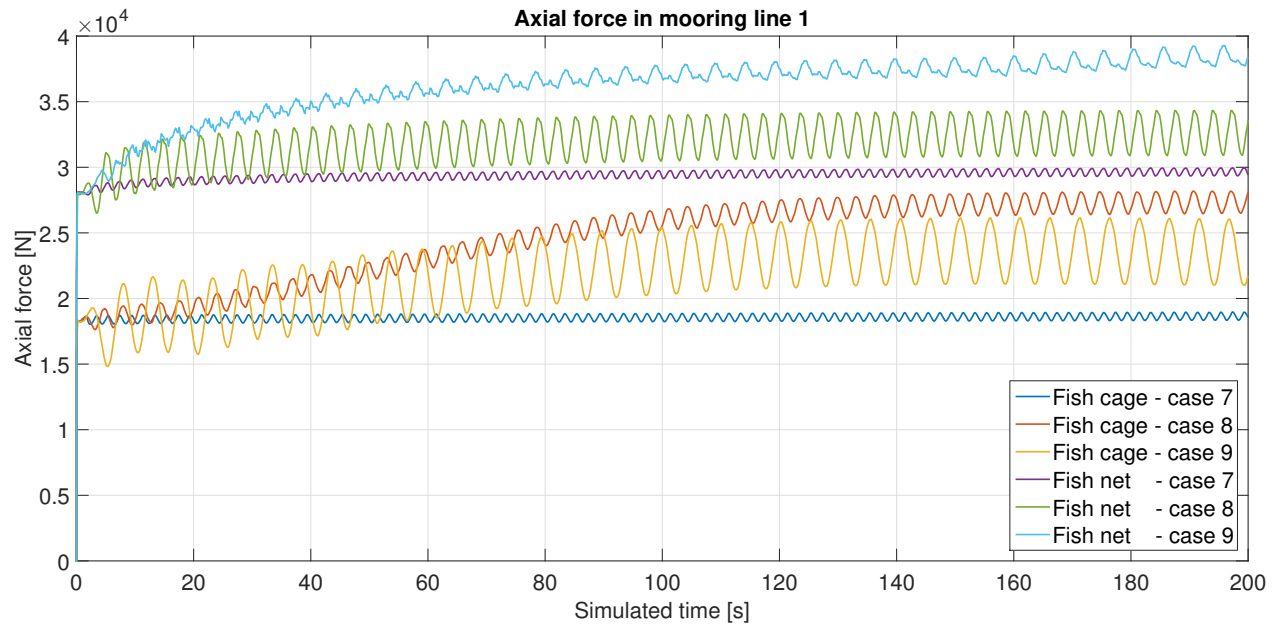


Figure 5.31: Axial force in mooring line 1 for case 7, 8 , and 9

Condition 10, 11, and 12

Loading condition 10, 11, and 12 are plotted in figure 5.32. The static starting tension have shifted even higher as a result of the higher current velocity and resulting drag force. Condition 12 for the fish cage have obtained a smoother plot line, with some of the ragged peaks removed. This is most likely a result of the higher mean tension in the mooring line, due to the higher current velocity, which restricts the load reduction in the wave trough, which again counteracts some of the snap loads. There is still a sharp peak at both top and bottom of the oscillations, but not as much as the previous condition. However, even though some of the sharp peaks have been removed, there is a notable increase in tension compared to case 9.

Condition 10 concerning the fish cage is still governed by current and static forces, and only experience small oscillations of tension around the static value. Case 11 maintains its sloping increase before it settles at a value higher than the static value. Interestingly, it is first at a current velocity of 0,6 m/s that the plotted line of case 12 and 11 follows almost the same path. Even though the wave condition with 2m wave height reaches the same level of tension as wave

condition with 1m wave height, it still exerts higher load variation because of the higher waves. More importantly, however, is the fact that the fish cage still has not reached the same level of tension as the fishing net, and that there is still a distinct separation of the results for both systems.

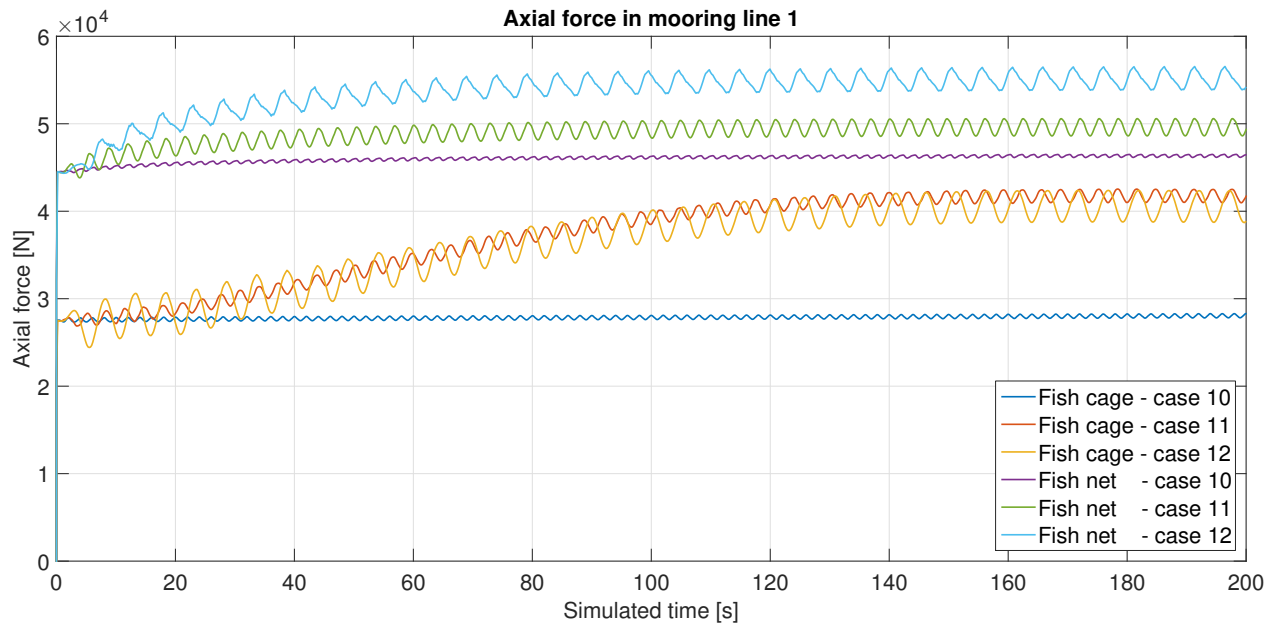


Figure 5.32: Axial force in mooring line 1 for case 10, 11 , and 12

6. Conclusions

This study, serves as an early investigation of the forces exerted on the mooring system of a fish farm with two different fish containment elements. The work carried out, sets out to check whether it would be possible to replace a fish net with a new closed egg-shaped fish cage, but also to determine if there is any purpose to proceed with the study after the evaluation of these first results.

A comparison study has been conducted regarding the mooring system of a regular fish net, and a closed cage shaped as an egg with a circular floating collar. Initially, the wave regimes and associated wave theory was established, as well as a set of wave and current conditions in accordance with the classification system in Norwegian Standard NS9415.

Even though a significant amount of wave forces are observed in the analytical approach, the same amount of forces are not evident in the dynamic simulations. This might be a result of the spherical shape that is used in the numerical model, in comparison to the regular cylinder that is used in the analytical approach, and the way it influences the wave interaction. Nevertheless, there is a large difference in forces. And even though the dynamic simulations don't capture these values as axial tension in the mooring lines, one should still acknowledge these forces as structural concerns. Secondly, the lack of a dampening effect from the mooring system, and the omission of movement in the hand calculation, may produce conservative results. At this point, model testing seems to be required to establish the dynamic effects of the fish cage.

The final models of both the fish net and the fish cage were modelled in AquaEdit, comprising the necessary membrane, beam, and truss elements, to make up the mooring system and the structures. The modeling approach of combining both beam elements and dense net mem-

branes for the fish cage was verified as robust a approach by Aquastructures, and captures the effect of the large water filled volume inside the fish cage.

Drag loads on the fish net were calculated with two different sinker tubes, and increasing marine growth. The results were compared to that of the fish cage, and are promising for all conditions. Nonetheless, these results are dependent on the accuracy of the drag coefficient of the fish cage, which is an estimated value that needs to be further refined to obtain accurate result.

An identical spread mooring system have been used for both setups, with the length of the bridle lines as the only differencing element between the two. The mooring lines use a synthetic fiber rope for the span with an extra length of anchor chain near the anchor to prevent lifting forces at the anchor. The tension plots for both systems converge for all simulations, but the more complicated fish cage model needs more computational time to reach convergence. The fish net with marine fouling produces the highest tension output throughout all tested conditions within the same mooring configuration, which makes the interchangeability of the fish cage with the fish net plausible. However, the results of the fish cage exposed to wave condition 3, with or without current, imply that there is some uncertain behavior linked to these conditions, most likely due to the waves that overtops the floating collar.

Although the combined wave and current simulations provide satisfactory results, it is necessary to point out that the fish net uses a growth coefficient of 50%, while the fish cage is assumed to maintain a clean, smooth surface. This value was chosen because the certification rules of NS9415 requires the operator to certify the system when the fish net has a growth coefficient of 50%. Based upon this, it is advisable to perform the same tests and simulations with a variable growth coefficient, to identify the effect of a variable growth coefficient for the fish cage as well.

7. Further Work

One should determine if it is acceptable to have waves overtopping the floating collar of the fish cage. And more attention should be focused on wave height relative to the freeboard height of the floating collar, if this is chosen as an acceptable event. The simulation model may also benefit from further refinement of the floating collar and the structure above the swl, due to the uncertain behavior of the results linked to the overtopping situation.

The mooring line composition (fiber rope mooring lines with chain on the seafloor) and material are highly influential factors, and different compositions and heavier mooring chains can be considered. Water depth was set to 100m throughout this thesis, but it is known to vary between different locations, and experiments at shallower waters should be conducted. Shallower water depths will influence the mooring lines and the necessary step out distance of the anchors. It would be hard to improve on the general results without more specific material data and features of both systems, as they tend to change with location of the fish farms.

The drag coefficient of the fish cage, C_D , is an estimated value with an associated uncertainty. Model test or CFD analysis may be used to establish a more reliable drag coefficient before any further studies are commenced, due to the influence this value has on the results.

It would be possible to analyze a higher number of environmental conditions, with even higher and longer waves. Secondly, it is important that the design value for the current are fully documented, taking tidal currents and storm surge currents into consideration. Nevertheless, the NS9415 standard requires the contractor to analyze each system with input from local, long term measurements at each location of interest. Thus, the usefulness of further studies without legitimate data will be questionable.

Bibliography

- Akva-Group (n.d.). Marine Fouling [Picture]. Available at: <http://www.akvagroup.com/Products/Cage%20farming%20aquaculture%20products/Net%20Cleaning%20Systems/effective-net-cleaning.jpg?w=767&h=386&bg=ffffff> Accessed [30.05.2017].
- Aquastructures (2014). *The AquaSim Package user manual*. DOC NO: TR-30000-2049-1.
- Aquastructures (n.d.). AquaSim 2.12 [Software Program]. Available at: <http://aquastructures.no/aquasim/> Accessed [01.02.2017].
- Badinotti Group (n.d.). Mooring Equipment [Online]. Available at: http://www.badinotti.com/prod_mooring.html Accessed [24.02.2017].
- Bergdahl, L. (2009). Wave-induced loads and ship motions. Technical report, Chalmers University of Technology, Göteborg.
- Berstad, A. J. and Heimstad, L. F. (2015). Numerical formulation of sea loads to impermeable nets. In *Proceedings of the VI International Conference on Computational Methods in Marine Engineering*. MARINE 2015, Rome, Italy.
- Berstad, A. J., Walaunet, J., and Heimstad, L. F. (2012). Loads from currents and waves on net structures. In *Proceedings of the ASME 2012 31st International Conference on Ocean, Offshore and Arctic Engineering*, number OMAE2012-83757, pages 95–104. OMAE2012, Rio de Janeiro, Brazil.
- Chadwick, E., Parsons, G., Sayavong, B., and Canada, N. R. C. (2010). *Evaluation of Closed-containment Technologies for Saltwater Salmon Aquaculture*. NRC Research Press, Ottawa, Ontario, Canada.

- Chakrabarti, S. (2005). *Handbook of Offshore Engineering (2-volume set)*. Elsevier Ocean Engineering Series. Elsevier Science, Burlington.
- Chakrabarti, S. K. (1987a). *Hydrodynamics of offshore structures*. Computational Mechanics Publications, Southampton.
- Chakrabarti, S. K. (1987b). *Hydrodynamics of offshore structures [Picture]*. Computational Mechanics Publications, Southampton. page 323.
- DNV GL (n.d.a). GeniE [Software Program]. Available at: <https://www.dnvgl.com/services/conceptual-modelling-of-offshore-and-maritime-structures-genie-89128> Accessed [26.01.2017].
- DNV GL (n.d.b). HydroD [Software Program]. Available at: <https://www.dnvgl.com/services/stability-analysis-tool-hydrod-14492> Accessed [09.02.2017].
- Eiva-Safex (n.d.a). Anchor chain [Picture]. Available at: <http://eiva-safex.no/havbruk/langlenket-galvanisert-kjetting/> Accessed [03.03.2017].
- Eiva-Safex (n.d.b). Buoyancy element [Picture]. Available at: <http://eiva-safex.no/wp-content/uploads/2016/05/Poleyform-Aqua.png> Accessed [05.03.2017].
- Eiva-Safex (n.d.c). Fiber rope [Picture]. Available at: <http://eiva-safex.no/havbruk/tau-og-trosser/> Accessed [05.03.2017].
- Eiva-Safex (n.d.). Fortøyningsbøyer [Online]. Available at: <http://eiva-safex.no/havbruk/fortoyningsboyer/> Accessed [24.02.2017].
- Çengel, Y. A. and Cimbala, J. M. (2014). *Fluid mechanics : fundamentals and applications*. McGraw-Hill, Boston, 3rd ed. in SI units edition.
- Faltinsen, O. M. (1990). *Sea loads on ships and offshore structures*. Cambridge ocean technology series. Cambridge University Press, Cambridge.
- FAO (2014a). The state of world fisheries and aquaculture, , food and agriculture organization of the united nations. Report, Food and Agriculture Organization of the United Nations, Rome, Italy.

- FAO (2014b). The state of world fisheries and aquaculture [Picture]. Available at: <http://www.fao.org/3/a-i3720e.pdf> Accessed [06.02.2017].
- Fiskeridirektoratet (2015). Rømmningsstatistikk [Online]. Available at: <http://www.fiskeridir.no/Akvakultur/Statistikk-akvakultur/Roemningsstatistikk> Accessed [06.02.2017].
- Fiskeridirektoratet (2016). Utviklingstillatelser [Online]. Available at: <http://www.fiskeridir.no/Akvakultur/Tildeling-og-tillatelser/Saertillatelser/Utviklingstillatelser> Accessed [06.02.2017].
- Gansel, L. C., Plew, D. R., Endresen, P. C., Olsen, A. I., Misimi, E., Guenther, J., and Jensen, Ø. (2015). Drag of clean and fouled net panels—measurements and parameterization of fouling. *PloS one*, 10(7):e0131051.
- Garrett, C. J. R. (1971). Wave forces on a circular dock. *Journal of Fluid Mechanics*, 46(1):page 129–139.
- Hauge Aqua (n.d.a). Anchoring system [Picture]. Available at: <http://www.haugeaqua.com/images/viewimage.aspx?id=63> Accessed [23.01.2017].
- Hauge Aqua (n.d.b). Technology [Online]. Available at: <http://www.haugeaqua.com/Technology/> Accessed [04.01.2017].
- Johnsen, I. A., Fiksen, ., Sandvik, A. D., and Asplin, L. (2014). Vertical salmon lice behaviour as a response to environmental conditions and its influence on regional dispersion in a fjord system. *Aquaculture Environment Interactions*, 5(2):127–141.
- Laksefakta (n.d.). Norsk Havbrukshistorie [Online]. Available at: <https://laksefakta.no/> Accessed [27.01.2017].
- Lien, A. M. and Volent, Z. (2012). Deformasjon av not og permaskjørt og krefter på fortøyning. Technical report, SINTEF. Language: Nor.
- Mark G. J. Hartl, D. W. and Davenport, J. (2006). Biofouling in the marine aquaculture industry, with particular reference to finfish – current status and future challenges: Marine

- estate research report. Technical report, Department of Zoology, Ecology and Plant Science, University College Cork.
- McCamy, R. C. and Fuchs, R. A. (1954). Wave forces on piles: A diffraction theory. Technical report, Tech. Memo No 69, U.S. Army Corps of Engineers, Beach Erosion Board.
- McCormick, M. E. (2010a). *Ocean Engineering Mechanics : With Applications*. Cambridge University Press, New York.
- McCormick, M. E. (2010b). *Ocean Engineering Mechanics : With Applications [picture]*. Cambridge University Press. page 322.
- Miles, J. and Gilbert, F. (1968). Scattering of gravity waves by a circular dock. *Journal of Fluid Mechanics*, 34(4):page 783–793.
- Miljøstatus (2015). Fiskeoppdrett – en næring i vekst [Online]. Available at: <http://www.miljostatus.no/Tema/Hav-og-kyst/Fiskeoppdrett/#heading1> Accessed [12.01.2017].
- Morison, J., Johnson, J., Schaaf, S., et al. (1950). The force exerted by surface waves on piles. *Journal of Petroleum Technology*, 2(05):149–154.
- Nærings- og fiskeridepartementet (2011). Forskrift om krav til teknisk standard for flytende akvakulturanlegg (NYTEK).
- Rosten, T. W., Ulgenes, Y., Henriksen, K., Terjesen, B. F., Biering, E., and Winther, U. (2011). Oppdrett av laks og ørret i lukkede anlegg - forprosjekt Utredning for Fiskeri og havbruksnæringens forskningsfond (FHF). Project number: 86021201 ISBN 978-82-14-05212-1, SINTEF.
- Sarpkaya, T. (2010). *Wave forces on offshore structures*. Cambridge University Press, Cambridge.
- Sarpkaya, T. and Isaacson, M. (1981). *Mechanics of wave forces on offshore structures*. Van Nostrand Reinhold, New York.
- Standard Norge (2009). NS9415.E:2009 Flytende oppdrettsanlegg: Krav til utforming, dimensjonering, utførelse, installasjon og drift.
- Sumer, B. M. and Fredsøe, J. (1997). *Hydrodynamics around cylindrical structures*, volume vol. 12 of *Advanced series on ocean engineering*. World Scientific, Singapore.
- US Cargo Control (n.d.). Anchor shackle bolt [Picture]. Available at: <http://images>.

uscargocontrol.com/1521-anchor-shackle-bolt-type-2-1-2-steel-55-ton_1_640.jpg Accessed [05.03.2017].

van Oortmerssen, G. (1971). The interaction between a vertical cylinder and regular waves. *Symposium on Offshore Hydrodynamics, Wageningen, August 25-26, 1971*, page 24.

Vónin (n.d.a). Connection plate [Picture]. Available at: https://duli17ghd8dbr.cloudfront.net/media/1538/vonin_aquaculture_mooring_system_faroe_islands.jpg?width=550 Accessed [05.03.2017].

Vónin (n.d.b). Vonin anchor [Picture]. Available at: https://duli17ghd8dbr.cloudfront.net/media/1215/vonin_anchor_3d.jpg?width=550 Accessed [05.03.2017].

A. Environmental Classification

This appendix include the wave and current classifications, described in the standard, NS9415.

A.1 Wave parameters

Wave classes	H_s [m]	T_p [s]	Description
A	0,0 - 0,5	0,0 - 2,0	Small exposure
B	0,5 - 1,0	1,6 - 3,2	Moderate exposure
C	1,0 - 2,0	2,5 - 5,1	Large exposure
D	2,0 - 3,0	4,0 - 6,7	High exposure
E	> 3,0	5,3 - 18,0	Huge exposure

A.2 Current parameters

Wave classes	U_c [m/s]	Description
a	0,0 - 0,3	Small exposure
b	0,3 - 0,5	Moderate exposure
c	0,5 - 1,0	Large exposure
d	1,0 - 1,5	High exposure
e	> 1,5	Huge exposure

B. Wave Forces by [Chadwick et al. \(2010\)](#)

Wave forces on a floating cylinder with diameter 20m and draft 8m, from “Evaluation of Closed-containment Technologies for Saltwater Salmon Aquaculture”

Table B.1: Horizontal wave forces [N] on one cylinder as presented by [Chadwick et al. \(2010\)](#)

Wave height [m]	T = 2s	T = 4s	T = 6s	T = 8s
0,5	39 498	273 863	570 678	634 730
1	78 996	547 727	1 141 802	1 269 459
2	157 993	1 139 933	2 283 603	2 538 918
3	236 989	1 643 180	3 425 405	3 808 378
4	315 826	4 567 206	4 567 206	5 077 837

C. Fish Net Deformation in Varying Current

This Appendix illustrates the deformation of the fish net in varying current, with no marine fouling. The subsequent drag loads have been presented in chapter 5.5.2

C.1 Sinker tube weight 78 kg/m

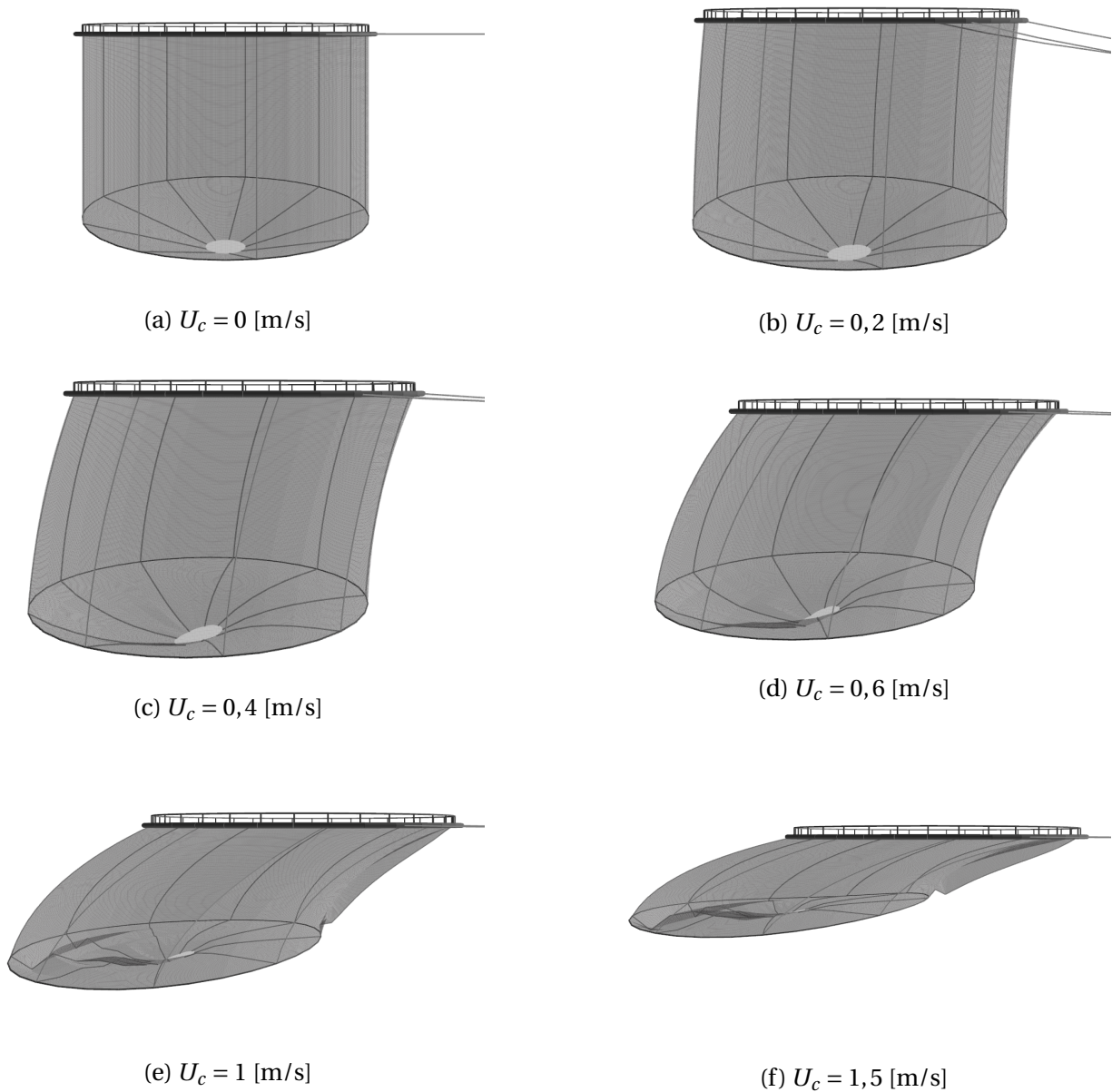
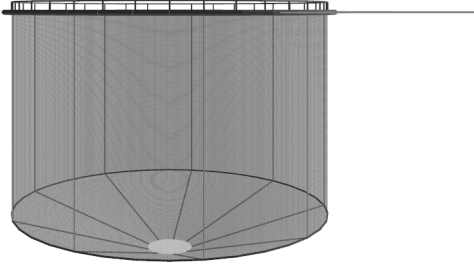
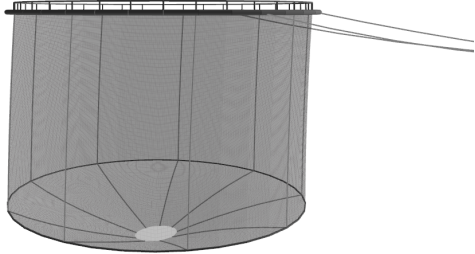


Figure C.1: Sinker tube weight, 78 kg/m

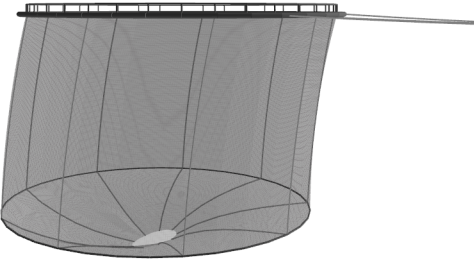
C.2 Sinker tube weight 135 kg/m



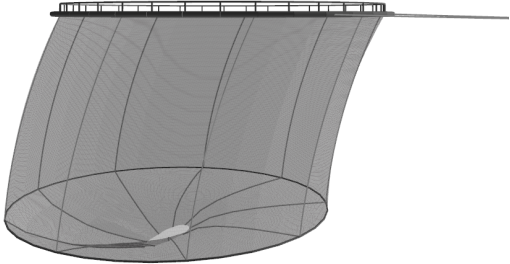
(a) $U_c = 0$ [m/s]



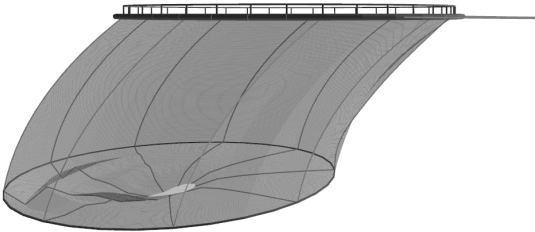
(b) $U_c = 0,2$ [m/s]



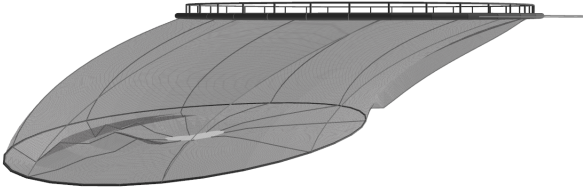
(c) $U_c = 0,4$ [m/s]



(d) $U_c = 0,6$ [m/s]



(e) $U_c = 1$ [m/s]



(f) $U_c = 1,5$ [m/s]

Figure C.2: Sinker tube weight, 135 kg/m

D. AquaSim Material Properties

This appendix include the input data for the different elements used in AquaSim.

D.1 Material properites for beam elements

Material	Custom
Mass density	953 [kg/m^3]
E-modulus	2,11E11 [N/m^2]
G-modulus	8,08E10 [N/m^2]

D.2 Material properites for floater elements in the fish net

Material	Plastic
Mass density	233,62 [kg/m^3]
Diameter	500 [mm]
Cross sectional area	0.19635 [m^2]
E-modulus	8E8 [N/m^2]
G-modulus	3,077E8 [N/m^2]

D.3 Mooring buoy properties

Node decorators	
Point load force (Z)	1,0462E4 [N]
Load type	0
Spring stiffness (Z)	8000 [N/m]
Type	BUOY

D.4 Net properties for fish net

Mask type	Type 1
Mass density	900 [kg/m ³]
E-modulus	1E9 [N/m ²]
Thread diameter	1,9995E-3 [m]
Pretension Y	5E-5
Pretension X	5E-5
Maskwidth Y	0,025 [m]
Maskwidth X	0,025 [m]
Growthcoefficient	1.0 - 1.5
Solidity 2D	15,9959 %
Solidity 2D included growth	15,99 - 23.99 %
Load type	M1: New Default

D.5 Net properties for dense net

Mask type	Type 1
Mass density	900 [kg/m^3]
E-modulus	1E9 [N/m^2]
Thread diameter	1E-3 [m]
Pretension X	5E-5
Pretension Y	5E-5
Maskwidth Y	5E-5
Maskwidth X	5E-5
Growthcoefficient	1.0 - 1.5
Solidity 2D	100 %

Drag coefficient	0.3
Lift coefficient, peak value	1,2
Density of fluid inside tank	1025 [kg/m^3]
Height of fluid inside tank relative to swl	0,0 [m]
Added mass coefficient horizontal motion	1,0
Added mass coefficient vertical motion	1,0
Bottom factor	1,0
Damping coefficient	0,0
Skin friciton coefficient	0,01
Type of diffraction load	McCamy - Fuchs

D.6 Mooring and bridle line 48mm properties

Mass density	1000 [kg/m^3]
E-modulus	1,8E9 [N/m^2]
Weight in air	1,81 [kg/m]
Diameter Y	0,048 [m]
Diameter Z	0,048 [m]
Drag coefficient Y	1,2
Drag coefficient Z	1,2
Added mass coefficient Y	1,0
Added mass coefficient Z	1,0

D.7 Anchor chain 36mm properties

Mass density	1,4E4 [kg/m^3]
E-modulus	1,1E11 [N/m^2]
Weight in air	28,0 [kg/m]
Diameter Y	0,07 [m]
Diameter Z	0,07 [m]
Drag coefficient Y	1,2
Drag coefficient Z	1,2
Added mass coefficient Y	1,0
Added mass coefficient Z	1,0

E. Properties for the time domain simulation

Table E.1: Simulated conditions with time domain parameters

Condition	H[m]	T_p[s]	C_x [m/s]	Pre- increment	Max iterations per step	Num total steps for waves	Num steps for one wave
1	0.5	2	0	5	500	3000	30
2	1	3.2	0	5	500	2500	40
3	2	5.1	0	5	500	2000	50
4	0.5	2	0.2	5	500	3000	30
5	1	3.2	0.2	5	500	2500	40
6	2	5.1	0.2	5	500	2000	50
7	0.5	2	0.4	5	500	3000	30
8	1	3.2	0.4	5	500	2500	40
9	2	5.1	0.4	5	500	2000	50
10	0.5	2	0.6	5	500	3000	30
11	1	3.2	0.6	5	500	2500	40
12	2	5.1	0.6	5	500	2000	50

[-] Time serie	
Preincrement	5
Max iterations pr step	500
Num total steps for waves	40
Num steps for one wave	20
Convergence criteria	1.0
Current reduction type	From initial shape ▼
Infinte depth	<input checked="" type="checkbox"/>
Depth(wave profile)	-1.0 m
[-] Bottom	
Bottom contact	<input checked="" type="checkbox"/>
Bottom depth	-100.0 m
Bottom parameter	1.0
Bottom friction	0.0
<input type="checkbox"/> Seed generation	
Number of seeds	0
Seed	0
Seed increment	0
[-] Advanced	
Water volume correction	None ▼
Reported steps	1
Convergence accelerator	0.0
Newmark damping	0.5
Analysis type	Normal ▼
Type of mass	Lumped mass ▼
Buckling/eigenperiod analysis	<input type="checkbox"/> ⋮
[-] Hydrodynamic properties	
Wave headings	90
Segments on hull	40
Segments on water surface	24

E. Numerical Formulation of Sea Loads to Impermeable Nets

VI International Conference on Computational Methods in Marine Engineering
MARINE 2015
A.J. Berstad, L.F. Heimstad

NUMERICAL FORMULATION OF SEA LOADS TO IMPERMEABLE NETS

Are Johan Berstad*, Line Fludal Heimstad†

Aquastructures
Kjøpmannsgata 21, 7013 Trondheim, Norway
e-mail: mail@aquastructures.no
web page: <http://www.aquastructures.no>

Key words: Numerical calculations, impermeable nets, AquaSim, Finite Element analysis.

Abstract. A load formulation has been introduced to the Finite Element program AquaSim, where the net is impermeable and water is hence not allowed to pass through the elements belonging to the impermeable net. This paper presents the theory of the load formulation, and presents three case studies where the load model is validated.

1 INTRODUCTION

The aquaculture industry has increased rapidly the last 30 years. In almost all fish farms, the fish is held contained in net cages. In 2009, the Norwegian standard, NS 9415, was revised, and in 2011 corresponding regulations were enforced. This largely increased the number of analysis being carried out on aquaculture structures.

Lice on farmed fish in Norway has increased concurrently with the growth of the aquaculture industry. In order to maintain the growth and the sustainability, the industry is forced to come up with solutions. Two suggestions, which is believed to reduce and perhaps eliminate lice on farmed fish, are closed flexible bags or stiffer structures and Lice-skirts mounted on the upper part of the net.

Common with both of these suggestions is that water can not flow through the net, since the material is impermeable. This introduces a significant change to the governing physics, where the usual Morison type load formulation applied to groups of twines is no longer applicable. The structure will behave as a large floating mass being withheld inside a thin sheet. The current is forced to flow around, and the waves are accompanied by diffraction or deformation of the impermeable net.

This paper presents the load formulation that has been introduced to the computer program AquaSim [1, 2, 3] for analysis to impermeable nets. AquaSim is a FE computer program used for the design of almost all fish farm systems in Norway, and is also in wide use in other countries doing offshore fish farming such as Chile and Australia.

2 THEORETICAL FORMULATION

2.1 Internal pressure and static equilibrium

Consider a tank filled with an arbitrary fluid. The tank can also be empty. Assume that the fluid inside the tank has a different water level than the fluid outside the tank, as shown in Fig. 1.

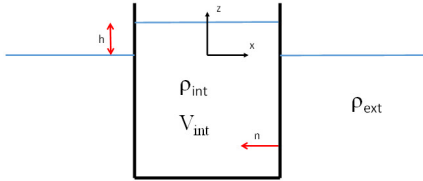


Figure 1: Tank in water

The tank has an inside volume, V_{int} . Load equilibrium for a net panel of the tank is found as:

$$F_n = gzA(\rho_{ext} - \rho_{int}) - ghA\rho_{int} \quad (1)$$

Where F_n is the normal force to a net panel pointing into the tank where a net is subdivided into several panels. More abbreviations is found at the end of this document. Positive value of h means the water level inside the tank is higher than the water level outside the tank. If the tank is empty the inside water density, ρ_{int} , will be zero.

Figure 2a and 2b shows a case were the inside water density is the same as the outside water density, but the water height, h , inside is one meter above the water level outside the cage. In this case the inside pressure leads to a deformation of the net going outwards (x-direction) and downwards (z-direction). Whether the net is deformed, or the cage moves downwards is decided by the stiffness of the net, relative to the stiffness of the water plane area.

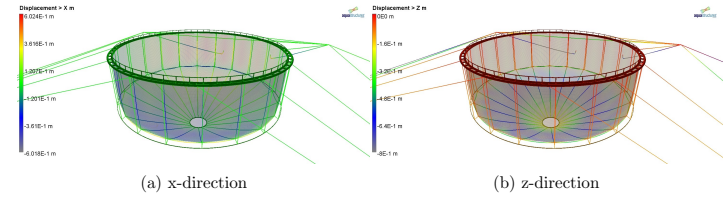


Figure 2: Deformation of the net. Inside water lever is one meter above the outside water level

2.2 Forces from current flow around cylinder

Impermeable nets may also be open at the top and at the bottom. For example skirts to avoid lice, i.e. lice skirts. This is shown in Fig. 3. In this case, the static pressure inside will be equal to the static pressure outside the net.

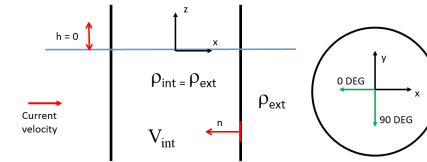


Figure 3: Dense net in current flow.

Consider a current velocity approaching along the x-axis. The current flow around a cylinder will introduce a velocity field which introduces a pressure field to the cylinder.

The pressure field around a cylinder is implemented to AquaSim in a simplified way as shown in Fig. 4. A drag and a lift coefficient is introduced. The pressure coefficient, C_p , upstream is expressed as:

$$C_p = 1 - (C_l + 1) \sin^4 \theta, \quad \text{for } 0^\circ \leq \theta \leq 90^\circ \quad (2)$$

Note that this corresponds to the analytical solution for an inviscid flow with $C_l = 3.0$. C_p at the leeward side of the cylinder is found as:

$$C_p = \min(1 - (C_l + 1) \sin^4(90 + (\theta - 90) \cdot 1.5) - C_{wake} \quad (3)$$

Where C_{wake} is found by matching the overall drag to the cylinder, to the drag force derived from the input drag and lift coefficients.

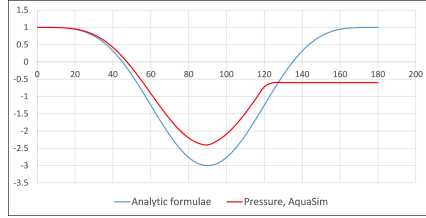


Figure 4: Pressure distribution around a cylinder as calculated in AquaSim.

Having found C_p as a function of the angle between the element in the horizontal plane, and the current flow the force acting on a net panel with an area, A , is found as:

$$F_n = \frac{\rho A C_p}{2} U_c^2 \quad (4)$$

The cross-flow principle is applied such that the U_c is the part of the current velocity normal to the element at the element fronting the current direction.

In addition a skin friction force, F_s , can be applied and may be expressed as:

$$F_s = \frac{\rho A C_s}{2} U_{tan}^2 \quad (5)$$

The skin friction part of the force is applied for the current flow in the tangential direction, both circumferential and along the length of the cylinder.

2.3 Wave force

For wave forces the pressure from the incident wave, i.e. Froude-Kriloff, and the pressure caused by the wave diffraction are calculated according to MacCamy and Fuchs theory [6].

In a regular sea with airy waves, the dynamic pressure from the incident wave is found as [4]

$$p_{FC} = \rho g \zeta \frac{\cosh k(z+h)}{\cosh kh} \sin(\omega t - kx) \quad (6)$$

For an irregular sea state the expression for the dynamic pressure is [4]:

$$p_{MF} = \sum_{n=1}^N \rho g \zeta_n \frac{\cosh k_n(z+h)}{\cosh k_n h} \sin(\omega_n t - k_n x + \epsilon_n) \quad (7)$$

In Eq. 7 N sinusoidal wave components are used to represent the wave spectrum, n means the n th sinusoidal wave component and ϵ_n is a random phase for each sinusoidal wave component.

The pressure caused by a diffracted wave around the surface of the cylinder with a radius r , according to [6] is:

$$p_{MF} = \rho g \zeta \frac{\cosh k(z+h)}{\cosh kh} \sum_{n=0}^{\infty} i [B_n H_n^1(kr)] \cos n\theta e^{-i\omega t} \quad (8)$$

Where:

$$B_n = -\epsilon_n t^n \frac{J'(kr)}{H^{(1)}(kr)} \quad (9)$$

In an irregular sea the pressure from the diffracted wave field along the surface is found as:

$$p_{MF} = \sum_{m=1}^N \rho g \zeta_m \frac{\cosh k_m(z+h)}{\cosh k_m h} \sum_{n=0}^{\infty} i [B_n H_n^1(kr)] \cos n\theta e^{-i\omega t + \epsilon_n} \quad (10)$$

The total pressure at a given point is then found as:

$$p = p_{FC} + p_{MF} \quad (11)$$

As the MacCamy and Fuchs theory for diffracted waves is valid for vertical cylinders, ρ_{MF} is multiplied with the vertical projection of the area.

2.3.1 Wave drift

Drift forces is proportional to the wave elevation squared and is hence a 2^{nd} order effect. It should therefore be found keeping all 2^{nd} order terms of the force in a 2^{nd} order perturbation approach. The wave potential may be expressed as [4]:

$$\phi = \phi_1 + \phi_2 \quad (12)$$

Where ϕ_1 is the 1^{st} order potential and ϕ_2 is the 2^{nd} order potential. Latter will not give any contribution to drift forces [4]. Hence, drift forces is found by keeping the 2^{nd} order terms when evaluating the Bernoulli equation in the 1^{st} order potential, given as:

$$p = \rho g z - \rho \frac{\partial \phi_1}{\partial t} - \frac{\rho}{2} \left\{ \left(\frac{\partial \phi_1}{\partial x} \right)^2 + \left(\frac{\partial \phi_1}{\partial y} \right)^2 + \left(\frac{\partial \phi_1}{\partial z} \right)^2 \right\} \quad (13)$$

Also, 2^{nd} order terms with a zero mean force can be omitted. Following [4] the terms given in Eq. 14 and Eq. 15, of the 1^{st} order potentials, are the ones contributing to drift forces:

$$p = -\rho g \int_0^\zeta z dz - p \frac{\partial \Phi_1}{\partial t} \Big|_{z=0\zeta} \quad (14)$$

and:

$$-\frac{\rho}{2} \int_{-\infty}^0 \left\{ \left(\frac{\partial \phi_1}{\partial x} \right)^2 + \left(\frac{\partial \phi_1}{\partial y} \right)^2 + \left(\frac{\partial \phi_1}{\partial z} \right)^2 \right\} dz \quad (15)$$

Which corresponds to the velocity squared term in the Bernoulli equation. Equation 14-15 are valid for infinitely deep cylinders. For the real case the integrals are performed from the bottom of the cylinders, as the lowest point.

It should be noted that by including the drift terms from Eq. 14 and Eq. 15 also a sum frequency load is introduced to the analysis. This is not the full sum frequency load effect, but only parts contributing to drift.

3 CASE STUDIES

3.1 Wave and current forces to cylinder

Two cylinder-shaped models have been established in AquaSim: One consisting of beam elements, and the other with impermeable membrane elements covering the circumference. Both models with the parameters given in Tab. 1. The length of the cylinders is situated vertically, i.e. in the negative z-direction from the sea surface and downwards, as shown in Fig. 5. The cylinder is kept from moving such that the velocity of the cylinder itself is negligible, and the wave length is large relative to the cylinder diameter. The long wave approximation [4] should give good results in this case, meaning that the results from these two models should have good correspondence.

Table 1: Cylinder particulars

Diameter [m]	4
Depth [m]	15
$\rho_w \left[\frac{kg}{m^3} \right]$	1025
C_d	1.2
ζ [m]	5
T [s]	10
$U_c \frac{m}{s}$	1.0

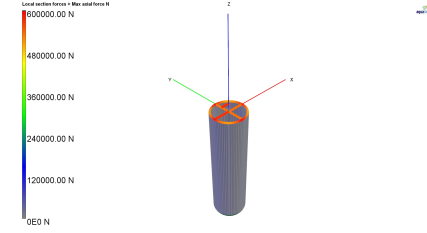


Figure 5: Vertical cylinder.

The Morrison equation [7], for a non-moving object, can be expressed as:

$$F = \rho C_m V \dot{u} + \rho C_d A u |u| \quad (16)$$

Where the first term in Eq. 16 is the inertia forces, and the second term is the drag forces.

3.1.1 Current loads

Figure 6 shows comparison between the Net model and the Beam model exposed to current only, and with three different drag coefficients, i.e. $C_d = 0.6$, $C_d = 1.2$ and $C_d = 2.0$. In this case, only the drag forces from Eq. 16 will apply. As seen from this figure there is a good correspondence between the results.

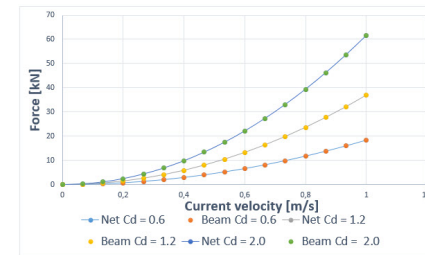


Figure 6: Comparison between the Net and Beam model exposed to current, and with different drag coefficients.

3.1.2 Wave and current loads

The inertia part of the forces is the results of the pressure distribution around the object, where F in the direction i can be expressed as:

$$F_i = \iint_S p n_i ds + a m_{i1} a_1 + a m_{i2} a_2 + a m_{i3} a_3 \quad (17)$$

Where n_i is the normal vector pointing into the object. For a case where the wave is long relative to the volume, the divergence theorem can be applied and Eq. 17 can be expressed as:

$$F_1 = \rho V a_1 + a m_{11} a_1 = \rho V (a_1 + a_1) = \rho V (1 + C_a) a_1 = \rho V C_m a_1 \quad (18)$$

For long waves the MacCamy and Fuchs theory should asymptotically lead to the same results as Eq. 18 with $C_m = 2.0$. The results with the Net and the Beam model, exposed to wave and current, are shown in Fig. 7. As seen from this figure there is a good correspondence between the results.

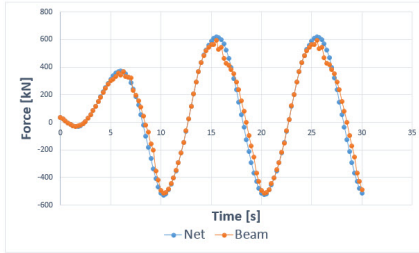


Figure 7: Net model and beam model exposed to wave and current.

3.2 Current forces to impermeable net - lice skirt

The load model implemented in AquaSim for impermeable net has been compared to model experiments performed by [5]. The impermeable net has a depth of 0.540 m, and the current velocity is in the range $U_c = 0.05 - 0.20 m/s$. The lice skirt corresponds to the situation shown in Fig. 3. The numerical model from AquaSim is shown in Fig. 8. The current is applied along the positive x-axis.

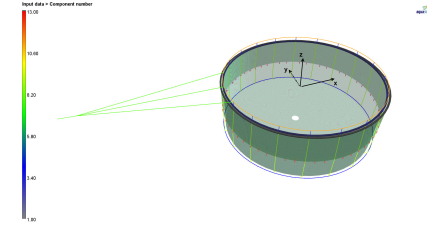


Figure 8: Numerical model in AquaSim with liceskirt.

The numerical results has been compared to the experimental results using a $C_d = 1.2$, and a $C_l = 2.0$. Four different values for C_f has been used, i.e. $C_f = 0.00$, $C_f = 0.12$, $C_f = 0.18$ and $C_f = 0.24$. The results are shown in Fig. 9.

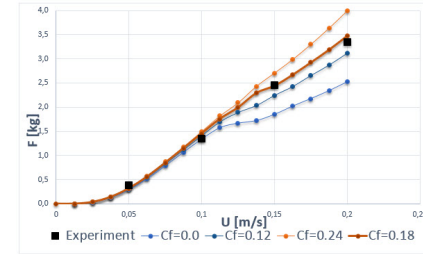


Figure 9: Numerical results compared to model experiments from [5], with $C_d = 1.2$, $C_l = 2.0$ and four different values for C_f .

3.3 Wave forces and response to SPAR buoy

Figure 10 shows two variations of a SPAR buoy modelled in AquaSim. In the Beam model the properties are distributed to beam elements. The properties includes load application from Morison's formulae [7] and added mass. For load application the Morison's formulae is applied for the beam with added mass coefficient of $C_a = 1.0$, giving a $C_m = 2.0$. The Net model consists of a net along the circumference of the cylinder. Loads are calculated on the net from MacCamy Fuchs theory [6]. Added mass is distributed to the net giving the same added mass as for the Beam model.

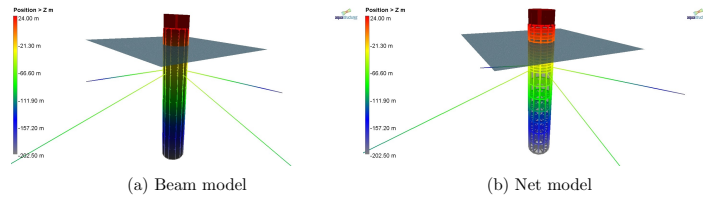


Figure 10: SPAR buoy

The main data for the analysed case, in both the Beam and the Net model, is given in Tab. 2.

Table 2: Particulars regarding the SPAR Buoy

Environment	
Wave amplitude [m]	5.0
Wave period [s]	22.6
SPAR buoy	
Diameter [m]	37.5
Depth [m]	200.0
COG	-102.5
COB	-100.0
Mass of structure [ton]	225435
Horizontal added mass [ton]	226416
Vertical added mass [ton]	0
Mooring	
Horizontal length [m]	481.25
Depth [m]	202.5
EA [kN]	170112
Pretension [kN]	4888
Weight per meter [kg/m]	185
Eigen period system	
Heave	28
Surge/sway [s]	219
Pitch/roll [s]	94
Yaw	Suppressed

Two variations of the Net model has been carried out: One where all load components, contributing to slow varying drift forces, are accounted for, and one Net model where 1st order forces are calculated to the actual free surface. The models are:

1. Beam model: All properties are distributed to a beam. Loads are calculated to the actual free surface, as shown in Eq. 14.
2. Net model with drift: A net is wrapped around the beams. All hydrodynamic loads are applied to the net, and not to the beam. The properties regarding the buoyancy are the same as for the Beam model. In addition to integrating to the free surface, Eq. 14, the load term of Eq. 15 is included.
3. Net model without drift: In this case the load term from Eq. 15 is not included, but all other load terms are the same.

A drag coefficient of $C_d = 1.2$ is applied to all the beam and membrane elements. For the mooring lines, a drag coefficient of $C_d = 1.3$ and a drag diameter of 142 mm has been applied.

The results from the analysis in AquaSim are shown in Fig. 11 and Fig. 12.

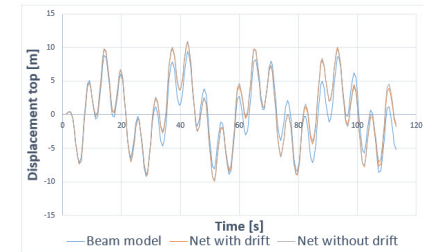


Figure 11: Comparison of motions, at the top, for the Beam model, the Net model with drift, and the Net model without drift.

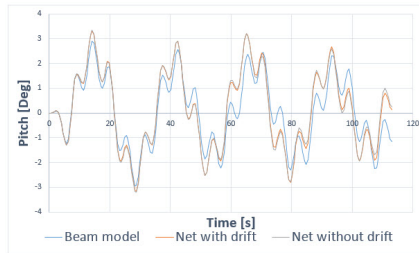


Figure 12: Comparison of rotations about the axis, normal to the flow, for the Beam model, the Net model with drift, and the Net model without drift.

As seen from Fig. 11 and Fig. 12 there is a good correspondence in the results. As this is a dynamic analysis, with the same loading to the two models, this shows that there is a good correspondence between the mass and the added mass. Whether one use the 2nd order terms from Eq. 14, or the 2nd order terms from Eq. 14 and Eq. 15 does not seem to have a large influence on the results in this case.

4 CONCLUSIONS

A load formulation for impermeable nets has been introduced to the Finite Element Program AquaSim. Three case studies is presented. The case studies validates the calculation of current and wave loads, and the application of mass and added mass. The case study performed on lice skirt, which deforms strongly in current, shows the importance of enabling skin friction. Using a skin friction coefficient of $C_f = 0.18$, 15 % of the drag coefficient give results fitting well with the empirical data.

For further work it is suggested to carry out more comparisons between model experiments, and numerical analysis.

Abbreviations

g	Acceleration of gravity	m/s^2
ζ	Amplitude of wave	
θ	Angle	Deg
A	Area	
J'_n	Bessel function, first derivative	
B_n	Coefficient	m
i	Complex unit (0,1)	
U_c	Current flow normal to the element	m/s
U_{tan}	Current flow tangential to the element	m/s
ρ	Density of fluid	kg/m^3
C_d	Drag coefficient	
ϵ	$\epsilon_0 = 0$ else 2	
F	Force	N
H_n^1	Hankel function, first kind	
C_l	Lift coefficient	
n	Normal vector	
C_p	Pressure coefficient	
C_s	Skin friction coefficient	
T	Time	s
h	Vertical distance	m
z	Vertical position	m
V	Volume	m^3
ω	Wave frequency	$2\pi/s$
k	Wave number	$1/m$

REFERENCES

- [1] Berstad, A.J. and Heimstad, L.F. and Walaunet, J. *Model Testing of Fish Farms for Validation of Analysis Programs*. Proceedings of the ASME 2014 33rd International Conference on Ocean, Offshore and Arctic Engineering OMAE2014, (June 8-13 2014), San Francisco, California. OMAE2014-24647.
- [2] Berstad, A.J. and Walaunet, J. and Heimstad, L.F. *Loads from Currents and Waves on Net Structures*. Proceedings of the ASME 2012 31st International Conference on Ocean, Offshore and Arctic Engineering OMAE2012, (July 1-6, 2012), Rio de Janeiro, Brazil. OMAE2012-83757.
- [3] Berstad, A.J. and Tronstad, H.Y. *Design Rules for Marine Fish Farms in Norway. Calculation of the Structural Response of such Flexible Structures to Verify Structural Integrity*. Proceedings of the ASME 2004 23rd International Conference on Ocean, Offshore and Arctic Engineering OMAE2004, (June 2004), Vancouver, Canada. OMAE2004-51577.
- [4] Faltinsen, O.M. *Sea Loads on Ships and Offshore Structures* Cambridge University Press (1990).
- [5] Lien, A.M. and Volen, Z. *Deformation of net and Permskirt and Forces on Mooring* (In Norwegian) Model experiments in flumetank. SINTEF Fisheries and Aquaculture (March 2012).
- [6] MacCamy, R.C et al. *Wave Forces on Piles: A Diffraction Theory*. Corps of Engineers, Washington, D.C, (December 1954).
- [7] Morison, J.R. and O'Brien, J.W. and Schaaf, S.A. *The Force Exerted by Surface Waves on Piles* Petroleum Transactions, AIME Vol. bold 189, 149-154 (1950).

G. Matlab Functions

```
% Find the wave number, k, by using the dispersion relation
% This script uses the kSolve function to calculate the wave number, k
% by iteration. Initial guess, x0, is set to 0.
```

```
% Constant parameters
```

```
g = 9.81;
rho = 1025;
```

```
% Wave period, T (s)
```

```
T = 3.2;
f = 1/T;
```

```
% Water depth (m)
```

```
h = 100;
```

```
% Initial guess
```

```
x0 = [0];
```

```
% Dispersion relation function to find wave number, k
```

```
[k,fval] = fsolve(@(k) kSolve(f,g,h,k), x0);
```

```
k
```

```
L = (g/(2*pi))*T^2*tanh(k*h)
```

Published with MATLAB® R2014b

```
% Solving Dispersion relation
```

```
function [k]= kSolve(f,g,h,k)
```

```
% Function that calculates the wave number, k.
```

```
% Format of call: kSolve(f,g,h,k)
```

```
% input: f, g, h, k
```

```
% output: wave number, k
```

```
% Authors: Ingrid K.Feyling & Siri M. Kalvig (October 2016)
```

```
omega = 2*pi*f;
```

```
k = omega^2-(g*k*tanh(k*h));
```

```
end % end of function
```

Published with MATLAB® R2014b

% Static mooring line calculations

```
clc
clear all

% Number of anchors
n = 2;

% Water depth (m)
h = 0:1:95;

% Horizontal load (N) - equal to drag load at
% current speed of X-[m/s]
H_x_total = 2152;
H_x_total = 8608;
H_x_total = 19369;
H_x_total = 121053;

% Divide by anchors
H_x = H_x_total/n;

% Stud-link chain size 1-3/4 inch
% Submerged weight/m (N/m)
W = 39;

% Distance to touchdown point (m)
L = (H_x/W)*acosh(((W*h)/H_x)+1);

Lmax = max(L)

% Geometric profile of catenary
y = (H_x/W)*(cosh((W/H_x)*L)-1);

% Touchdown point to anchor
x2 = -70:1:0;
indexmax2 = find(max(x2) == x2);
y2 = zeros(1,indexmax2);

% Coordinates of touchdown point
x_td = 0;
y_td = 0;

% Length of catenary
% The total length is calculated when x = Lmax
s = (H_x/W)*sinh((W*Lmax)/H_x)

% Vertical force in Newton
V = W*s

% Total tension, Newton
T = sqrt((H_x^2)+(V^2))
```
